Dissecting the neuronal circuitry of the sleep homeostat

Lea Ballenberger

Department of Physiology, Anatomy and Genetics

Harris Manchester College

University of Oxford

A thesis presented for the degree of

Doctor of Philosophy

Trinity 2025

Acknowledgements

This thesis would not exist if it wasn't for all the people who have supported me throughout the process.

First and foremost, I would like to thank my supervisor Gero Miesenböck for giving me the opportunity to join his lab. I am grateful for the chance to work in this highly stimulating environment for the past five years and for everything I learned on the way. I am indebted to him for his support, scientific guidance and everything he taught me during these years. I would also like to thank my second supervisor Stephen Goodwin for his support and kindness.

I would like to thank my funding body, Boehringer Ingelheim Fonds, for the financial support, but also for all the amazing people I got to meet throughout the years. I am proud to be part of this community.

The work in the lab would not have been achievable if it wasn't for the people who taught me, and who shared every day in the lab with me. I would like to thank everybody in the CNCB that I crossed paths with throughout the years. Especially, I would like to thank Katerina Christodoulou and Anissa Kempf who helped me start off in the lab. Olof Rorsman, thanks for making the struggles lighter by sharing them. Timothy Wong and Paola Vargas Gutierrez, who became and remained friends. Haram Park, Paul Volkmann, Eleftheria Vrontou, Alina Krebbers, Celina Hartmann, Bhagyashree Senapati and so many others, thank you for your support and advice! I am grateful for all the technical and scientific support to Raffaele Sarnataro, Clifford Talbot, Peter Hasenhütl as well as everybody else in the lab and CNCB. A special thanks goes out to Ruth Brain,

Fiona Woods and Rebecca Busby without whom the CNCB would not function, and to Sarah Noujaim for her support.

Life in Oxford would not have been the same without all my friends here. These five years are so special because of you. Thank you to Leoni Boyle, Lucille Duquenoy, Leonie Hoff, Maxime Kayser, Olivia McGinnis, Ashwin Miriyala, Monty Ochocki, Jonas Schuff, Madeline Tatum, Penny Zacharopoulou, and many more. Thank you to Anne Fleischmann, Annika Sachs dos Santos and Janine Utz who have been with my for all those years and supported me in all my struggles and achievements. I am so glad for your support throughout all stages. Thank you to Annie and Amelia who supported me in the hardest times.

A special thanks goes out to my flatmates in these years: Melody Li, Josef Lolacher and Eddie Toma. You have seen me at my best and at my worst. I am forever grateful for all the late night chats after hard days of work that helped me stay sane, you will forever be my Oxford home.

I am glad you joined for the last stretch of my PhD, and I am so happy for what it turned out to be. Thank you Henni, for everything so far and everything that will come.

Last, I want to thank the people whose unconditional support has been with me throughout all my life and who brought me to where I am right now, my parents Andrea and Gerd, and my brother Tim. This thesis is dedicated to you.

Lea Ballenberger, Oxford 18th June 2025

Table of Contents

List of Figures **ix**

List of Tables **xi**

List of Abbreviations **xii**

Abstract **xiii**

1 Introduction **1**

1.1 Sleep . . . 1

1.1.1 The two process model of sleep regulation . . . 2

1.2 *Drosophila melanogaster* as a model organism . . . 3

1.2.1 Neurotransmitter systems . . . 5

1.2.2 Studying neural circuits in *Drosophila* . . . 5

1.3 Sleep in *Drosophila* . . . 7

1.3.1 Sleep stages in *Drosophila* . . . 8

1.3.2 Dorsal fan-shaped body neurons . . . 9

1.3.2.1 Sensing sleep need . . . 10

1.3.2.2 Controversy . . . 11

1.3.2.3 Sleep related inputs . . . 12

1.3.3 R5 neurons in sleep regulation . . . 13

1.4 Aim . . . 15

2 Materials and Methods **16**

2.1 Fly strains and husbandry . . . 16

2.2 *Drosophila* stocks . . . 16

2.3 Connectome analysis . . . 21

2.4 Sleep behavioural experiments . . . 22

2.5 Two-photon calcium imaging . . . 23

2.6 Patch-clamp electrophysiology . . . 24

2.6.1 Optogenetics . . . 24

2.6.2 Toxins . . . 25

2.6.3 Targeted ATP and glutamate application . . . 25
2.6.4 Analysis of electrophysiology data . . . 25
2.7 Immunohistochemistry . . . 26
2.8 Confocal Microscopy . . . 26
2.9 Quantification and statistical analysis . . . 27

3 Connectome analysis of dFB neurons 28
3.1 Introduction . . . 28
3.1.1 The *Drosophila* connectomes . . . 28
3.1.2 Heterogeneity within dFBNs . . . 29
3.2 Results . . . 30
3.2.1 dFBNs receive synaptic inputs in the superior protocerebrum and the fan-shaped body . . . 30
3.2.2 Postsynaptic connections of dFBNs target interneurons in the FB . . . 33
3.2.3 Connections of dFBNs are largely conserved between connectome datasets . . . 35
3.3 Discussion . . . 40
3.3.1 Not all known inputs to dFBNs can be verified via the connectome . . . 40
3.3.2 Known synaptic outputs of dFBNs are present in the connectome . . . 41
3.3.3 Sensory inputs arrive in the SP . . . 42

4 Behavioural screen of neurons connected to dFBNs 44
4.1 Introduction . . . 44
4.2 Results . . . 45
4.2.1 Sleep behavioural screens identify several neurons of interest . . . 45
4.2.1.1 Neuronal activation alters sleep in multiple genotypes . . . 45
4.2.1.2 Neuronal inhibition alters sleep in multiple genotypes . . . 47
4.2.2 Anatomical analysis verifies overlap with dFBNs . . . 50
4.2.3 Testing functional connectivity between R56E07-GAL4 and dFBNs reveals monosynaptic connection . . . 53
4.2.3.1 Calcium imaging reveals connection between neurons . . . 55
4.2.3.2 Optogenetic activation of dFBNs induces a strong depolarization in patch-clamp recordings . . . 57

4.2.3.3 R56E07-GAL4 neurons receive synaptic input from dFBNs 59
4.2.4 Chemogenetic activation of dFBNs via P2X2 induces a strong depolarization . . . 62
4.2.4.1 Chemogenetic activation of dFBNs induces response in downstream neurons . . . 63
4.2.4.2 The function of R56E07-GAL4 neurons upstream of dFBNs 65
4.2.5 Generation of split lines to target pontine neurons more specifically . 67
4.2.5.1 CX neurons in R56E07-GAL4 are responsible for the reduction in sleep . . . 68
4.2.5.2 R56E07 split-GAL4 lines label different number of cells . . 69
4.3 Discussion . . . 71
4.3.1 GAL4 lines often target unknown additional cell types . . . 72
4.3.2 Caveats of TrpA1 activation . . . 73
4.3.3 Synaptic connectivity testing remains difficult . . . 74

5 dFBNs project onto wake-promoting hDeltaF neurons 76
5.1 Introduction . . . 76
5.2 Results . . . 80
5.2.1 Connectome analysis of hDeltaF neurons . . . 80
5.2.1.1 Presynaptic connections of hDeltaF neurons are mainly formed by dFBNs . . . 80
5.2.1.2 hDeltaF neurons target cells encoding goal angle . . . 84
5.2.2 Behavioural analysis of hDeltaF neurons reveals wake-promoting effect 85
5.2.2.1 Activation of hDeltaF neurons reduces sleep . . . 87
5.2.2.2 Inhibiting synaptic output from hDeltaF neurons does not affect sleep . . . 92
5.2.3 Electrophysiological analysis of the connection from dFBNs to hDeltaF neurons . . . 98
5.2.3.1 Optogenetic stimulation of dFBNs elicits response in hDeltaF neurons . . . 98
5.2.3.2 The connection between dFBNs and hDeltaF neurons is driven by glutamate . . . 103

5.3 Discussion . . . 108
5.3.1 hDeltaF neurons connect a sleep centre with neurons encoding goal angle representation . . . 110
5.3.2 The role of hDeltaF neurons in the control of sleep . . . 112
5.3.3 Functional connection of dFBNs onto hDeltaF neurons . . . 114

6 Connections between the EB and the dFB 117
6.1 Introduction . . . 117
6.2 Results . . . 118
6.2.1 Manipulation of hDeltaK neurons increases wake . . . 118
6.2.2 Inhibition of serotonergic ExR3 neurons increases wake . . . 127
6.3 Discussion . . . 132
6.3.1 Opposing manipulations of hDeltaK lead to the same behavioural output . . . 132
6.3.2 hDeltaK neurons target dFBNs . . . 134

7 Discussion 138
7.1 Main findings . . . 138
7.2 Limitations . . . 139
7.3 Implications . . . 141
7.3.1 The connection between a sleep control centre and a navigational centre . . . 141
7.3.2 The synaptic connections of dFBNs . . . 144
7.4 Future directions . . . 146

8 Supplementary Data 147
Supplementary Data . . . 147

List of Figures

3.1 Presynaptic connections of dFBNs 31
3.2 Postsynaptic connections of dFBNs 34
3.3 Comparison of presynaptic connections of dFBNs 36
3.4 Comparison of postsynaptic connections of dFBNs 38

4.1 Thermogenetic screen for sleep behaviour 46
4.2 Kir2.1 inhibition screen for sleep behaviour 48
4.3 Confocal image of specific GAL4-driver lines 50
4.4 GRASP staining 51
4.5 DenMark staining 53
4.6 Optogenetic activation leads to an increase in GCaMP7f signal. 54
4.7 Calcium imaging reveales connection to R56E07 56
4.8 Patch-clamp recordings reveal a strong depolarization during optogenetic stimulation 58
4.9 Connection from dFBNs to R56E07 can be detected 60
4.10 Connection from dFBNs to R56E07-GAL4 is monosynaptic 61
4.11 ATP applications depolarize P2X2-expressing dFBNs strongly 63
4.12 Chemogenetic activation of dFBNs elicits response in R56E07-GAL4 neurons 64
4.13 Patch-clamp recordings of dFBNs upon R56E07-GAL4 stimulation 66
4.14 Patch-clamp recordings reveal a monosynaptic connection from R56E07-GAL4 onto dFBNs 67
4.15 R56E07 split-GAL4 behaviour 69
4.16 Expression pattern of R56E07-GAL4 split-GAL4 lines 70

5.1 Main synaptic connections of dFBNs 77
5.2 Presynaptic connections of hDeltaF neurons 81
5.3 Comparison of presynaptic connections of hDeltaF neurons between datasets 82
5.4 Postsynaptic connections of hDeltaF neurons 83
5.5 Comparison of postsynaptic connections of hDeltaF neurons between datasets 84
5.6 Activation of hDeltaF neurons reduces sleep 86
5.7 Further parameters of hDeltaF neuronal activation 88

5.8 hDeltaF split-GAL4 expression is the same in all sexes 91
5.9 *shibire^{ts}* expression in hDeltaF changes sleep architecture 93
5.10 No change in sleep upon EKO expression in hDeltaF neurons in mated female flies 95
5.11 Increased wake during EKO expression in hDeltaF neurons in male flies . . 96
5.12 hDeltaF neurons receive monosynaptic input from dFBNs, recordings at -30 mV 99
5.13 hDeltaF neurons receive monosynaptic input from dFBNs, recordings at -60 mV 101
5.14 No leaky CsChrimson expression detected in hDeltaF neurons with patch clamp recordigns 102
5.15 Glutamate depolarizes hDeltaF neurons when held at -60 mV 104
5.16 Glutamate elicits complex response in hDeltaF neurons when held at -30 mV 105
5.17 GluCl knockdown in hDeltaF neurons does not change sleep 107
5.18 Sleep parameters of GluCl knockdown in hDeltaF neurons 109

6.1 hDeltaK neurons are strongly connected to dFBNs 119
6.2 Activation of hDeltaK neurons decreases sleep 120
6.3 Blocking hDeltaK neuronal output decreases total sleep as well as sleep depth 123
6.4 hDeltaK form a monosynaptic connection with dFBNs 125
6.5 dFBNs' connection onto hDeltaK neurons remains unclear 126
6.6 dFBNs connection onto hDeltaK neurons cannot be detected 127
6.7 Activation of ExR3 neurons fragments sleep 128
6.8 Blocking synaptic output in ExR3 neurons decreases sleep 130
6.9 Serotonin expression in ExR3 neurons 132

S1 Changes in movement during thermogenetic screen for sleep behaviour . . . 147

List of Tables

2.1 List of fly stocks 16

List of Abbreviations

ACh ..... acetylcholine

AD ..... activation domain

AP ..... action potential

AstA ..... allatostatin-A

ATR ..... all-*trans* retinal

CNS ..... central nervous system

CX ..... central complex

DBD ..... DNA binding domain

dFB ..... dorsal fan-shaped body

dFBN ..... dorsal fan-shaped body neuron

EB ..... ellipsoid body

EEG ..... electroencephalogram

FB ..... fan-shaped body

FW ..... FlyWire

GFP ..... green fluorescent protein

GluCl ..... glutamate-gated chloride channel

GRASP ..... GFP reconstitution across synaptic partners

HB ..... hemibrain

HD ..... head direction

KD ..... knockdown

KO ..... knockout

LFP ..... local field potential

MB ..... mushroom body

NGS ..... normal goat serum

NO ..... paired noduli

NREM ..... non-rapid eye movement

NT ..... neurotransmitter

PB ..... protocerebral bridge

PBS ..... phosphate-buffered saline

PBST ..... PBS with Triton-X

PFA ..... paraformaldehyde

PTX ..... picrotoxin

REM ..... rapid eye movement

RMP ..... resting membrane potential

ROS ..... reactive oxygen species

SD ..... sleep deprivation

SG ..... subesophageal ganglion

SHY ..... synaptic homeostasis hypothesis

SIP ..... superior intermediate protocerebrum

SLP ..... superior lateral protocerebrum

SMP ..... superior medial protocerebrum

SP ..... superior protocerebrum

TTX ..... tetrodotoxin

UAS ..... upstream activation sequence

VNC ..... ventral nerve cord

Abstract

Sleep is essential to every animal's life and sleep deprivation can be detrimental to the animal's health and wellbeing. The timing and length of sleep are tightly regulated by the circadian rhythm and the homeostatic process. In the fruit fly *Drosophila melanogaster*, the homeostatic control of sleep was mapped to neurons projecting to the dorsal fan-shaped body (dFBN). These neurons change their firing rate with increasing sleep pressure and subsequently induce sleep in the animal. While the molecular mechanisms involved in sensing sleep pressure in dFBNs are being delineated, their synaptic connections have not been analysed functionally. Here, I analysed the published connectomes to identify relevant connected cell types and found strong synaptic connections to and from interneurons in the fan-shaped body. I performed a behavioural screen to delineate the role of sleep regulation in these connected neurons and found several cell types that might be relevant in the sleep control circuitry. dFBNs connect strongest to hDeltaF neurons, which form columnar neurons in the fan-shaped body, and I showed that these neurons have wake-promoting effects upon activation. I further studied two cell types that connect dFBNs to another sleep regulatory centre, the ellipsoid body, and manipulating these neurons also revealed wake-promoting effects. Further analysis of the synaptic connection of dFBNs and hDeltaF neurons via patch-clamp electrophysiology uncovered a synapse of dual polarity, suggesting that one neurotransmitter, glutamate, can be both inhibitory and excitatory between the same synaptic partners. Overall, dFBNs are interconnected with many different cell types and their synaptic connection might be more diverse than expected, suggesting a modulatory role on downstream circuits.

1 | Introduction

1.1 Sleep

Sleep is immensely important for animals and humans alike. The sleep behaviours of many different animals have been studied to date, and none has been found that does not sleep. This suggests that sleep is evolutionarily conserved and essential for life, despite its associated risks for animals in the wild [1–3]. Sleep is first and foremost defined on a behavioural level: it is a reversible state of quiescent immobility accompanied by an increased arousal threshold, homeostatic control and often a preferred posture [4]. Further, sleep can be distinguished from quiet wake based on the neural activity pattern in electroencephalogram (EEG) recordings as well as muscular activity [3–5]. In humans and many animals, sleep can further be divided into two different stages: rapid eye movement (REM), which is associated with dreaming [6, 7], as well as non-rapid eye movement (NREM) [3, 5]. Interestingly, animals do not need a central nervous system (CNS) to sleep, as was shown in studies of the jellyfish *Cassiopea* [8] and *Hydra vulgaris* amongst others [9].

To understand the importance of sleep, many scientists study the effects of sleep deprivation (SD). One of the first documented SD studies was performed in 1894: Marie de Manaceine sleep deprived dogs and found that the absence of sleep for a few days led to premature death in these animals, while the absence of food could be sustained for much longer without detrimental effects [10]. Many studies followed, with one of the most famous by Allan Rechtschaffen who sleep deprived rats, compared them to yoked animals to control for stress artifacts, and found that SD led to significant physiological impairments, in

several cases lethal to the animal [11].

While it is undeniable that sleep is important, the reason why we sleep has still not been fully understood. There are several, not mutually exclusive hypotheses for why we sleep. The two most prominent ones are the synaptic homeostasis hypothesis (SHY) and the need for clearance. SHY states that sleep is necessary to downscale the synapses that were built and strengthened during wakefulness [12, 13]. Support for this hypothesis comes from many species, including fruit flies [14, 15], zebrafish [16, 17], rodents [18, 19] and humans [20]. Further, sleep is believed to aid in the process of clearing the brain of toxins and metabolites that have accumulated during wake [21, 22]. Recent evidence suggests that the glymphatic system is responsible for this clearance during sleep, and an increased flow of cerebrospinal fluid has been shown during NREM in mice [21], humans [23] and birds [24]. Even in *Drosophila*, a sleep stage necessary for brain clearance has been defined [25]. Further, sleep was shown to be necessary to prevent damage by and for the clearance of reactive oxygen species (ROS) [26, 27]. To uphold these necessary functions and balance these with the associated risks and drawbacks, sleep needs to be precisely regulated.

1.1.1 The two process model of sleep regulation

There are two parallel systems that control sleep: the circadian clock and the homeostatic system [28, 29]. The two process model of sleep regulation by Alexander Borbély states that these two processes interact to control the timing and length of sleep [28]. While the circadian clock functions to synchronize the sleep-wake cycle with the external environment, the homeostatic system measures increasing sleep pressure during the waking time, and dissipates it during the sleep period [28, 30]. Consequently, sleep deprivation increases sleep need, and to compensate the following sleep period needs to be longer or more intense. A

sleep homeostat must be recording the accumulated time spent awake and translate this to subsequent periods of sleep to maintain a healthy balance. Sleep homeostasis refers to this regulatory process of maintaining a stable balance between sleep and wakefulness in the animal and to correct for any lack of sleep. The homeostatic control of sleep has not been fully understood and will form the main focus of this thesis.

The circadian clock, on the other hand, has been well studied and the 24-hour rhythm of most animals has been traced back to a transcription-translation feedback loop [31, 32]. The groundbreaking experiments that led to the understanding of the circadian clock were performed in *Drosophila melanogaster* [31, 32] and in subsequent studies, these findings were ultimately translated to mammals [33]. This is one example showing the usefulness of understanding basic principles in a simple model organism, like the fly, before translating them to more complex organisms like mice or humans.

1.2 *Drosophila melanogaster* as a model organism

For more than a century, *Drosophila melanogaster* has been used as a model organism for the study of genetics, starting with the identification of the first genes and their inheritance pattern [34]. The field moved on to the discovery that single genes can influence certain behaviours, a finding that also led to the discovery of the molecular basis of the circadian clock [35, 36]. In the year 2000, the whole genome of *Drosophila melanogaster* was sequenced [37, 38], after only two other, smaller, eukaryotic genomes had been published, those of *Saccharomyces cerevisiae* [39] and *C. elegans* [40, 41].

Following whole genome sequencing, another huge project was taken on by the fly community: mapping the whole connectome of the CNS of the fly. Advances of the past five

years have produced detailed maps for every single neuron in the female fly brain [42–45]. This effort was continued to generate the connectome of the ventral nerve cord (VNC), the fly's equivalent of the spinal cord, as well as its connections to the brain [46–49].

The description of the connectome has helped the generation of more precise tools for the study of single cell types. The GAL4/UAS system has been well established in the fly [50–52]. Here, the transcriptional activator GAL4 is inserted into the genome after a specific enhancer sequence that will control its expression [50, 51]. To control gene expression, transgenes will be encoded after a UAS (upstream activation sequence) and transcription can only be induced in cells that also express GAL4 [50, 51]. A more refined version of this system is the split-GAL4 approach: here, the GAL4 is split into its two domains: the DNA binding domain (DBD) and the transcription activation domain (AD) [53, 54]. Both domains can be expressed using different promoters. As the GAL4 protein can only induce transcription once the DBD and the AD domain are combined, transgene expression will be restricted to the subset of cells that express both GAL4 domains [53, 54]. The number of GAL4 and split-GAL4 lines available to target specific subsets of neurons is ever-increasing, with recent advances offering tools that target neurons with single cell-type specificity [52, 55, 56]. This allows researchers to precisely study and control subsets of neurons, and target transgene expression to the desired group of cells. Further, a plethora of RNAi and shRNA lines to knockdown (KD) gene expression is available for a wide range of transcripts [57–61] and CRISPR-Cas9 knockout methods are now widely established in *Drosophila* [62–65].

1.2.1 Neurotransmitter systems

Neurotransmission in *Drosophila* happens via fast-acting neurotransmitters, such as acetylcholine, GABA and glutamate, as well as neuropeptides that can act hormone-like or as neuromodulators [66, 67]. The effect of neurotransmitters depends on the respective receptor on the postsynaptic partner. Acetylcholine is the main excitatory neurotransmitter in *Drosophila*: it acts either via nicotinic receptors, which are ligand gated ion channels or via less abundant muscarinic receptors, which are G-protein-coupled receptors [68–70]. GABA is the main inhibitory neurotransmitter in the fly, acting via ionotropic $GABA_A$ Cl^- channels or metabotropic, G-protein-coupled $GABA_B$ receptors [71–73]. Glutamate can excite, modulate or inhibit its postsynaptic partners, depending on the receptors they express. Through glutamate, the postsynaptic cell can be depolarized via ionotropic glutamate receptors, such as AMPA, kainate or NMDA receptors, it can be modulated via metabotropic receptors, but it can also be inhibited via the glutamate-gated chloride channel (GluCl) [70, 74–78].

1.2.2 Studying neural circuits in *Drosophila*

Next to genetic and anatomical information about the brain, gathered from the genome and the connectome, physiological descriptions are needed to understand a functional neural network. Several advances in the second half of the 20th century have made it possible to study the electric activity of neurons: Hodkin and Huxley first described the ionic currents underlying action potentials (APs) on the giant squid axon [79]. To study circuits and ion channels, patch-clamp recording was developed by Erwin Neher and Bert Sakmann [80, 81], for which they received the Nobel Prize in 1991. Only at the end of the last century,

the technique was introduced in fly research with the first *in-vivo* recordings in the CNS of *Drosophila* embryos by Baines and Bate [82]. Wilson and Laurent were the first to record neural activity in adult *Drosophila*, where they recorded odour responses in projection neurons and local neurons of the antennal lobe [83].

To verify a connection between neurons, several different methods can be used, each with their advantages and disadvantages. Connections can be tested either via anatomical proximity, or via functional connectivity where the postsynaptic neuron responds to a presynaptic stimulation. In *Drosophila*, anatomical proximity can be tested by GFP reconstitution across synaptic partners (GRASP) [84], where close proximity of split GFP proteins allows them to reconstitute to form a functional protein whose fluorescence can be detected [85–87]. While this method is technically rather easy, it does not offer temporal resolution nor the sensitivity necessary for certain questions.

Functional connectivity can be tested via stimulation of presynaptic neurons, e.g. via opto- or chemogenetic activation, and recording of downstream responses via calcium imaging or patch-clamp electrophysiology. In *Drosophila* most studies use calcium imaging as readout, as it is technically less challenging, even though it is not as precise [88–91]. Patch-clamp recordings of the downstream neuron allow for detection of synaptic events that might otherwise be invisible in calcium imaging recordings [92–94].

To distinguish monosynaptic from polysynaptic connections, the gold standard in mammalian research is to measure the time between the presynaptic action potential and the postsynaptic potential, which can be achieved via double patch-clamp recordings [87, 95]. Polysynaptic events have a longer latency, which can be used to distinguish them from monosynaptic transmission events [87]. In invertebrates like *Drosophila*, this approach is

less reliable because synaptic events might not propagate fully to the soma, as the synapse is often located far away from the cell body [87, 95]. While dual patch-clamp recordings to test synaptic connections are possible in *Drosophila* [96], they are very rarely used due to the technical difficulty. An alternative approach that can be used in the fly is opto- or chemogenetic stimulation of the presynaptic neuron while recording from the postsynaptic neuron in the presence of tetrodotoxin (TTX), which blocks action potentials by inhibiting voltage-gated sodium channels and subsequently prevents polysynaptic transmission [87, 88, 93, 94, 97]. To further understand which neurotransmitter is present in the synapse, different pharmacological antagonists for the specific receptors can be added to the synapse, to block the relevant transmission [98]. Addition of high concentrations of picrotoxin (PTX), for example, blocks the glutamate-gated chloride channel [76] and can therefore be used to demonstrate that glutamate induces inhibition at a certain synapse.

1.3 Sleep in *Drosophila*

Drosophila melanogaster is an ideal model organism to study different levels of neuroscience: we can examine the molecular composition of single cells, analyse functional connections between neurons, investigate neuronal network activity *in-vivo* and study the resulting behaviour. The fly meets all of the previously mentioned criteria for a sleep state [4, 99, 100]: flies tend to sleep mostly at night, exhibit an increased arousal threshold, show homeostatic control of sleep, and even have a preferred sleeping position [99–101]. Further, sleep in the fly shows differences between the sexes [102–104], as well as an age dependent change, just like in humans: the amount of sleep is high in young mammals and flies, stabilises until adulthood, and decreases with old age [99]. As EEG recordings cannot be performed in *Drosophila*, the widely used definition of sleep is based on the

behavioural criteria of five minutes or longer of sustained inactivity, which is correlated with an increased arousal threshold [99, 100]. Using this behavioural criteria of inactivity, we can define a sleep state in the fly in contrast to the wake state during times of activity. Further, flies show certain sleep behaviours that are associated with the sleep state: they sleep in bouts of different durations, mostly at night and during the mid of the day, they can show varying overall amounts of total sleep, depending on external or internal factors (such as age, feeding state or external temperature) and have a reduced arousal threshold [99, 100, 105].

1.3.1 Sleep stages in *Drosophila*

Sleep in mammals can be classified in different sleep stages [3], which is also thought to apply to fruit flies [25, 106]. While sleep in *Drosophila* appears to correlate with a reduction in local field potentials (LFP) in the brain when compared to wakefulness, it was found that even within a sleep bout LFP activity changed correlating with the time since falling asleep [106, 107]. Further, different sleep stages can be identified on a behavioural level: sleep depth varies throughout a sleep bout, the metabolic rate of a fly decreases with deeper sleep stages and particularly deep sleep stages correlate with an increase in proboscis extensions [25, 106, 108]. Information from multi-channel electrophysiology, behavioural inputs, as well as machine learning can now be combined to reliably identify several different sleep stages [109, 110]. It has been shown that specifically deep sleep stages are subject to a stricter homeostatic control, highlighting that different sleep stages fulfil essential roles [111].

Drosophila sleep has been intensely studied since its discovery [112–114]. In the quest to understand its regulation, researchers have studied external influences, such as feeding and

starvation, temperature and social interaction [105], or have focussed on finding genes or brain regions that regulate sleep [112–114]. So far, more than 200 different genes have been identified to be involved in its regulation [113], underlining the plethora of different pathways and influences on fly sleep.

1.3.2 Dorsal fan-shaped body neurons

One of the main brain regions associated with the homeostatic control of sleep is the dorsal fan-shaped body (dFB). The fan-shaped body (FB) is a highly conserved region in the central complex (CX) of the fly. The CX describes a collection of neuropils in the centre of the brain of insects that consists of several distinct neuropils: the protocerebral bridge (PB), the ellipsoid body (EB), the FB and the paired noduli (NO) [115]. Early studies suggested the CX to be involved in many different behaviours, mainly motor control, navigational behaviours, and sensory integration [115–119].

The FB can be subdivided into nine horizontal layers, as well as roughly nine vertical columns (exact number depends on the cell type) [44]. Recent years have provided substantial evidence that the FB is the place of path integration, vector based computations and navigational outputs in the fly brain [94, 120–123]. Here, neurons are encoding the travelling direction and compute the fly's location in space [94, 121]. The FB seems to be especially tuned to receive input from different sensory modalities, such as odour information or wind flow, and then use this information to shape resulting navigational strategies [94, 121, 123–125].

The homeostatic control of sleep was pinpointed to the dorsal area of the FB: neurons projecting to the dFB (dFBNs) are tangential neurons that encode the sleep need of the animal [126–133]. In most studies, these neurons have been labelled by the R23E10-GAL4

driver [126–129, 131]. dFBNs constitute a group of 10-15 neurons per hemisphere, with their cell bodies on both hemispheres of the brain, and their neurites in the superior protocerebrum (SP) and in layer 6 and 7 of the FB [43, 44]. Several different lines of research have provided evidence that the population is heterogeneous, as was shown by their electrical characteristics, their response to specific signalling molecules and their receptor expression patterns [127, 134, 135]. Their role in regulating sleep behaviour has been identified via a behavioural screen, where artificial activation of these neurons induced sleep in the animal [126]. Further work has suggested an enhanced excitability of these neurons as well as an increase in overall activity, measured by elevated average calcium activity after sleep deprivation [127, 132] and in the evening, when sleep pressure is higher [91]. Higher activity in dFBNs was further shown in early stages of development, correlating with increased sleep pressure in young flies [136]. dFBNs are believed to communicate with each other, as shown by the connectome data [43, 44], as well as their oscillatory activity [132] and gap junctions, the latter possibly coupling them to non-dFBNs [137, 138]. A knockdown of innexin, which is the main building block of gap junctions, decreased sleep depth and overall amount, likely by reducing the synchronised activity of these cells [137].

1.3.2.1 Sensing sleep need

The importance of dFBNs in the regulation of sleep has become clearer over time and how these cells sense increasing sleep need is slowly being untangled. Early work suggested that the firing pattern of these cells changed during the course of the day, in relation to sleep need, with the cells being more active during times of high sleep pressure [91, 127]. This increase in firing rate is dependent on the potassium channel Shaker and its β-subunit Hyperkinetic [131]. The co-factor NADPH is bound to Hyperkinetic and can be reduced

to $NADP^+$, via increases of ROS and lipid peroxidation products, which in turn increases the firing rate of the neurons [131, 139]. Increasing sleep pressure enhances ROS as a by-product from mitochondrial electron transport chains and decreases the size and fission of mitochondria in dFBNs [131, 133]. Further it was shown that artificially increasing fission specifically in dFBNs decreased sleep [131, 133]. This suggests that changes in mitochondrial dynamics are not (only) a result of lost sleep, but might themselves be causal for the changes in sleep by reducing ATP levels in the neurons [133].

1.3.2.2 Controversy

While substantial evidence supports the role of dFBNs in the control of sleep, recent publications have put this into question [140, 141]. Close examination of the R23E10-GAL4 driver discovered off-target expression in areas in the brain outside of the dFB as well as in the VNC, and activation of these neurons alone appeared to be able to induce sleep [140, 142]. A long-term imaging study of different neurons in the fly brain suggests that the activity of dFBNs correlates with the feeding and walking state of the animal, rather than a sleep pressure signal [141]. Further, activation of R23E10-GAL4 neurons seems to induce a sleep state that differs from spontaneous sleep as measured by the simultaneously recorded calcium activity of several thousand neurons [143], while also inducing microbehaviours [144]. Activation of dFBNs using the 104y-GAL4 driver, which labels many off-targets, showed much higher LFP in acute activation of dFBNs when compared to spontaneous or drug induced sleep [145].

The above evidence questions the tools that were used for previous experiments, and the problem likely stems from the broad expression pattern of the R23E10-GAL4 line. To circumvent unspecific labelling, several efforts have now generated split-GAL4 driver lines

that label subsets of dFBNs [55, 132, 144, 146]. Activating several of these subsets, without any expression in the VNC, still increases sleep without inducing microbehaviours [55, 132, 144].

These advances make it clear that only a subpopulation of dFBNs is responsible for the increase in sleep upon activation, while other neurons (in the FB or in the VNC) might be responsible for the induction of microbehaviours [144]. Importantly, the correct stimulation protocol is also relevant to observing a reliable induction of sleep [132].

1.3.2.3 Sleep related inputs

dFBNs receive several sleep- or wake-promoting signals, some of which have been mapped to specific neurons, while for others only the signalling molecule, but not the responsible neuron is known. So far, three wake- and two sleep-promoting inputs to dFBNs have been described: first, dopamine was shown to be a wake-promoting signal that directly acts on dFBNs and inhibits their activity [85, 128, 147]. Applications of dopamine hyperpolarized dFBNs and subsequently induced locomotion [128]. The source of dopamine was mapped to PPL1 or PPM3 neurons [85, 147]. The second wake promoting signal has been hypothesized to come from hDeltaK neurons, which form interneurons in the FB [148]. hDeltaK neurons were shown to be necessary for increased wakefulness following social isolation, and based on connectome data this effect was suggested to act via dFBNs, but no direct evidence has been provided [44, 148]. The third wake-promoting input to dFBNs was described to stem from pontine neurons in the FB [90]. hDeltaK neurons are pontine neurons too, but were not labelled in that study, hence more work is needed to identify how different pontine neurons influence sleep behaviour [90].

Further, there are two sleep-promoting inputs to dFBNs: serotonin, as well as indirect

signalling from R5 neurons. The source of serotonin has not yet been found, but knockdown of the serotonin receptor 5-HT2B in a subset of dFBNs decreases sleep [135]. Further, the same manipulation impaired sleep rebound after SD, underlining serotonergic signalling as necessary for sleep induction or maintenance [135]. The last known sleep-promoting input to dFBNs stems from R5 neurons in the EB [130]. While R5 neurons do not form direct synapses onto dFBNs, it was shown that activation of R5 neurons increases the calcium signal in dFBNs [91, 130]. Further, the connection between dFBNs and R5 neurons seems to be reciprocal, with the strength of their influence on one another changing depending on the time of day [91].

1.3.3 R5 neurons in sleep regulation

R5 neurons are a group of ring neurons in the EB. In general, neurons in the EB respond to visual features [149], are necessary for memory in visual-navigational tasks [150, 151], encode the heading direction of the animal [152–154] and control the length and architecture of sleep [86, 155, 156].

Activation of R5 neurons induces sleep during as well as after the stimulation [130]. Here, sleep need is encoded in delta oscillations, and increasing sleep pressure increases their neuronal activity [130, 157]. Further, the oscillations are shaped by wake- and sleep-promoting inputs indirectly from circadian neurons [158, 159]. One of the downstream partners of R5 neurons are EPG neurons, whose activation themselves increases sleep [96, 160]. Not only the activity of these neurons, but also the connection between R5 and EPG neurons seems to be shaped by sleep pressure: sleep deprivation strengthens the synaptic connection in terms of number of cells that are connected, as well as synaptic strength between these two neurons [96], which can also be seen by the increase of active

zones in R5 neurons after SD [130]. Further, artificial brain-wide increase of bruchpilot, an important constituent of the active zone, increased sleep as well as calcium activity within these neurons [161, 162]. Last, blocking synaptic output of R5 neurons inhibits homeostatic rebound after a night of sleep deprivation [163].

R5 neurons and dFBNs are reciprocally connected via helicon cells (also called ExR1 cells) [91, 129]. Helicon cells receive inhibitory input from dFBNs via Allatostatin-A (AstA), and removal of the AstA receptor in helicon cells leads to a decrease in sleep [129]. Downstream, helicon cells project onto R5 neurons [129], while also receiving excitatory input from these neurons [91]. Helicon cells respond to visual stimuli and their activation induces movement, which is likely gated by their connection onto EPG neurons [91, 129].

1.4 Aim

This overview makes it clear that dFBNs do not act on their own to control sleep in *Drosophila*, but rather are part of a wider neuronal circuitry that receives information about sleep and wake states, and then translates increasing sleep pressure onto the organism.

The aim of this thesis is to understand how dFBNs are embedded in their local neuronal circuitry. While the role of dFBNs in the homeostatic regulation of sleep has been explored, their connections have not been analysed in detail. Further, their anatomical position places them at the centre of navigational control, suggesting additional, so far unexplored, neural circuits. This raises the questions of what signals are received by dFBNs, how they transmit their sleep promoting information, and whether they are involved in shaping the navigational behaviour of the fly.

To this end, three aims were explored:

1. What are the connections of dFBNs?
2. How do these connections shape the sleep behaviour of the animal?
3. What is the functional composition of the connection between dFBNs and their synaptic partners?

2 | Materials and Methods

2.1 Fly strains and husbandry

Flies were raised on standard agar food at 25 °C in 12 hour light/12 hour dark cycles, unless otherwise specified. 3–5-day-old mated female flies were used for the majority of sleep behavioural experiments; exceptions clearly labelled. For patch clamp and calcium imaging experiments, only female flies were used. For thermogenetic experiments, TrpA1 and shibire^{ts} experiments, flies were raised at 21 °C. For experiments with Gal80^{ts}, flies were raised at 18 °C. Flies for optogenetic experiments were raised in the dark, and transferred for 1-2 days onto food containing 2 mM all-*trans* retinal (Molekula) in DMSO upon eclosion. Flies for *trans*-Tango stainings were grown at 18 °C and dissected four weeks after eclosion for stronger transgene expression.

2.2 *Drosophila* stocks

Fly stocks were acquired from Bloomington *Drosophila* stock centre (BDSC), the Vienna *Drosophila* Resource Centre (VDRC) and the in house stock collection of the Centre for Neural Circuits and Behaviour (CNCB). Fly stocks SS04919, SS61641, SS54676, SS63089 were kind gifts from G. Rubin (Janelia), before their original publication [55].

Table 2.1: List of fly stocks

Genotype	**Source+ID**
R23E10-GAL4	CNCB
Continued on next page	

Table 2.1 – continued from previous page

Genotype	Source+ID
CS;UAS-myrGFP;QUAS-mtdTomatoX3HA (*trans*-Tango)	Gilestro lab [164]
Canton-S	CNCB
w[1118];P{y[+t7.7]w[+mC]=GMR56E07-GAL4}attP2 (R56E07-GAL4)	BDSC #39153
w[1118];P{y[+t7.7]w[+mC]=GMR45F08-GAL4}attP2 (R45F08-GAL4)	BDSC #49565
w[1118];P{y[+t7.7]w[+mC]=GMR9D11-GAL4}attP2 (R9D11-GAL4)	BDSC #40731
w[1118];P{y[+t7.7]w[+mC]=GMR29A11-GAL4}attP2 (R29A11-GAL4)	BDSC #49881
w[1118];P{y[+t7.7]w[+mC]=GMR24E05-GAL4}attP2 (R24E05-GAL4)	BDSC #49081
w[1118];P{y[+t7.7]w[+mC]=GMR14F05-GAL4}attP2 (R14F05-GAL4)	BDSC #49257
w[1118];P{y[+t7.7]w[+mC]=GMR17H12-GAL4}attP2 (R17H12-GAL4)	BDSC #49276
w[1118];P{y[+t7.7]w[+mC]=GMR38C04-GAL4}attP2 (R38C04-GAL4)	BDSC #49990

Continued on next page

Table 2.1 – continued from previous page

Genotype	Source+ID
w[1118];P{y[+t7.7]w[+mC]=GMR24C07-GAL4}attP2 (R24C07-GAL4)	BDSC #49074
w[1118];P{y[+t7.7]w[+mC]=GMR24A05-GAL4}attP2 (R24A05-GAL4)	BDSC #49055
w[1118];P{y[+t7.7]w[+mC]=GMR72H04-GAL4}attP2 (R72H04-GAL4)	BDSC #39800
w[1118];P{y[+t7.7]w[+mC]=GMR78A01-GAL4}attP2 (R78A01-GAL4)	BDSC #39985
w[1118];P{y[+t7.7]w[+mC]=GMR22H05-GAL4}attP2 (R22H05-GAL4)	BDSC #49002
w[1118];P{y[+t7.7]w[+mC]=GMR24B11-GAL4}attP2 (R24B11-GAL4)	BDSC #49070
R22H10-GAL4	CNCB
w[1118];P{y[+t7.7]w[+mC]=GMR88A06-GAL4}attP2 (R88A06-GAL4)	BDSC #46847
w[1118];P{y[+t7.7]w[+mC]=GMR83H09-GAL4}attP2 (R83H09-GAL4)	BDSC #41311
w[1118];P{y[+t7.7]w[+mC]=R24E06-p65.AD}attP40; P{y[+t7.7]w[+mC]=Tdc2-GAL4.DBD}attP2 (tdc-GAL4)	BDSC #68298
w[*];P{w[+mC]=Tdc2-GAL4.C}2 (tdc2-GAL4)	BDSC #9313

Continued on next page

Table 2.1 – continued from previous page

Genotype	Source+ID
w[1118];P{y[+t7.7]w[+mC]=GMR16H07-GAL4}attP2 (R16H07-GAL4)	BDSC #48747
w[1118];P{y[+t7.7]w[+mC]=GMR64A11-GAL4}attP2 (R64A11-GAL4)	BDSC #39289
w[1118];P{y[+t7.7]w[+mC]=GMR46C02-GAL4}attP2 (R46C02-GAL4)	BDSC #50257
w[1118];P{y[+t7.7]w[+mC]=GMR21C04-GAL4}attP2 (R21C04-GAL4)	BDSC #48932
w[1118];P{y[+t7.7]w[+mC]=GMR68B06-GAL4}attP2 (R68B06-GAL4)	BDSC #39458
w[1118];P{y[+t7.7]w[+mC]=GAL4.1Uw}attP2 (empty-GAL4)	BDSC #68384
UAS-TrpA1	CNCB
UAS-Kir2.1; Gal80ts	CNCB
w[1118];Py[+t7.7]w[+mC]=GMR23E10-lexAattP40 (R23E10-LexA)	BDSC #52693
UAS-tdTomato	CNCB
w[*];P{y[+t7.7]w[+mC]=CoinFLP-LexA::GAD.GAL4}attP40 P{w[+mC]=lexAop-rCD2.RFP}2;P{w[+mC]=UAS-CD4-spGFP1-10}3, P{w[+mC]=lexAop-CD4-spGFP11}3/TM6C, Sb[1] (GRASP)	BDSC #58755

Continued on next page

Table 2.1 – continued from previous page

Genotype	Source+ID
w[1118];L[1]/CyO;P{w[+mC]=UAS-DenMark}3, P{w[+mC]=UAS-syt.eGFP}3 (DenMark)	BDSC #33065
w[1118]; P{y[+t7.7] w[+mC]=20XUAS-IVS-jGCaMP7f}su(Hw)attP5 (UAS-GCaMP7f)	BDSC #80906
w[1118]; PBac{y[+mDint2] w[+mC]=20XUAS-IVS-jGCaMP7f}VK00005 (UAS-GCaMP7f)	BDSC #79031
LexAop-CsChrimson::tdTomato	CNCB
UAS-mCD8::GFP	CNCB
y[1]w[*];P{w[+mC]=UAS-Rnor \ P2rx2.L}3 (UAS-P2X2)	BDSC #91222
UAS-CsChrimson::tdTomato	CNCB
w[1118];P{y[+t7.7]w[+mC]=R72G03-p65.AD}attP40 (R72G03-AD)	BDSC #71128
w[1118];P{y[+t7.7]w[+mC]=R91D10-p65.AD}attP40; P{y[+t7.7]w[+mC]=R56E07-GAL4.DBD}attP2 (R91D10-AD;R56E07-DBD, hDeltaF-GAL4)	BDSC #88490
w[1118];Py[+t7.7]w[+mC]=R65B12-p65.ADattP40 (R65B12-AD)	BDSC #71110
UAS-RedStinger; UAS-GFP	CNCB
w[1118];P{y[+t7.7]w[+mC]=p65.AD.Uw}attP40; P{y[+t7.7] w[+mC]=GAL4.DBD.Uw}attP2 (empty split-GAL4)	BDSC #79603
UAS-shibire^{ts}	CNCB

Continued on next page

Table 2.1 – continued from previous page	
Genotype	**Source+ID**
y[1]w[*];P{w[+mC]=UAS-EKO[+]}222a P{w[+mC]=UAS-EKO[+]}222b (UAS-EKO)	BDSC #40974
107971KK GluCl RNAi#1	VDRC
105754KK GluCl RNAi#2	VDRC
UAS-GluCl-4xgRNA, UAS-Cas9 (CRISPR GluCl)	CNCB
w[1118];P{y[+t7.7]w[+mC]=VT014202-p65.AD}attP40; P{y[+t7.7 w[+mC]=VT039497-GAL4.DBD}attP2/TM6B,Tb[1](SS63089)	G. Rubin (Janelia) [55]
w[1118];P{y[+t7.7]w[+mC]=R72G03-p65.AD}attP40; P{y[+t7.7] w[+mC]=VT039497-GAL4.DBD}attP2/TM6B,Tb[1] (SS54676)	G. Rubin (Janelia) [55]
w;VT023810-p65ADZp in attP40/CyOTb; VT004983-ZpGdbd in attP2 (SS61641)	G. Rubin (Janelia)
w; VT010661-p65ADZp in attP40; VT010063-ZpGDBD in attP2 (SS04919)	G. Rubin (Janelia)

2.3 Connectome analysis

Connectome data was analysed using custom written MATLAB code. The Hemibrain dataset was downloaded in version hemibrain v1.2.1 [43, 165], and subsequently analysed in MATLAB. Flywire data was downloaded [42, 45, 166, 167] and preprocessed in R, then the data was extracted and analysed further in MATLAB, using the same scripts as for the hemibrain dataset. For both datasets, connections with less than 3 synapses and connections to neurons that were not annotated were excluded from the analysis. dFB

neurons were analysed as one group of neurons: the connections of all dFBNs were summed and studied together. Connections are studied as relative of the total connections of all dFBNs. For analysis in cell type families: cell types were grouped based on their annotated name.

2.4 Sleep behavioural experiments

Flies were collected on days 1-3 post eclosion, loaded into individual 65 mm glass tubes and placed in Trikinetics *Drosophila* Activity Monitors on days 3-5. The flies' activity was tracked for three days, using a single infrared beam in the middle of the tube and beam crosses are translated into activity. Sleep was classified as min. 5 minutes of inactivity, per standard definition in the field [99, 100]. Experiments were conducted at 25 °C under a constant 12-hour light/12-hour dark schedule. For thermogenetic experiments with TrpA1, baseline sleep was recorded on the first day after loading, at 21 °C. Thermogenetic induction was performed on the second day of the experiment, for 24 hours at 29 or 31 °C. Recovery sleep was recorded on day 3 of the experiment at 21 °C. For experiments with $Gal80^{ts}$, flies were collected into two groups, one group housed at 18 °C and the other group at 31 °C. After 2 days, flies were loaded into sleep monitors and behaviour was tracked for 3 days, at 18 °and 31 °C. For studies looking at virgin female flies, these were collected upon eclosion, and then aged appropriately. They were used for experiments at the same age as mated female flies, but housed without males since eclosion. 2-3 independent replicates were performed for every behavioural experiment. Immobile flies or flies that died during the experiment were excluded from the analysis. Data was acquired in 1 min and 30 min bins and analysed using the Sleep and Circadian Analysis MATLAB Program (SCAMP), by C. Vecsey [168, 169]. Several analyses can be performed based on the movement data

of the flies: total sleep, number and mean duration of sleep episodes, P(Wake), P(Doze) and activity counts per time awake. P(Wake) and P(Doze) are probabilities based on the changes from activity to inactivity states and vice versa: P(Wake) describes the probability to start moving, after a period of inactivity and P(Doze) describes the probability to stop moving after a period of activity [110]. Experimentally it was shown that P(Wake) and P(Doze) describe the sleep depth and the sleep pressure of the animal, respectively [110].

For thermogenetic experiments, data was plotted as the change to baseline day, according to the following formula:

$$\frac{(day2/3 - day1)}{day1}$$

2.5 Two-photon calcium imaging

For calcium imaging, 3-4 day old female flies were anaesthetized on ice and head-fixed to a custom made chamber with eicosane (Sigma). The cuticle was opened to gain visual access to the brain. The brain was perfused with extracellular solution containing 103 mM NaCl, 3 mM KCl, 5 mM TES, 8 mM trehalose, 10 mM glucose, 7 mM sucrose, 26 mM $NaHCO_3$, 1 mM NaH_2P0_4, 1.5 mM $CaCl_2$, 4 mM $MgCl_2$ (all Sigma) at pH 7.3, constantly bubbled with Carbogen (5% CO_2 and 95% Oxygen). 2-photon laser scanning microscopy was performed with excitation wavelength of 930 nm (Chameleaon Ultra II, Coherent), adjusted with a Pockels cell (302RM, Conoptics), focussed by a 20x, 1.0 NA water immersion objective (W-Plan-Apochromat, Zeiss), signal was detected with GaAsP photomultiplier tubes (Hamamatsu Photonics), and imaged with a frame rate of 32,79 Hz. The microscope was controlled through ScanImage. Change in fluorescence of region of interest was divided by the mean background signal.

2.6 Patch-clamp electrophysiology

In-vivo targeted patch-clamp recordings were performed on female flies aged 1-4 days post eclosion. Flies were briefly anaesthetized on ice, then head-fixed to a custom made chamber with eicosane (Sigma). To gain access to the cells of interest, cuticle, fat tissue, trachea and perineural sheet were removed manually. The brain was constantly perfused using the same extracellular solution as used for 2-photon imaging. Cells were visualized under a Olympus U-CMAD3 microscope, using brightfield to illuminate the field of vision and the cells, and then using a LED to specifically visualise the GFP tag in the cells of interest. Borosilicate glass electrodes with filament (Sutter instrument) were pulled using the DMZ Universal Electrode Puller (Zeitz-Instruments), to a resistance of 8-12 MΩ, adjusted to the targeted cell type. Internal solution to fill the patch pipettes consisted of 140 mM potassium aspartate, 10 mM HEPES, 1 mM KCl, 4 mM MgATP, 0.5 mM Na_3GTP, 1 mM EGTA (all Sigma) adjusted to a pH of 7.3. Using these solutions, the chloride reversal potential at room temperature is at -122 mV. Data was acquired with the Multiclamp 700B amplifier (Molecular Devices) and digitized with Digidata 1440A (Molecular Devices). Only one cell per fly was patched.

2.6.1 Optogenetics

For optogenetic experiments, CsChrimson-expressing cells were stimulated using a red LED at 625 nm (Thorlabs, M625L3), focussed on the fly's head. Stimulation protocols were controlled by pClamp and the TTL triggered pulse was simultaneously recorded in the software. Red light stimulation was repeated 10 times per sample, results were averaged per fly.

2.6.2 Toxins

To test the identity of synaptic connections, different toxins were added to the extracellular solution and perfused onto the brain. Sufficient incubation time was allowed for toxins to bind to their targets and exhibit their effects. Tetrodotoxin (TTX, Tocris and HelloBio) was used at a concentration of 1 μM, picrotoxin (PTX, Sigma) at a concentration of 100 μM.

2.6.3 Targeted ATP and glutamate application

For P2X2-activation experiments, glass electrodes were filled with 1 mM ATP (Sigma) in extracellular solution. Glass pipettes were placed in the dendritic tree of GFP-labelled dFB neurons and 50 ms pulses of ATP were pressure ejected using a Pressure Application System (PDES - Pneumatic Drug Ejection System, PDES-02DX, npi) at 1 bar. Ejections were TTL-triggered.

To apply glutamate onto hDeltaF neurons, 1 mM glutamate (Sigma) in extracellular solution was filled into glass electrodes. These were placed into the fan-shaped body, location was confirmed with test pulses. Glutamate was pressure ejected in 50 ms pulses.

2.6.4 Analysis of electrophysiology data

To compare changes in membrane voltage between several cells, the area under the curve was calculated, during the time of light stimulation of dFBNs. For this, the traces were normalized to the first 4 seconds of recordings, and changes in voltage were therefore a change from baseline. Resulting numbers are either positive (for excitatory responses) or negative (for inhibitory responses).

2.7 Immunohistochemistry

Brains and ventral nerve cord were dissected in phosphate-buffered saline (PBS, Fisher Scientific) from adult female flies, unless otherwise specified. Tissues were fixed for 20 min at room temperature in 4 % paraformaldehyde (PFA, Electron Microscopy Sciences), washed with 0.5% PBST (PBS with Triton-X) and blocked with 10% normal goat serum (NGS, Sigma) in PBST for one hour at room temperature or at 4 °C over night. Samples were then incubated with primary antibodies (1:250 rabbit anti-Serotonin (Sigma); 1:1000 chicken anti-GFP (Abcam), 1:500 rabbit anti:tdTomato (Takara), 1:10 mouse nc82 anti-bruchpilot (DSHB)), in 10% NGS in PBST for 48 hours at 4 °C, washed with PBST and incubated with secondary antibody (1:500 anti-chicken conjugated to Alexa 488 (Thermo Fisher Scientific), 1:500 anti-rabbit conjugated to Alexa 555 (Thermo Fisher Scientific), 1:500 anti-mouse conjugated to Alexa 633 (Thermo Fisher Scientific)) in 10% NGS in PBST over night. Tissue was mounted with Vectashield (Vector laboratories) and stored at 4 °C until imaging. For GRASP analysis, no antibodies were used, to avoid unspecific binding.

2.8 Confocal Microscopy

Stained brains and VNC were imaged on a Leica TCS SP5 confocal microscope. Pictures were acquired using a water immersion 25x objective. Pictures were processed using Fji/ImageJ, contrast and brightness was adjusted to enhance visibility.

2.9 Quantification and statistical analysis

Sleep data was analysed in Prism (GraphPad). Electrophysiology data was analysed using MATLAB (Mathworks). For statistical significance calculations of sleep data, data was tested for normal distribution using the D'Agostino & Pearson test. Statistical significance was then calculated with ordinary one-way ANOVA or an unpaired t-test for normally distributed data, and Kruskal-Wallis or Mann-Whitney U test for not normally distributed data.

3 | Connectome analysis of dFB neurons

3.1 Introduction

3.1.1 The *Drosophila* connectomes

In recent years, a huge milestone has been achieved: the connectome of the adult fly brain [42–45]. A full wiring pattern of an animal was first studied in 1986 by White, Southgate, Thomson and Brenner, who published "the mind of a worm" [170]. More recently, computationally aided efforts to delineate the connectomes of more animals have resulted in the connectome of the nematode *C. elegans* [171] and the *Drosophila* larva [172]. The connectome of the brain of the adult fruit fly is the first of its kind of an adult, and is now available in two different datasets [42–45]. It was quickly followed by the connectome of the male [46, 47] and the female VNC [48], as well as the reconstitution of the descending and ascending neurons that form the connection between brain and VNC [49]. This huge effort has generated vast amounts of data and tools that can guide and verify future and past research.

The first published connectome dataset was the hemibrain (HB) [43, 44]. Here, a part of a 5-day-old female brain, covering most of the central area of the brain including the central complex, was completely imaged and reconstructed to identify 25,000 neurons and roughly 20 million synapses present in this area [43]. The second effort, FlyWire (FW), analysed the complete brain of a 7-day-old female fly, resulting in the full adult fly brain, a resource that contains almost 140,000 neurons and more than 50 million synapses [42, 45, 173]. Both groups used an electron microscopy approach with slightly different preparation

techniques and resolution [42, 43]. As both approaches target an overlapping section of the adult female brain, the conservation of the wiring pattern, as well as potential individual differences between single flies can be examined [173].

Most importantly, the wiring diagram shows a high level of stereotypy, including synapse counts [173]. Some of the differences between datasets highlight potential caveats: first, cell type numbers can vary not only between brains, but even within hemispheres [173]. Next, not all cell types between connectomes can be matched, which means that the classification of cell types that was presented in the hemibrain, cannot be verified in all cases in the FAFB dataset [173]. Last, some cell types from the hemibrain needed to be divided into subgroups [173]. Since publication of the connectomes, even further advances have been made: machine-learning algorithm based neurotransmitter predictions allow us to understand the polarity of the synapse based on the dataset [174] and a huge library of new split-GAL4 lines has been made available, based on the new cell type classifications [55].

One caveat that will surely be solved soon, is that the currently publicly available brain datasets are from one sex only. Sex differences in the brain are known to exist, as for example *doublesex*-expressing neurons have been described to be sexually dimorphic and show differences in morphology and connectivity [175, 176]. Comparing the male and female connectome will be necessary to understand whether there might be further differences than have been unknown so far.

3.1.2 Heterogeneity within dFBNs

In order to study the synaptic connections of dFBNs, it is necessary to understand what neurons are labelled by the most widely used driver to label these neurons: R23E10-GAL4

[127–129, 131]. Morphologically, it was shown that this driver labels roughly a dozen tangential neurons with axons projecting to the dorsal fan-shaped body, and dendrites in the three areas of the superior protocerebrum (SP): superior medial protocerebrum (SMP), superior intermediate protocerebrum (SIP) and superior lateral protocerebrum (SLP) [44, 127, 177]. Differences in electrophysiological properties and receptor expression patterns suggested a heterogeneous group of neurons [127, 134, 135]. In the hemibrain dataset, the neurons in the R23E10-GAL4 driver that project to the dFB have been identified to consist of several different cell types (numbers of neurons in brackets): FB6A (6), FB6C_a (2), FB6C_b (5), FB6E (2), FB6G (2), FB6I (2), FB6Z (2), FB7A (6) and FB7K (4) [44]. Interestingly, this means that the R23E10-GAL4 driver does not only label different cell types in the same area, but cell types that project to two different layers of the FB.

In this chapter, the connectome data was used to study how dFB neurons are embedded in their neuronal circuitry, aiming to understand which neurons might be most relevant in the regulation of sleep. First, I studied the presynaptic neurons that form the input into dFBNs, and the postsynaptic neurons that form the output pathway. And second, I compared the HB data to the FW data, to verify whether the results would remain consistent between datasets.

3.2 Results

3.2.1 dFBNs receive synaptic inputs in the superior protocerebrum and the fan-shaped body

The neurons within the driver that are (or are not) relevant for the regulation of sleep are not yet known, hence the connections of all individual cell types were considered

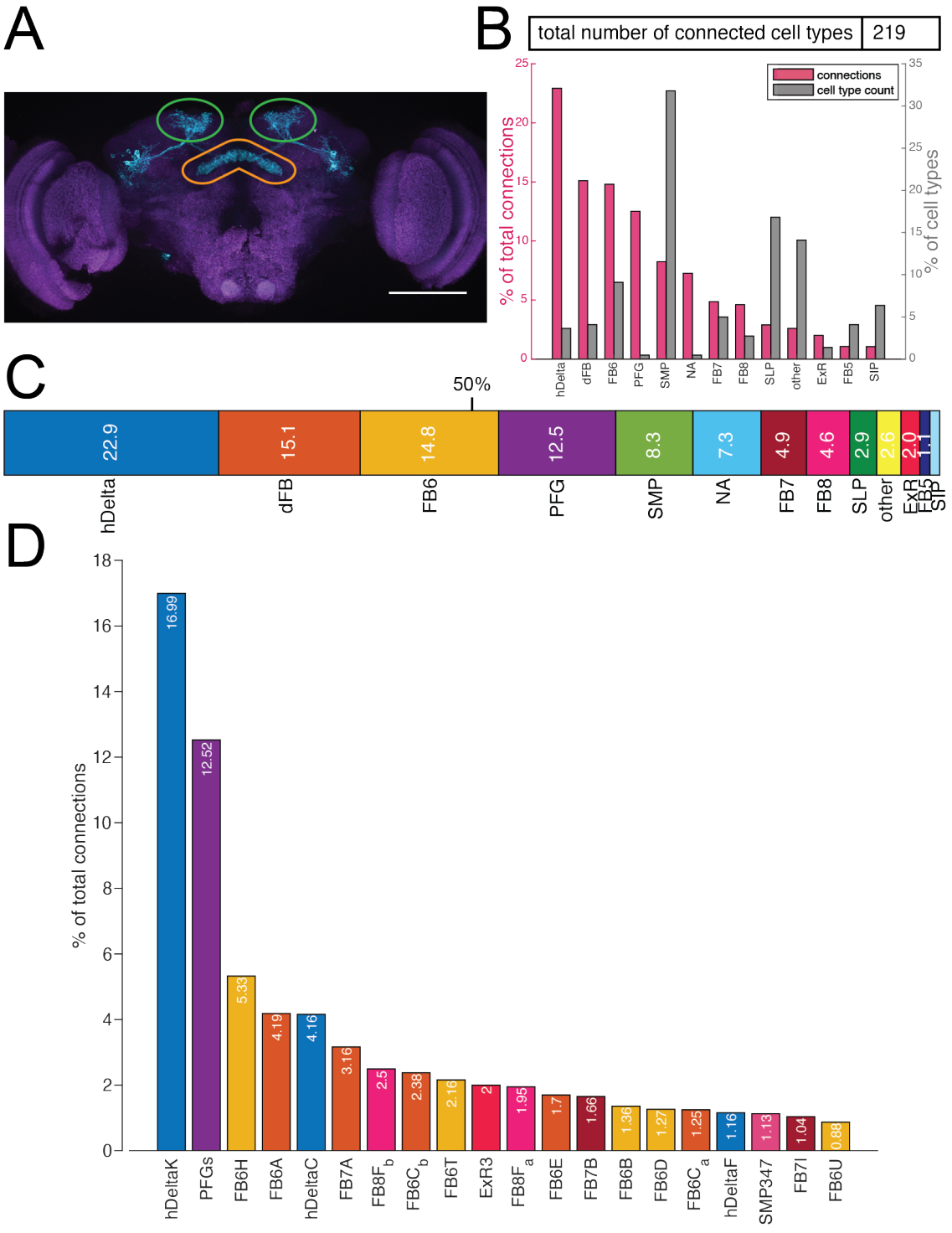

Figure 3.1: dFBNs receive synaptic input in the SP and the FB, from a wide variety of cells. A) Immunostaining of R23E10-GAL4 labelled neurons (cyan) in a *Drosophila* brain (nc82 staining, magenta). Maximum intensity projection of the whole brain. Neurites in both hemispheres of the superior protocerebrum are outlined by green circles, neurites in the FB outlined in orange. Scale bar = 100 µm. (Caption continued on next page.)

Figure 3.1: (Continued from previous page.) B) Presynaptic connections of dFBNs grouped into cell type families and plotted as % of total connections of dFBNs (pink), together with the number of cell types in % of all cell types connected presynaptic to dFBNs (grey). C) Cell type families forming synaptic inputs to dFBNs plotted horizontally for easier visibility, connections add up to 100%. NA = not annotated = truncated cells. Cell type groups with a connection strength of less than 1% are summed up as 'other'. D) The 20 strongest connected cell types are plotted in % of total connections of dFBNs. Data is sorted by connection strength. Bars are colour coded according to groups in C). Connections with less than 3 synapses were excluded. Raw data obtained from Hemibrain v1.2.1 [43, 165].

of equal relevance and analysed together to get a connectivity pattern for all dFBNs in the following analysis. They receive inputs in two different brain regions: the superior protocerebrum and layer 6 and 7 of the fan-shaped body (Fig. 3.1A). Overall dFBNs were heavily embedded in their local neuronal network: In total, dFBNs received inputs from 219 different cell types (Fig. 3.1B). To understand the connections better, cell types were categorized in bigger cell type families (e.g. all cells in layer 6, excluding the ones that are part of dFBNs, were summarized as 'FB6'). When describing presynaptic inputs to dFBNs at the level of cell type families, it became clear that columnar hDelta neurons formed by far the biggest input (Fig. 3.1B). This was followed by inputs of dFBNs themselves as well as other neurons in layer 6 of the FB (Fig. 3.1B). Together, these three groups of cell types formed more than 50% of all inputs to dFBNs (Fig. 3.1C). Besides the number of connections, the number of individual cell types in each of the cell type families were also examined. Here, an interesting picture became apparent: while hDelta and dFB neurons formed strong inputs, these connections were formed by few cell types. On the other hand, the inputs in the SP region were weak, with each cell type forming incoming synapses with less than 1% of synapse strength, but there were many different cell types that formed these synapses (Fig. 3.1B), suggesting that many different pathways converge here.

When examining individual cell types, certain neurons stood out due to the vast number of synapses they form with dFBNs: Almost one third of inputs was formed by only two cell

types: hDeltaK and PFG neurons (Fig. 3.1D). The third strongest connection was formed by FB6H, a dopaminergic neuron [55, 174]. Next came connections of dFBNs themselves, where the strongest synaptic inputs came from FB6A and FB7A (Fig. 3.1D). Overall, a lot of the connections in the FB area were other tangential neurons, or local interneurons. Non-tangential neurons that received inputs from an area outside the FB and transmit it onto the FB region of dFBNs were few, notable examples include: hDeltaK (receiving inputs from the EB), PFGs (inputs from the PB) and ExR3 neurons (inputs in the EB) (Fig. 3.1).

3.2.2 Postsynaptic connections of dFBNs target interneurons in the FB

To develop an intuition for the postsynaptic partners of dFBNs, a *trans*-Tango staining was performed: by using this technique all neurons are genetically equipped with a glucagon-receptor and a tdTomato reporter that will be transcribed upon receptor activation [178]. The cell population of interest is targeted with a GAL4 driver to expresses GFP as well as a membrane-bond glucagon, which will induce transcription of tdTomato in postsynaptic cells [178]. *trans*-Tango expression was analysed in flies with a R23E10-GAL4 driver where GFP was expressed in dFBNs, and tdTomato in downstream neurons (Fig. 3.2A). Overall, a diverse collection of neurons were labelled with tdTomato, of which the majority had neurites in the FB and the SP, as this was where they connected with dFBNs. The labelled neurons were almost exclusively in the dorsal half of the brain. Identification of single cell types based on the staining was difficult and often unreliable, hence further analysis of the postsynaptic partners was performed based on the connectome data.

The strongest output of dFBNs targeted hDelta neurons, a connection that made up more than one third of postsynaptic connections (Fig. 3.2B). Further downstream connections

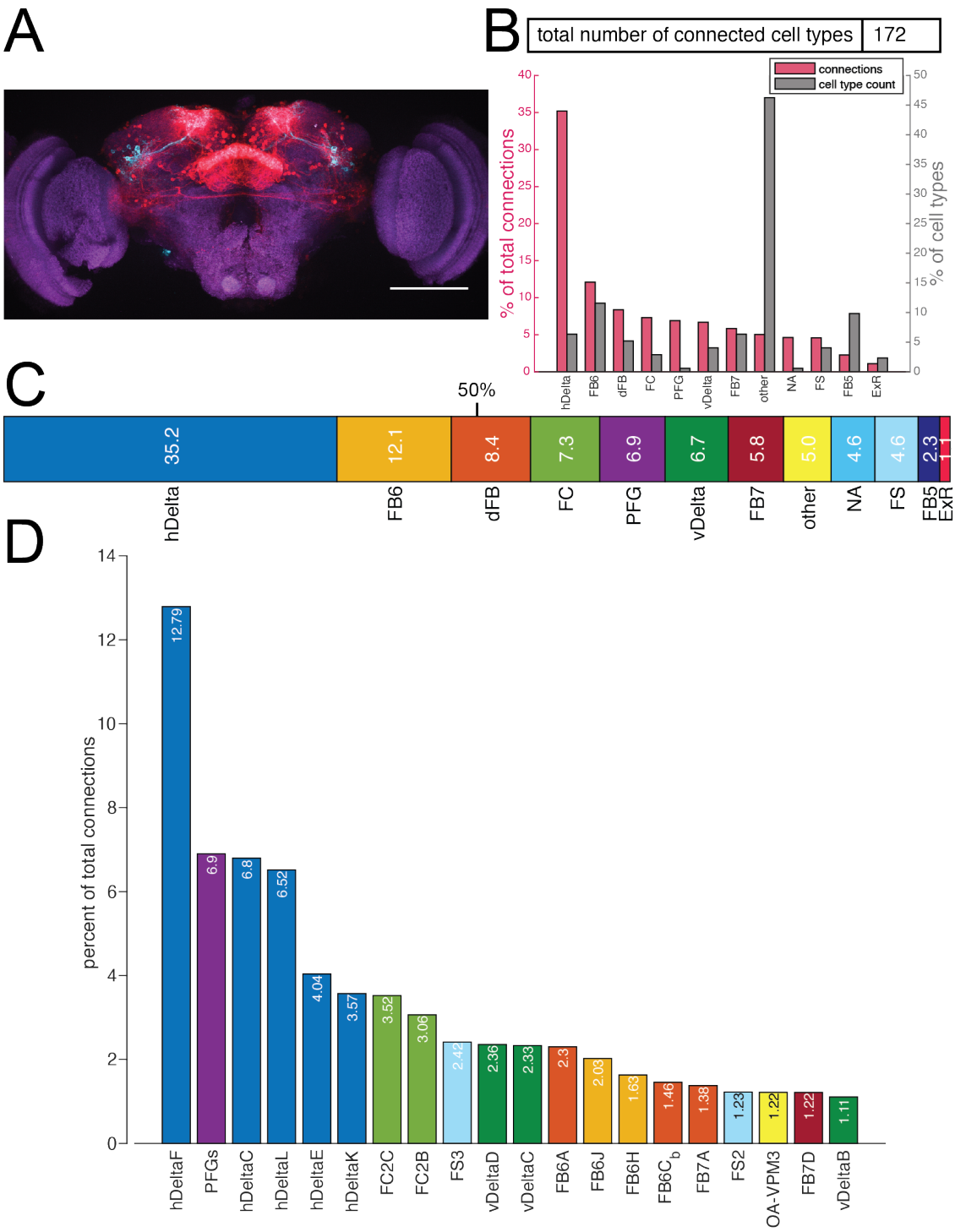

Figure 3.2: Postsynaptic connections of dFBNs target mainly cells in the FB. A) Immunostaining of *trans*-Tango expression, with R23E10-GAL4 driven GFP (cyan), and tdTomato expression (red) in downstream connected neurons. Maximum intensity projection Scale bar = 100 µm. B) Cell type families (pink) are plotted as percent of total postsynaptic connections of dFBNs, left y-axis. Number of cell types (grey) are plotted in % of all postsynaptic cell types, right y-axis. (Caption continued on next page.)

Figure 3.2: (Continued from previous page.) C) Postsynaptic connections of R23E10-GAL4 labelled neurons grouped into cell type families, plotted horizontally for easier visualisation. Connections plotted here add up to 100%. D) The 20 strongest connected neurons are plotted in % of total connections of dFBNs. Data is sorted by connection strength. Bars are colour coded according to groups in C). Connections with less than 3 synapses are excluded. Raw data obtained from Hemibrain v1.2.1 [43, 165]

targeted neurons in layer 6 of the FB, dFBNs and non-dFBNs, as well as FC, PFGs, vDelta and FB7 neurons, all with connection strengths between 12.1 and 5.8 % (Fig. 3.2C). Unlike the presynaptic connections of dFBNs, no cell type families stood out for having a large number of cell type counts (Fig. 3.2B). Analysing individual cell types revealed that there was one main postsynaptic partner: hDeltaF neurons (Fig. 3.2D). The second strongest connection were PFG neurons, which interestingly also formed the second strongest input to dFBNs. Next, there were four types of columnar neurons, hDeltaC, L, E and K before dFBNs targeted FC2C and FC2B cells (Fig. 3.2D). Overall, all top 10 postsynaptic partners were either columnar neurons in the FB, or outputs of the FB, suggesting that the main computations downstream of dFBNs were interneurons in the FB or goal encoding neurons (Fig. 3.2D, [123]).

3.2.3 Connections of dFBNs are largely conserved between connectome datasets

All previous analyses were performed on the data derived from the hemibrain dataset [43, 44]. To verify their reliability, they were subsequently compared to the FlyWire dataset [42, 45, 173]. Identifying dFBNs in the FW dataset already pointed to a difference: a different nomenclature had to be used, as not all cells from hemibrain could be reliably mapped in the FlyWire dataset [173]. This resulted in a reallocation of HB cell types to FW types: several different HB cell types were merged into one new FW cell type (e.g. FB6C and

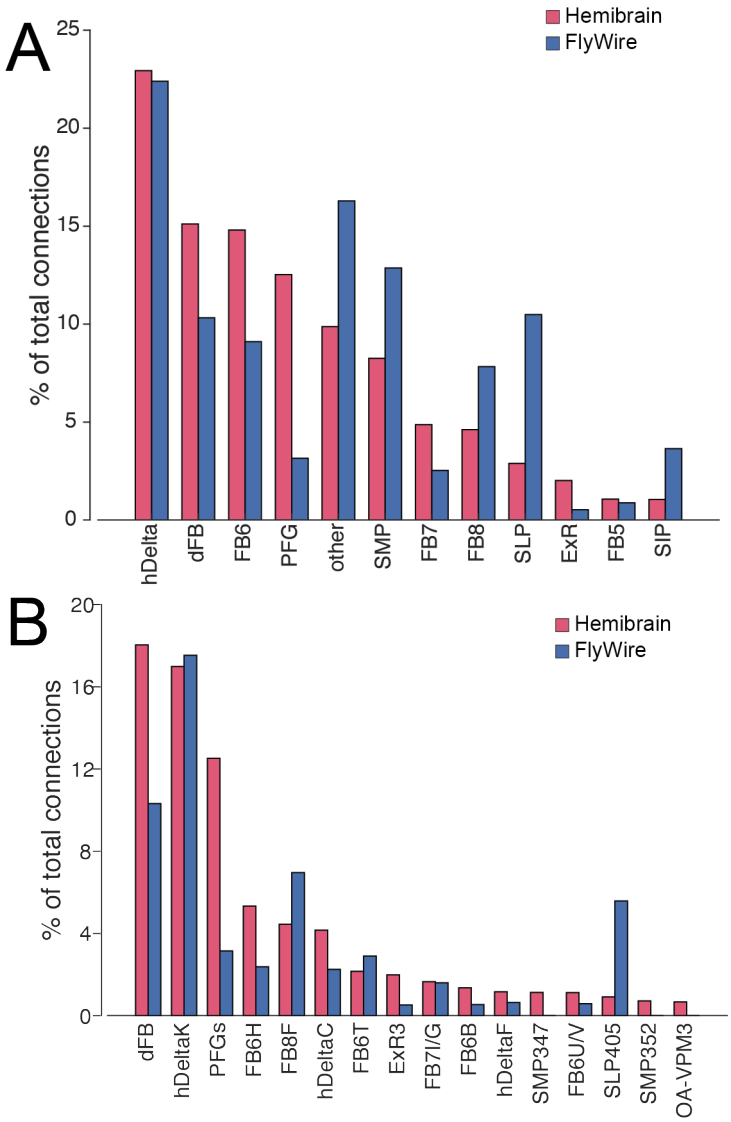

Figure 3.3: Presynaptic connections of dFBNs compared between the hemibrain and FlyWire dataset. A) Connections grouped by cell type families. B) Strongest presynaptic connections, comparison of individual cell types. Cell types that cannot be identified exactly between datasets have been summarized. Data is plotted as % of total connections of dFBNs in the respective dataset.

FB6I merged into CB.FB6E3), some HB cell types had to be split into several FW cell types (e.g. FB7A split into CB.FB7AE1 and CB.FB7E2, the latter also contains other HB cell types) and some remained their own cell type, simply with a new name (FB6Z was renamed CB.FB6E1) [173]. In summary, the dFBNs in the FW dataset were (number of neurons in brackets): CB.FB6E1 (2), CB.FB6E3 (7), CB.FB6E4 (10), CB.FB7E1 (7), CB.FB7E2 (11). It is noteworthy that two HB cell types were included in this allocation that used to be separated in the HB dataset (namely FB6D and FB7B).

Presynaptic connections of dFBNs could be detected from 271 cell types (Fig. 3.3), which was roughly 50 cell types more than in the HB dataset. Grouping the connections in cell type families showed that the strongest input in both datasets came from hDelta neurons, representing the same proportions in both datasets (Fig. 3.3A). Apart from this, almost all other identified cell type families showed clear differences between the datasets. The FW data suggested weaker inputs in the FB area, by dFBNs, FB6 neurons, PFGs and FB7 neurons (Fig. 3.3A). Stronger inputs were identified in the SP region where connection strength seemed to be doubled to almost 27% in FW compared to the 13% in the HB data (Fig. 3.3). Also inputs in FB layer 8 were increased in the FW dataset (Fig. 3.3A).

At the level of individual cell types, one of the biggest differences laid in the connection strength of PFG neurons: the FW data suggested only roughly one fourth of connection strength, namely 3.2% instead of 12.5% in the HB data (Fig. 3.3B). Also, connections from dFBNs and FB6H were reduced by almost half. Stronger connected cell types were FB8F and SLP405, for example (Fig. 3.3). A few cell types had shown connectivity in the HB data, did not present any connections in the FW data: SMP347, SMP352 and OA-VPM3 neurons showed connections between 0.6-1.1% in HB, but no connections in FW.

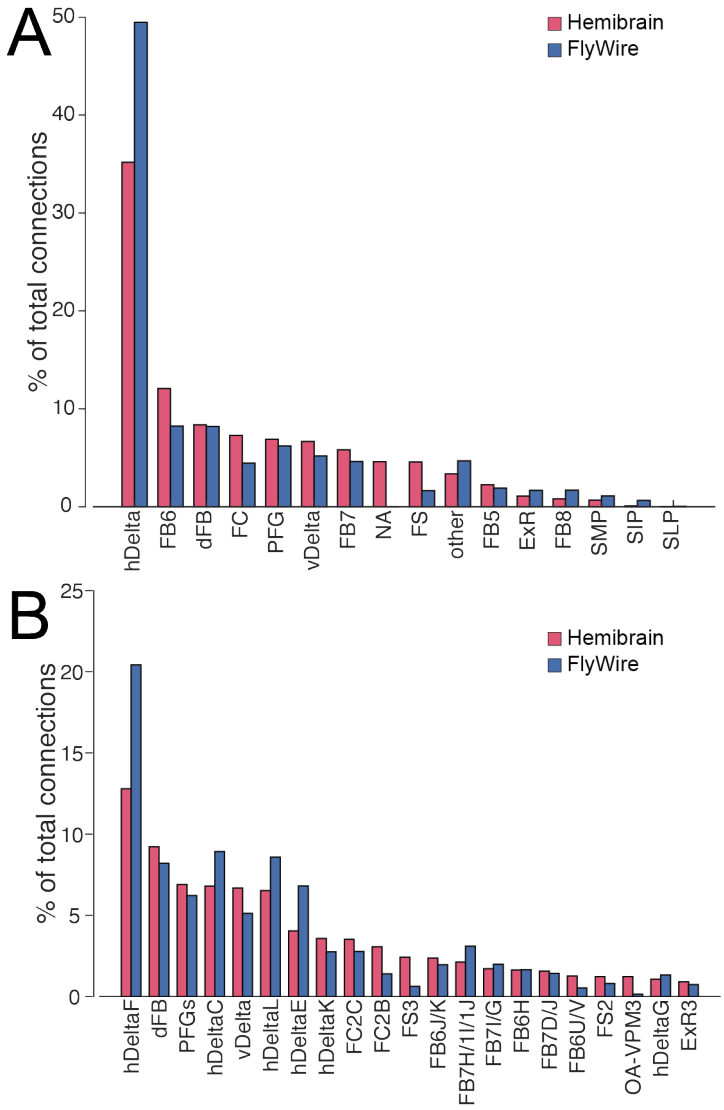

Figure 3.4: Postsynaptic connections of dFBNs compared between the hemibrain and FlyWire dataset. A) Connections grouped by cell type families. B) Strongest postsynaptic connections, comparison of individual cell types. Cell types that cannot be identified exactly between datasets have been summarized. Data is plotted as % of total connections of dFBNs in the respective dataset.

Comparing the postsynaptic connections between datasets revealed fewer differences than the presynaptic connections (Fig. 3.4A). The absolute number of postsynaptic cell types were almost identical, with 166 cell types in FW and 172 in HB. A major increase in connection strength in the FW dataset could be found in the connection to hDelta neurons. Here, the percentage of connections increased from an already high connection strength of 35.2% to almost 50% (Fig. 3.4A). In turn, most other connections were slightly reduced.

In the HB dataset, hDeltaF was already the strongest connection with almost 13%, but the FW data suggests the connection could be even stronger and make up more than 20% of output synapses (Fig. 3.4B). Also the connections to most other hDelta neurons were stronger in the FW dataset, suggesting more interconnectivity in the FB. On the other hand, several of the connections that signal outside of the FB were reduced: FC2C, FC2B, FS3 and FS2 were all lower in FW, with FC2B reducing their connections by 50% (3% versus 1.4%) and FS3 even reducing down to one fourth (2.4% in the HB versus 0.6% in FW).

Again, the connection to OA-VPM3 presented a big difference: while in HB it had more than 1000 postsynaptic contacts, in the FlyWire dataset there were only 65 output synapses (1.23 vs. 0.14%).

It should be emphasized that it is not yet known where these differences come from, whether they are based in biological differences or if at least some of these differences are also due to technical or annotation differences.

3.3 Discussion

The connectome offers a fantastic resource to understand, map and study neural circuits in the fly brain. In this chapter, I showed that dFBNs connect upstream and downstream to a vast number of neurons, with connection strengths varying between a few very strong connections and many rather weak connections (Fig. 3.1, fig. 3.2). This alone shows the strength and weakness of the connectome at the same time: the data that can be extracted is extensive, but finding and focussing on the relevant connections can be difficult. A main finding is that dFBNs receive input at two distinct anatomical locations: the SP and the FB (Fig. 3.1B). This contradicts the previously held belief that the inputs would be only at the dendritic tufts in the SP region [129], but is supported by the findings that pre- and postsynaptic sites are often located in the same neurites [43].

3.3.1 Not all known inputs to dFBNs can be verified via the connectome

Several sleep- or wake-promoting connections to and from dFBNs have been suggested in previous studies. Surprisingly not all of them can be verified with the connectome and therefore likely represent indirect connections. First, it was shown that dFBNs are bidirectionally connected to R5 neurons [91], although the connection from R5 to dFBNs is likely indirect [130]. Their likely connection is via ExR1/helicon cells [91, 129] which do connect to dFBNs, even though not strongly. Further there is a serotonergic input [135] that might stem from ExR3 neurons or from FB6H, as both neurons have been predicted to express serotonin [55, 174]. Interestingly, only one neuron in dFBNs seems to express 5-HT2B, the sleep promoting serotonin receptor [135]. Further neurons that have been suggested to be upstream of dFBNs are circadian pacemaker neurons, namely

LPN and SLP neurons [179]. While LPN neurons had been shown to be in anatomical proximity [179], they do not appear in the connectome as direct inputs, suggesting that the functional experiments performed in that study detect an indirect connection, rather than a monosynaptic one. Interestingly, these two groups of neurons were found because of their overlap with an AstA-GAL4 line. Recent evidence suggests that hDeltaK neurons, the strongest input to dFBNs, express AstA [55]. Potential off-target expression of their split-GAL4 approach that might unknowingly label hDeltaK neurons as well, might have led to the observed connectivity [179]. PI neurons have been suggested to be coupled to dFBNs via gap junctions [137]. Unfortunately, the resolution of the EM does not allow for detection of electrical synapses, hence this connection cannot be verified with the present dataset [138]. Last, dopamine has been shown to hyperpolarize dFBNs and act as a strong wake-promoting signal [128, 132, 179]. This signal likely stems from a single PPL1 neuron [147] that is identified as FB6H in the hemibrain [44]. This connection could be verified by the connectome, while future work will need to prove that FB6H actually expresses dopamine as NT, and not just on RNA levels [55]. Interestingly, recent work could only detect the dopaminergic input onto dFBNs in the SP region, and not in the FB [132]. FB6H neurons are expected to overlap with dFBNs in the SP and the FB, so either these neurons only release dopamine onto dFBNs in the SP, or there is a second dopaminergic input in the SP region.

3.3.2 Known synaptic outputs of dFBNs are present in the connectome

Known downstream partners of dFBNs are helicon cells [129], octopaminergic cells [179, 180] and dopaminergic cells [132]. The connection to helicon cells can be confirmed with the connectome data, but the connection is weak and makes up only 0.15% of total connections

in the HB dataset or 0.93% in the FW data [129]. This suggests that connection strength does not necessary imply importance of a connection, a topic we will revisit in chapter 7. Further, it was shown that dFBNs inhibit arousal-promoting octopamine neurons, which might likely be explained by the connection of dFBNs to OA-VPM3 [179, 180]. Surprisingly, this connection differed a lot between the two datasets, where the connection was almost negligible in the FW dataset, but well maintained in the HB data. VPM3 neurons only have one neuron per hemisphere, with their neurites spanning several different areas of the brain, and their cell bodies located in the subesophageal ganglion (SG) [181]. The SG is not covered by the hemibrain, which might have led to different attribution of the detected neurites. Last, recently feedback inhibition from dFBNs onto their dopaminergic input was shown [132]. This could likely be represented by the connection of dFBNs onto FB6H neurons that might form the dopaminergic input to dFBNs, as discussed above.

It is important to consider that dFBNs were treated as one homogeneous group of neurons for the data presented here. This approach is simplistic, and overlooks the differences that the individual subtypes of dFBNs might have.

3.3.3 Sensory inputs arrive in the SP

A lot of inputs target dFBNs in the superior protocerebrum. It is hard to pinpoint functions to single neurons here, as very little information is know, and the definition of these neuronal subtypes have only started with the preparation of the first connectome [43, 44]. The SP mainly acts as a relay hub, receiving different sensory information and transmitting it further onto FB neurons, amongst others [182–186]. The mushroom body, the neuropil for learning and memory, as well as the lateral horn, which is involved in innate olfactory behaviour, provide input to the SP, which suggested a role for the SP as

a higher order olfactory processing node [182–184, 187]. The SLP further receives input from taste projection neurons as well as sweet tasting neurons from the leg [186, 188]. The SMP receives sweet tasting projections, but not from the leg, as well as projections that induce water seeking [183–186].

One of the SLP neurons presents an interesting case in the comparison between datasets: In the FlyWire dataset SLP405 presents the second strongest input to dFBNs, while the connection is much weaker in the HB data. SLP405 comprises a group of 37 neurons, predicted to be cholinergic [42, 45, 174], and might indicate the importance of the inputs from the SP to the dFBNs. Also visual information seems to be conveyed here: MBON19 encodes visual information and transmits it onto SMP347 and SMP349, both of which project onto dFBNs [189]. Overall, SP input in general might provide dFBNs with different modalities of sensory information. On the other hand, the inputs in the FB area of dFBNs stem mainly from hDelta neurons, such as hDeltaK. These neurons have been implied in sleep loss following social isolation [148], as well as olfactory navigation [124, 190, 191]. How these different kinds of inputs interact will need further investigation.

While synaptic connections can now easily be mapped computationally, they need to be studied *in vivo* to determine their importance in the organism. The following chapters will focus on the behavioural effects of some of the neurons mentioned here, as well as their functional connectivity to dFBNs.

4 | Behavioural screen of neurons connected to dFBNs

4.1 Introduction

Following on the previous chapter, here the theoretical knowledge was transferred onto a functional level and the influence on the sleep behaviour of the connected neurons was studied. While dFBNs have been shown to regulate sleep [126, 128, 129], it remains unclear whether the connected neurons also regulate aspects of sleep, or encode different information. A common approach to detect neurons involved in the regulation of sleep is to perform a behavioural screen, using thermogenetic activation of TrpA1 of different neuronal GAL4 drivers and detect resulting changes in sleep phenotypes [55, 130]. TrpA1 is a cation channel that can be expressed in the neuronal population of interest by using the GAL4/UAS system [192]. The channel changes its conformation with differences in temperature. Increasing the environmental temperatures above 25 °C will open the ion channel, making it permeable to cations, and induce action potential firing in the neurons of interest [192]. At lower temperatures the ion channel will remain closed and neural activity will remain unchanged [192]. Thermogenetic activation of neurons therefore allows precise temporal and spatial control of neuronal depolarization, and allows researchers to compare natural sleep behaviour with sleep behaviour during neuronal activation.

Using this approach, I performed a thermogenetic screen, using a wide range of GAL4 drivers that cover different neurons connected to dFBNs. This screen identified several hits that changed their sleep behaviour upon activation. These GAL4 lines were analysed further, and I could verify their overlap with dFBNs. Last, I studied the functional connections from dFBNs to the downstream neurons by patch-clamp electrophysiology,

where I was able to detect a monosynaptic connection.

4.2 Results

4.2.1 Sleep behavioural screens identify several neurons of interest

4.2.1.1 Neuronal activation alters sleep in multiple genotypes

Using virtual fly brain [193, 194] and NeuronBridge [195], 24 different GAL4 lines were chosen for a thermogenetic screen, based on their overlap with neurons connected to dFBNs from the connectome analysis in chapter 3. The different GAL4 lines used here target 11 different cell groups: pontine neurons in the FB (hDelta and vDelta neurons), ExR3 and ExR1 neurons, neurons in the bulb, octopaminergic neurons (VPM3), SMP neurons, FC2 neurons, 5-HTPMPD01 neurons and FB6N neurons (Fig. 4.1).

All these lines were tested and analysed for changes in total sleep during the activation day and on the day after heat activation, the so-called rebound day (Fig. 4.1A). Changes in sleep were analysed and compared to the change in sleep in the empty GAL4 control. Neuronal activation induced significant increases or decreases in sleep with nine GAL4 lines (Fig. 4.1B). Importantly, activating different neurons in the same subgroup did not consistently elicit the same response. Strong reductions in sleep could be detected in four lines: R56E07-GAL4, R24B11-GAL4, R83H09-GAL4 and R46C02-GAL4 (Fig. 4.1B). Both lines targeting the octopaminergic neuron VPM3 induced a minor reduction in sleep upon activation (Fig. 4.1B). R24A05-GAL4 and R22H10-GAL4, targeting ExR3 and ExR1 neurons respectively, and the R23E10-GAL4 line significantly increased sleep when activated (Fig. 4.1B). These three lines also showed increased activity accompanying their increase in sleep (supplemental figure S1). Apart from that, only R45F08-GAL4 showed

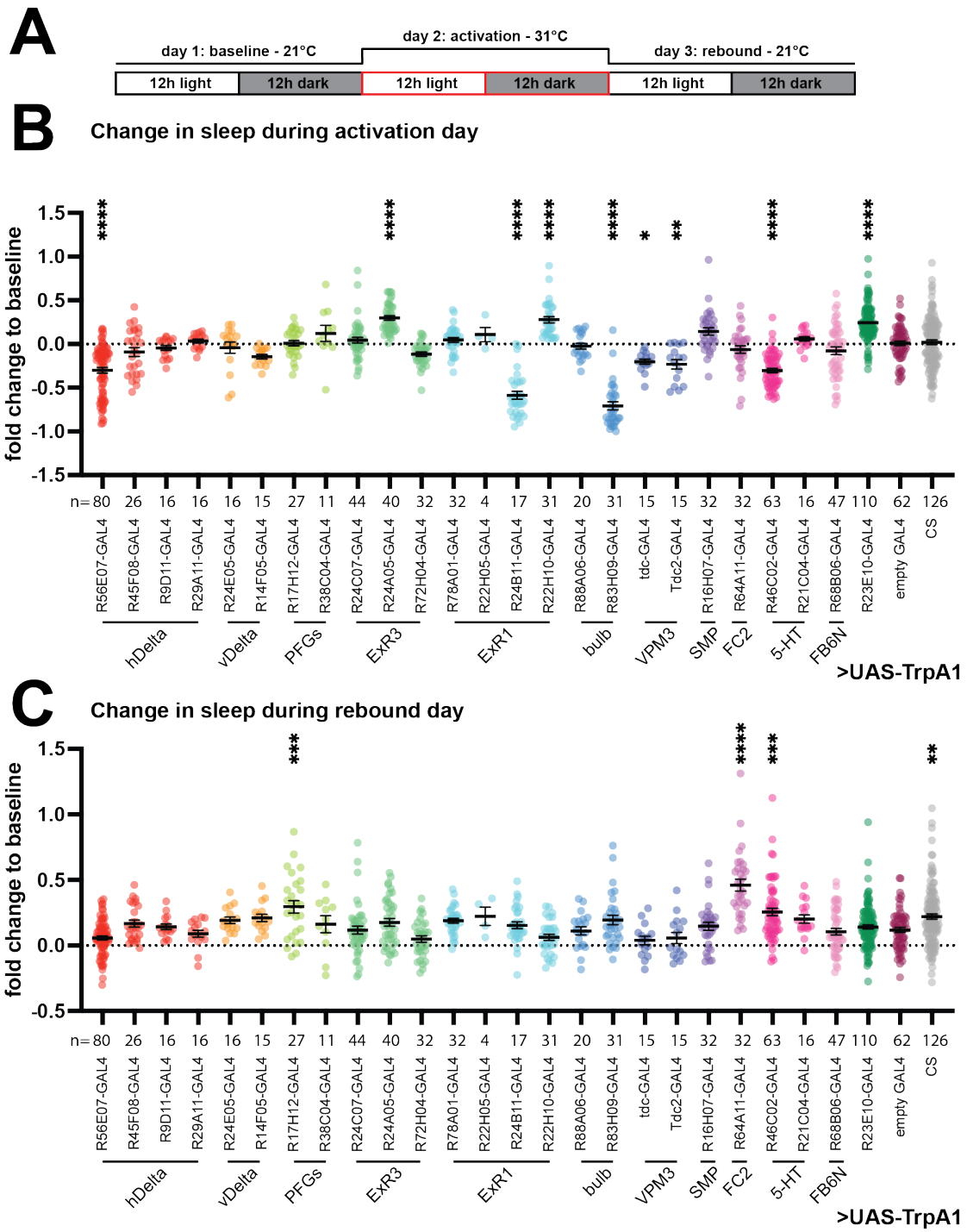

Figure 4.1: Thermogenetic screen of 24 GAL4 lines reveals several lines that increase and decrease sleep. A) Schematic description of the experimental setup: baseline sleep was measured at 21 °C, followed by an activation day at 31 °C and a recovery day, again at 21 °C, all with a 12h light/12h dark cycle. B) Change in total sleep during neuronal activation of 24 GAL4 lines targeting 11 groups of cell types. (Caption continued on next page)

Figure 4.1: (Continued from previous page.) C) Change in total sleep during 24h of the recovery day. Fold change in sleep compared to baseline day is plotted. Significance was compared to the empty GAL4 control group and calculated by one way ANOVA with Holm-Šídák. Stars indicate significance as follows: **** = $p < 0.0001$, *** = $p < 0.001$, ** = $p < 0.01$, * = $p < 0.05$, ns = $p > 0.05$. Individual dots represent single flies, bars represent mean ± SEM.

a strong increase in movement, which did not seem to affect the flies' sleep behaviour (supplemental figure S1, fig. 4.1B). None of the remaining 15 lines showed differences in their sleep behaviour nor their activity levels (Fig. 4.1B, supplemental figure S1).

Notably, on day three of the experiment, all genotypes showed a slight increase in sleep compared to the baseline day (Fig. 4.1C). A few lines stood out due to their significant increase in sleep on this day, compared to the empty GAL4 control: R17H12-GAL4, R64A11-GAL4 and R46C02-GAL4. Also the parental control with an undriven UAS-TrpA1 transgene showed a significant increase in sleep compared to the empty GAL4 (Fig. 4.1C).

4.2.1.2 Neuronal inhibition alters sleep in multiple genotypes

While neuronal activation can give an insight into what information neurons transmit while depolarized, inhibiting these neurons can show if they are necessary for that behaviour. Neurons can be inhibited by expression of Kir2.1 [196, 197]. This inward rectifying K^+-channel hyperpolarises the resting membrane potential and inhibits spontaneous action potential firing [197]. To prevent developmental effects that might confound the behavioural phenotype, transgene expression was inhibited with $GAL80^{ts}$. This protein acts as genetic repressor of GAL4 expression and therefore prevents expression of any UAS transgenes below a restrictive temperature [198, 199]. Flies carrying the $GAL80^{ts}$ and UAS-Kir2.1 transgenes were crossed to different GAL4 lines, raised at 18 °C and collected

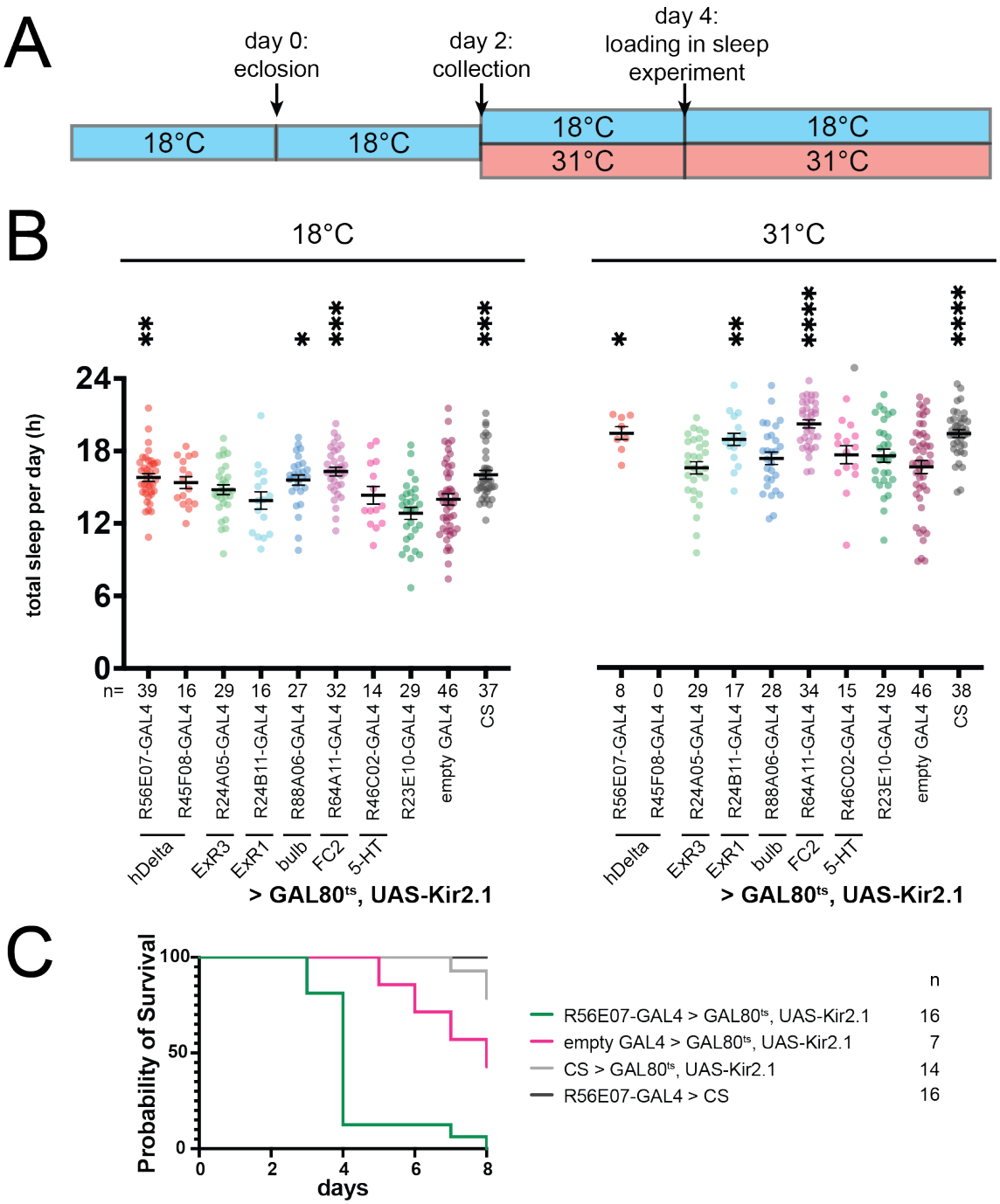

Figure 4.2: Kir2.1-inhibition screen reveals several lines that increase sleep when inhibited. A) Flies were raised at 18 °C, collected on day 2 after eclosion and subsequently housed at 18 °C and 31 °C to remove GAL80 inhibition in one group. After 2 days, flies were loaded into sleep monitors and activity was recorded at 18 °C and 31 °C. B) Total sleep in *GAL4 > UAS-Kir2.1, GAL80^{ts}* flies at 18 and 31 °C. Colour coding as in figure 4.1. (Caption continued on next page)

Figure 4.2: (Continued from previous page.) Significance was compared to the empty GAL4 control group and calculated by one way ANOVA with Holm-Šídák. Stars indicate significance as follows: **** = $p < 0.0001$, *** = $p < 0.001$, ** = $p < 0.01$, * = $p < 0.05$, ns = $p > 0.05$. Individual dots represent single flies, bars represent mean ± SEM. C) Survival plot at 31 °C for *R56E07-GAL4 > GAL80^{ts}, UAS-Kir2.1* flies and parental controls.

two days after eclosion. Flies were subsequently housed at either 18 °C, where GAL80 repressed GAL4, and at 31 °C, which removed the GAL80 block and therefore allowed Kir2.1 expression in the cells of interest (Fig. 4.2A).

The amount of total sleep was compared between the experimental group and the empty-GAL4 control. Already at 18 °C a difference between several groups and the control group could be detected: R56E07-GAL4, R88A06-GAL4 and R64A11-GAL4 showed an increase in sleep compared to the empty GAL4 group (Fig. 4.2B), potentially due to incomplete suppression via GAL80^{ts} [65]. Interestingly also the parental control that carried the transgenes but no GAL4 showed a significant increase in sleep. When flies were housed at temperatures that remove the GAL80^{ts} block, here 31 °C, an increase in sleep could be detected in the same groups, plus the R45F08-GAL4 and R24B11-GAL4 (Fig. 4.2B). Strikingly, two genotypes appeared very unhealthy when Kir2.1 expression was driven: R56E07-GAL4 and R45F08-GAL4 expressing flies housed at 31 °C were mostly dead by the time the experiment finished. In the case of R56E07-GAL4, 27 out of 35 flies died during the experiment, which left only eight flies to be analysed. For R45F08-GAL4, no flies survived the full length of the experiment (Fig. 4.2B). To see if this was reproducible, a separate experiment was conducted where flies were loaded into sleep monitors without having been accustomed to 31 °C beforehand. The flies were analysed for their survival in the following days, and the experiment was stopped after eight days. Almost all flies that expressed Kir2.1 in R56E07-GAL4 died during the experiment, while

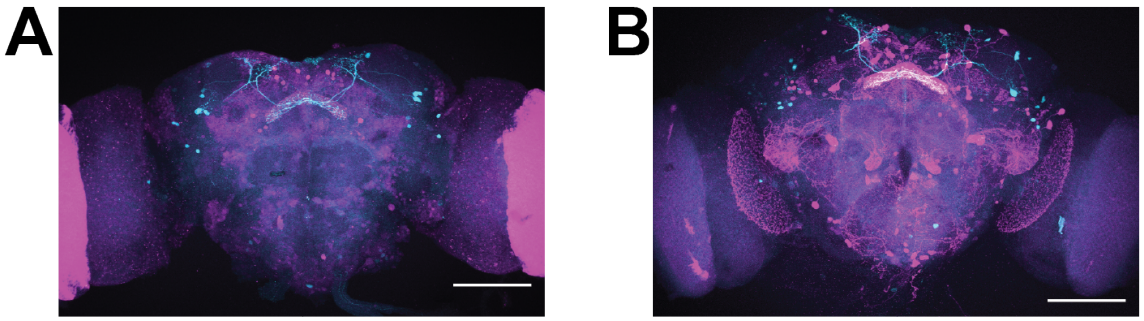

Figure 4.3: Expression pattern of R56E07-GAL4 and R24A05-GAL4. A) Maximum intensity projection of the confocal image of the whole brain of *R56E07-GAL4 > UAS-tdTomato* (magenta) *R23E10-LexA > LexAop-GFP* (cyan) flies. B) Confocal image of *R24A05-GAL4 > UAS-tdTomato* (magenta) *R23E10-LexA > LexAop-GFP* (cyan) flies. Scale bars: 100 μm.

control flies survived (Fig. 4.2C).

From this screen, R56E07-GAL4 and R24A05-GAL4 were selected for further evaluation, based on two main reasons: first and foremost, they were chosen based on their strong and reliable decrease and increase in sleep. And second, these drivers were especially interesting because of the cell types they target. R56E07-GAL4 targets columnar neurons in the fan-shaped body, and has a restricted expression pattern, reducing off-target effects (Fig. 4.3A). R24A05-GAL4 on the other hand is predicted to target ExR3, a neuron that receives inputs in the EB and therefore connects the two brain regions, but it also labels several other cells (Fig. 4.3B).

4.2.2 Anatomical analysis verifies overlap with dFBNs

To verify the overlap of the GAL4 lines with connections to dFBNs, morphologic analyses were performed. First, the anatomical proximity and potential synaptic connectivity to dFBNs was studied. This was analysed by green fluorescent protein (GFP) reconstitution across synaptic partners (GRASP) [84], whereby one part of a split GFP was expressed by a GAL4 driver of interest, in our case R23E10-GAL4, R22H10-GAL4, R24A05-GAL4 and

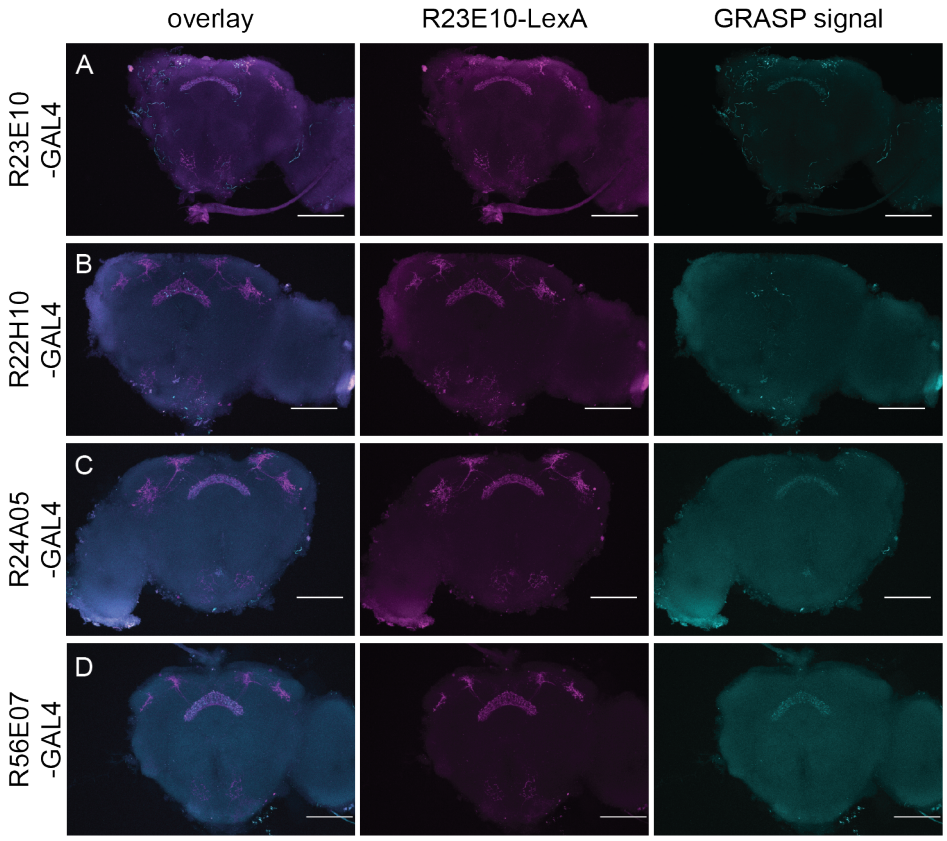

Figure 4.4: GRASP staining reveales close proximity between dFBNs and potential connections. A) GRASP signal (cyan) revealed close proximity between R23E10-GAL4 and R23E10-LexA (magenta) labelled neurons mainly in the FB and the SP. B) GRASP signal (cyan) revealed close proximity between R22H10-GAL4 and R23E10-LexA (magenta) labelled neurons only sparsely in the FB. C) GRASP signal (cyan) revealed close proximity between R24A05-GAL4 and R23E10-LexA (magenta) labelled neurons weakly in the FB and SP. Gain was increased to 250% to detect signal. D) GRASP signal (cyan) revealed close proximity between R56E07-GAL4 and R23E10-LexA (magenta) labelled neurons weakly in the FB. Gain was increased to 250% to detect signal. Scale bar: 100 μm.

R56E07-GAL4, and the second part of the split GFP was expressed by a LexA driver, in our case R23E10-LexA [200] (Fig. 4.4). A GRASP signal could be detected where neurons of R23E10-LexA and the GAL4 driver were close enough to each other for their split GFP to reconstitute and form a functional GFP unit. As this approach was not directed, it could not be concluded which neurons were pre- or postsynaptic.

R23E10-GAL4 was used as a positive control. Here, a GRASP signal could be detected in the FB as well as in the superior protocerebrum (Fig. 4.4A). Helicon cells, labelled by

R22H10-GAL4, have known functional connections to dFBNs [129] and this driver line was therefore used as a proof of principle for the system. Here, several dots in the FB could be detected, proving that the neurons were sparsely connected (Fig. 4.4B). Analysing brains with split GFP expression in R24A05-GAL4 revealed a signal in the FB, and a sparse signal in the SP (Fig. 4.4C). Last, neurons expressing split GFP in R56E07-GAL4 revealed a GRASP signal in the FB only (Fig. 4.4D). Overall, the two lines are in close proximity of dFBNs, suggesting a potential synaptic connection.

To better understand the functional anatomy of these neurons, the dendritic marker DenMark was expressed in these neurons as well as synaptotagmin::GFP, which labelled presynaptic vesicles [201]. Here, dendrites were labelled with mCherry and presynapses with GFP, which would help to visualize where the neurons receive synaptic input, and where they target postsynaptic partners. The R56E07-GAL4 line exhibited dendritic arborisations predominantly in the EB and FB, while the synaptic output was located to the neurites within the FB (Fig. 4.5A), suggesting that these neurons receive input in the EB and transmit information to the FB. R24A05-GAL4 on the other hand revealed dendritic regions in the FB, but also in many other regions, underlining the broad expression pattern of this line (Fig. 4.5B). Synaptic vesicles were primarily located in the FB and the optic lobe (Fig. 4.5B). Overall, the R24A05-GAL4 line's expression pattern proved to be too broad to map the behavioural effects to specific neurons. For this reason, the remainder of this chapter focuses on the neurons labelled by the R56E07-GAL4 line.

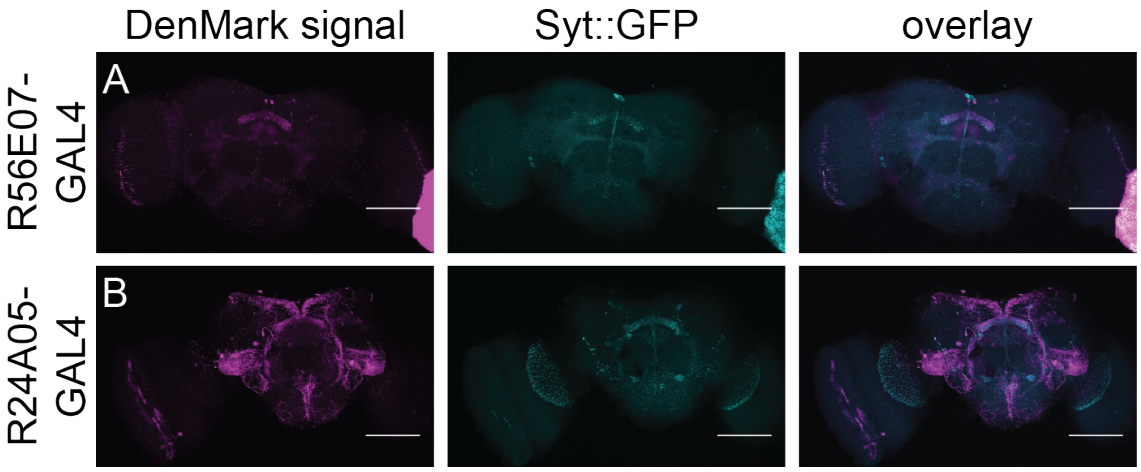

Figure 4.5: R56E07-GAL4 and R24A05-GAL4 have the majority of their synaptic vesicles in the FB. Staining against the dendritic marker DenMark (magenta) and the synaptic vesicle marker synaptotagmin (Syt, in cyan) in A) R56E07-GAL4 neurons and B) R24A05-GAL4 neurons. Scale bars represent 100 μm.

4.2.3 Testing functional connectivity between R56E07-GAL4 and dFBNs reveals monosynaptic connection

Anatomical proximity is necessary but not conclusive for synaptic connectivity. The previous results hinted at a connection between R56E07-GAL4 neurons and dFBNs, but further proof was needed that they actually form synapses between the neurons. Functional connectivity can be proven by optogenetically activating one group of neurons while simultaneously recording the neuronal response in the potential downstream neurons. Adding tetrodotoxin (TTX) isolates monosynaptic connections [93]: as TTX blocks sodium channels, no action potentials (AP) can be generated. Hence, optogenetic activation will depolarize a neuron, lead to synaptic release and the response can be measured on the monosynaptically connected downstream neurons. If connections are polysynaptic, the intermediate neuron cannot generate APs, hence the signal cannot be transmitted further.

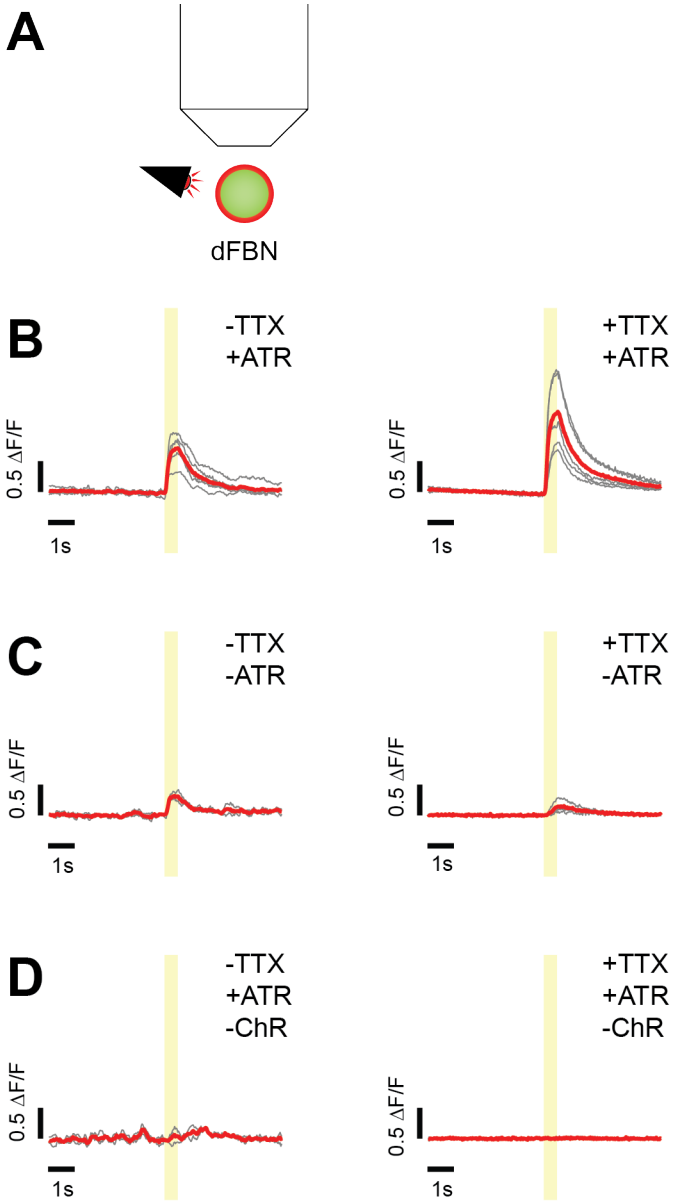

Figure 4.6: Optogenetic activation of dFBNs leads to in increase in GCaMP7f signal. A) Recordings were performed from dFBNs expressing GCaMP7f and CsChrimson during light stimulation. B) Calcium imaging traces of *R23E10-GAL4 > UAS-GCaMP7f, R23E10-LexA > LexAop-CsChrimson*. Flies were fed with ATR. n = 5 flies. C) Calcium imaging traces of *R23E10-GAL4 > UAS-GCaMP7f, R23E10-LexA > LexAop-CsChrimson*. Flies were not fed with ATR. n = 3 flies. D) Calcium imaging traces of *R23E10-GAL4 > UAS-GCaMP7f*. Flies were fed with ATR. n = 3 flies. 500 ms of light stimulation is represented by yellow shading. Grey traces indicate mean of 5 light pulses per fly. Red traces indicate mean of all flies of the same condition. ChR = CsChrimson.

4.2.3.1 Calcium imaging reveals connection between neurons

The first approach to record synaptic responses was by 2-photon imaging of GCaMP7f activity in the downstream neurons [202]. Changes in fluorescence equate to the changes of calcium levels in the cells, which is commonly used as a readout of neural activity. As a proof of concept, flies were analysed that expressed CsChrimson in dFBNs using the R23E10-LexA driver, and simultaneously expressed GCaMP7f under control of the R23E10-GAL4 driver (Fig. 4.6A) [203]. Light stimulation to activate CsChrimson led to a clear depolarization of the cells (Fig. 4.6B). In *Drosophila* all-*trans* retinal (ATR) needs to be added artificially to the food of the fly for several days before the experiment, to make the opsins light-sensitive [203]. Hence the widely used control of optogenetic experiments in *Drosophila* research is to use the same genotype but not feed the animals with ATR. This shall leave the channel inactive and therefore not induce a depolarization when stimulated with light.

Stimulation of CsChrimson in the absence of supplemented ATR still induced changes in calcium levels that were roughly half the size of the response with ATR (Fig. 4.6C). Adding TTX reduced the response further, but did not completely abolish it (Fig. 4.6C). Therefore, a second negative control was tested, where flies did not express CsChrimson, but were fed with ATR. Here, no response to the light stimulus could be detected (Fig. 4.6D), suggesting that a Chrimson-negative control was a better control than using the same genotype without ATR addition.

To test whether R56E07-GAL4 neurons are indeed connected to dFBNs, GCaMP7f was expressed in these neurons, and changes in calcium were recorded while activating dFBNs (under control of the R2310-LexA driver, fig. 4.7A). Activation of dFBNs elicited an

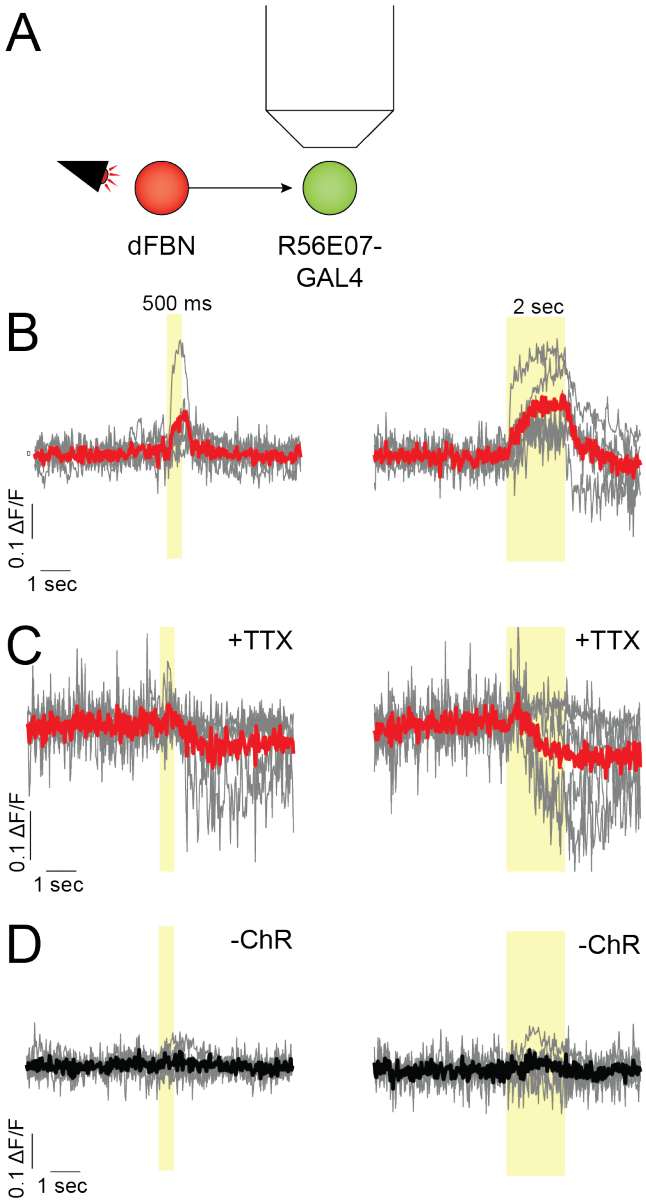

Figure 4.7: Optogenetic activation of dFBNs elicits excitatory response in R56E07-GAL4 neurons when recording calcium activity. A) *R23E10-LexA>LexAop-CsChrimson::tdTomato* neurons were activated with red light, while *R56E07-GAL4>UAS-GCaMP7f* neurons were recorded from. B) GCaMP7f signal in R56E07-GAL4 neurons during 500 ms and 2 sec activation of dFBNs. n = 5 flies. C) GCaMP7f recordings in R56E07-GAL4 neurons during 500 ms and 2 sec activation of dFBNs in the presence of TTX. n = 5 flies. D) Control GCaMP7f recordings in R56E07-GAL4 neurons during 500 ms and 2 sec light stimulation, without Chrimson expression. n = 5 flies. All flies were fed with ATR. Yellow shading indicates light stimulation. Grey traces indicate mean of 5 light pulses per fly. Red traces indicate mean of all flies of the same condition. ChR = CsChrimson.

excitatory response in R56E07-GAL4 neurons (Fig. 4.7B). Addition of TTX removed the excitation almost completely, and potentially uncovered a delayed inhibition (Fig. 4.7C). It needs to be noted that TTX also blocked any action potentials in R56E07-GAL4 neurons, which reduced the potential amplitude of the response in these neurons dramatically. To test if the excitation seen in the first experiment was due to a light artefact, I recorded from the same neurons in flies that did not express CsChrimson. Here, no response was detected during light stimulation (Fig. 4.7D), suggesting that the results obtained were specific for the connection between the two neurons.

4.2.3.2 Optogenetic activation of dFBNs induces a strong depolarization in patch-clamp recordings

As the amplitudes of the responses detected with GCaMP were relatively low, and a potential inhibition was hard to verify, the next experiments were performed instead by recording synaptic responses via patch-clamp electrophysiology. This experiment limited recordings of responses to one neuron at a time, but allowed more options to control and manipulate the neuron.

Recordings were performed from GFP- and CsChrimson-expressing dFBNs *in-vivo* during light stimulation, which should elicit a strong depolarization (Fig. 4.8A). A light pulse led to an immediate depolarization of the stimulated neuron which was not reduced in strength or timing by the addition of TTX (Fig. 4.8B). Next, I recorded from neurons expressing CsChrimson and GFP, but without supplementation of ATR. Recordings from these neurons still elicited a depolarization in response to the light stimulus (Fig. 4.8C). The effect remained visible when TTX was added to the bath (Fig. 4.8C). Overall, this observation was in line with the previous experiment, where the same effect was observed

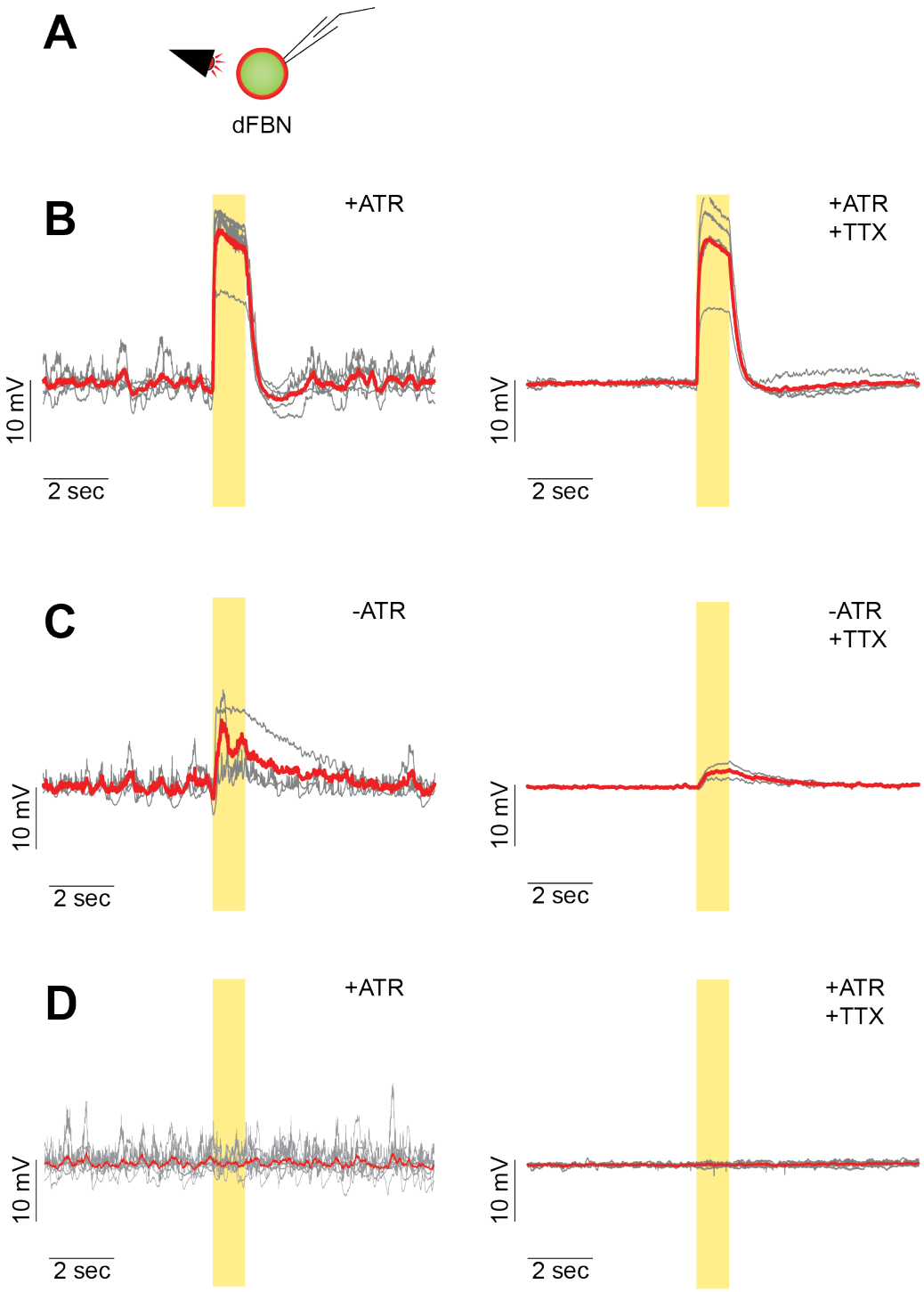

Figure 4.8: Optogenetic stimulation of dFBNs elicits strong depolarization. Full caption on next page.

Figure 4.8: (Continued from previous page.) A) Patch-clamp recordings were performed from *R23E10-LexA>LexAop-CsChrimson::tdTomato, R23E10-GAL4>UAS-mCD8::GFP* neurons during red light stimulation. B) Patch-clamp recordings of dFBNs showed a strong depolarization in response to a light pulse. Flies were fed with ATR. n = 5 cells. Strong depolarization remained consistent, when TTX was added to the bath. n = 4 cells. C) Recordings from dFBNs showed a slight depolarization even when flies were not fed with ATR. n = 3 cells. The depolarization remained present when TTX was added to the bath. n = 2 cells. D) *R23E10-GAL4>UAS-mCD8::GFP; +>LexAop-CsChrimson* expressing neurons with supplemented retinol did not respond to light stimulation. n = 9 cells. Also no response to light when TTX was present. n = 7 cells. Yellow shading indicated red light stimulation of 1 sec. Each grey line represents the mean of one cell. Red line indicates mean of all recordings of the same genotype. One cell per fly was patched.

via calcium imaging (compare figure 4.6). Recording from flies without CsChrimson expression, but with ATR supplementation, led to a much cleaner control: light stimulation did not elicit any detectable changes in membrane voltage of the targeted neuron (Fig. 4.8D).

4.2.3.3 R56E07-GAL4 neurons receive synaptic input from dFBNs

Next, to replicate and verify the results obtained with the GCaMP7f recording, flies were used that expressed CsChrimson under the control of the R23E10-LexA driver, as well as GFP under control of R56E07-GAL4 (Fig. 4.9A). Patch clamp recordings of R56E07-GAL4 neurons revealed that stimulation of dFBNs elicited a clear response in these neurons (Fig. 4.9B). Interestingly, the responses were not homogeneous, but differed strongly between cells, without changing throughout the recording (Fig. 4.9C). Comparing the different responses in detail, 6 out of 7 cells responded to an activation of dFBNs. In the cells that reacted, several different responses could be observed: first, three cells showed an excitatory response to dFBN activation (cell 1, 4 and 5 in fig. 4.9C). Second, two cells responded with an inhibition to the light activation (cell 3 and 7 in fig. 4.9C). And last, one cell responded with a very clear and immediate inhibition, followed by a clear excitation (cell 6 in fig. 4.9C). It needs to be noted that all cells were at different resting membrane

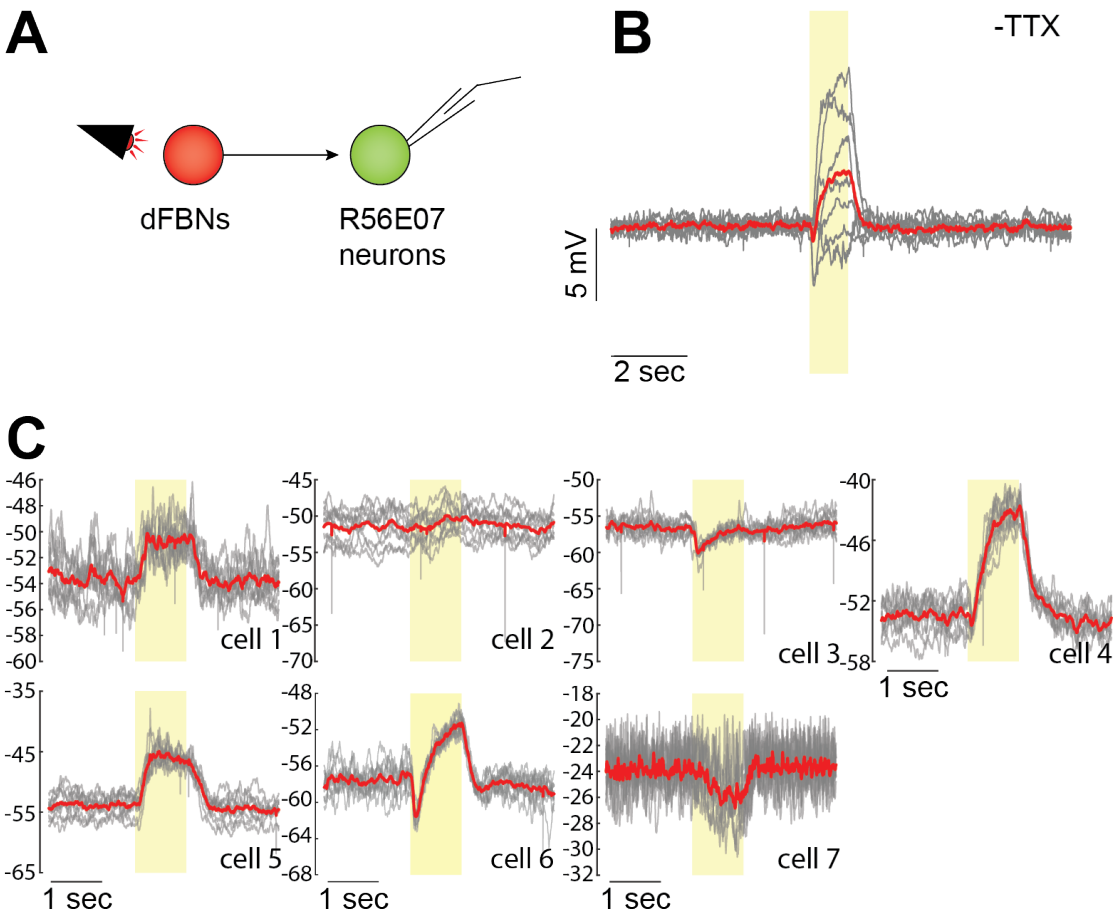

Figure 4.9: Optogenetic stimulation of dFBNs elicits response in R56E07-GAL4 neurons. A) Patch-clamp recordings of *R56E07-GAL4>UAS-mCD8::GFP* neurons during red light stimulation of *R23E10-LexA>LexAop-CsChrimson::tdTomato*. B) Normalized responses from all neurons to the activation of dFBNs showed an excitatory response. Recordings are normalized to the first 4 seconds of each sweep. Mean response of each cell is plotted in grey, with the mean of all responses plotted in red. n = 7 cells. C) Individual cells are plotted, with the 10 repeats of light activation plotted in gray and the mean of these repeats plotted in red. Yellow shading indicates red light stimulation.

potentials (RMP) when the experiments were performed. It could be expected that the RMP affected the response of the cell to the incoming stimulus, but even cells at the same RMP showed opposite responses (e.g. cell 3 and cell 5, fig. 4.9C).

To test whether these changes in membrane voltage were elicited mono- or polysynaptic by dFBNs, TTX was added to the bath of the same cells that had been recorded previously (Fig. 4.10A). Overall, the responses of R56E07-GAL4 neurons to the activation

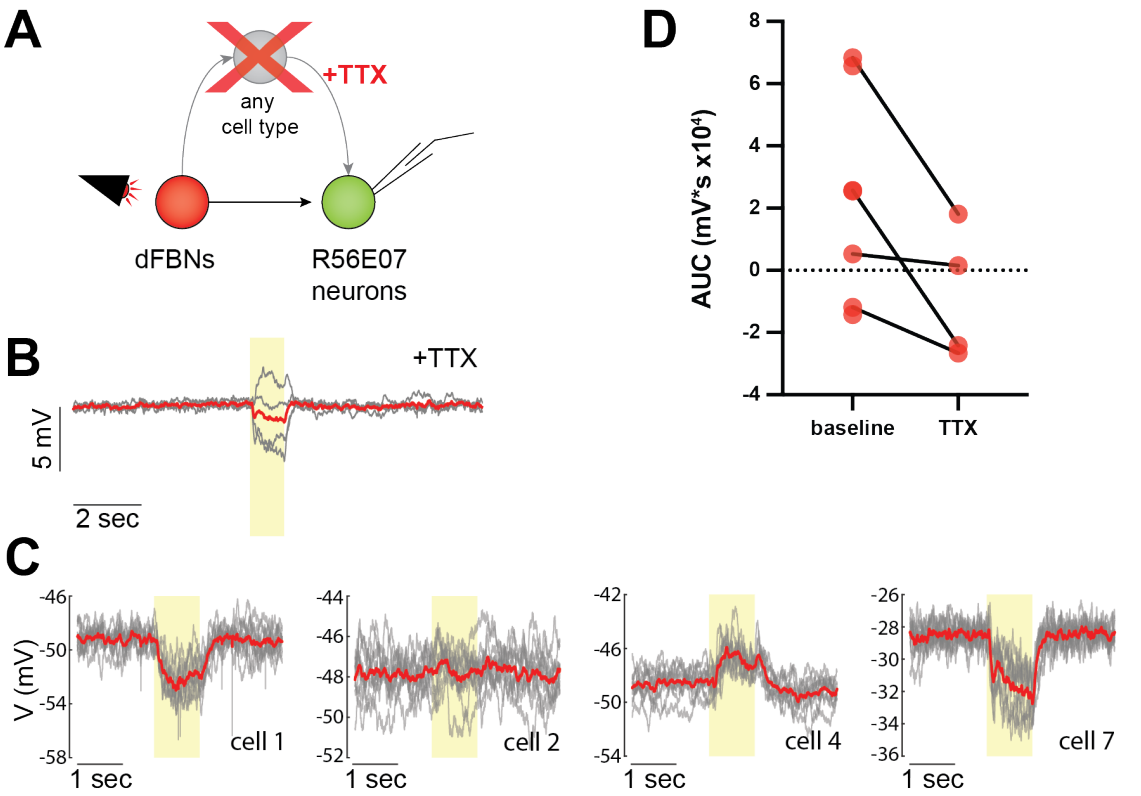

Figure 4.10: Optogenetic stimulation of dFBNs elicits a monosynaptic response in R56E07-GAL4 neurons. A) Patch-clamp recordings of *R56E07-GAL4>UAS-mCD8::GFP* neurons during red light stimulation of *R23E10-LexA>LexAop-CsChrimson::tdTomato* in the presence of TTX to block polysynaptic connections. B) Normalized responses from all neurons recorded with TTX showed an overall small inhibition, following activation of dFBNs. Recordings are normalized to the first 4 seconds of each sweep. Mean response of each cell is plotted in grey, with the mean of all responses plotted in red. n = 4 cells. C) Individual cells are plotted, with the 10 repeats of light activation plotted in grey and the mean of these repeats plotted in red. The 4 cells showed different responses to the activation of dFBNs. Cell labels correspond to the cell labels in figure 4.9C. D) Quantification of the area under the curve of the response in R56E07-GAL4 neurons during the light stimulation of dFBNs revealed an overall downward trend. n baseline = 7 cells, n TTX = 4 cells.

of dFBNs appeared to be mainly inhibitory, which due to the presence of TTX had to be monosynaptic (Fig. 4.10B). Studying individual responses in detail revealed again a heterogeneous response: 3 out of 4 cells responded to the light activation of dFBNs, two with inhibition and one with excitation (Fig. 4.10C). Interestingly, the response in cell 1 changed polarity and became inhibitory in the presence of TTX (compare fig. 4.10C to fig. 4.9C). Quantifying the change of the responses to light, by calculating the area under

the curve during light stimulation, a downward trend could be detected: all connections showed less excitation and more inhibition, but due to the low sample size no statistical significance could be detected (Fig. 4.10D). Overall, this indicates that R56E07-GAL4 neurons are monosynaptically connected downstream of dFBNs, but the nature of the connection needs to be studied further.

4.2.4 Chemogenetic activation of dFBNs via P2X2 induces a strong depolarization

While the downstream population might consist of several cell types that might differ in their response to dFBN activation, a second caveat was studied here: dFBNs themselves are heterogeneous, and the LexA driver does not label the exact same population of neurons as the GAL4 driver line. To resolve this issue, a second approach to test the connectivity between dFBNs and R56E07-GAL4 neurons was used. To label the downstream population, the R56E07-GAL4 driver needed to be used. To now also be able to use R23E10-GAL4 driver to label all dFBNs, a strategy was needed that allowed local activation of neurons, based on their morphological differences. Flies were generated that expressed GFP as well as P2X2, an ATP-gated cation channel [204, 205], so ATP applications could be targeted to the distant neurites of dFBNs, without activating R56E07-GAL4 neurons simultaneously.

ATP was ejected onto the neurites in the SP of dFBNs, while patch-clamp recordings were performed from R23E10-GAL4 labelled cell bodies (Fig. 4.11A). A 50 ms application of ATP onto P2X2-expressing dFBNs elicited a large-amplitude, prolonged depolarization for more than two seconds (Fig. 4.11B). While all recorded neurons depolarized following the application of ATP, the traces did not fully overlap in terms of amplitude and length of

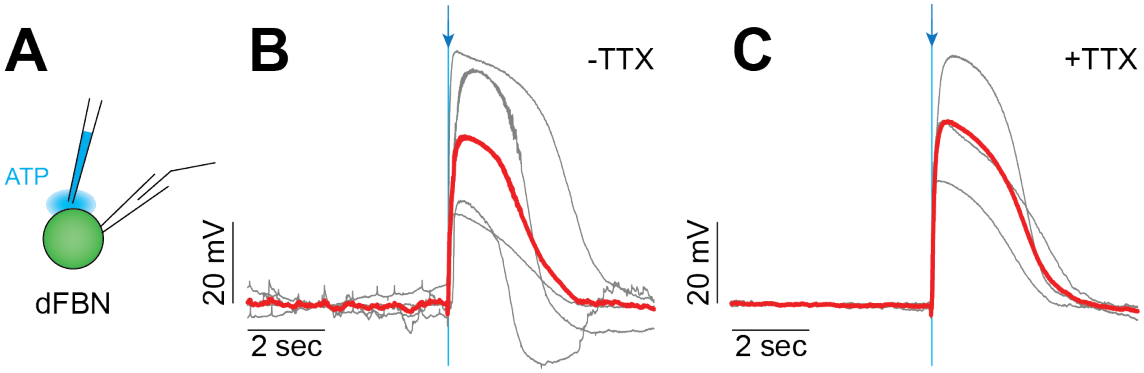

Figure 4.11: ATP applications depolarize P2X2-expressing dFBNs strongly. A) Patch-clamp recordings of *R23E10-GAL4 > UAS-mCD8::GFP, UAS-P2X2* during ATP application. B) Patch-clamp recordings revealed a strong depolarization of the cell membrane after pressure ejection of ATP. n = 4 cells, with 10 repeats of ATP application. C) Addition of TTX did not decrease the response to ATP. n = 3 cells. ATP was applied to the neurites in the SP of dFBNs. ATP application marked by a blue shade and arrow (50 ms). Grey lines indicate mean of single cell, red line indicates mean of all cells.

depolarization (Fig. 4.11B). This was likely due to the ejection pipette placed in different positions in the neurites and thus ATP might have diffused more or less until it reached the target receptors. While TTX blocked action potentials in all neurons, it did not affect the depolarization upon ATP application (Fig. 4.11C). To confirm that ATP applications were locally restricted, test pulses of microejections with a fluorescent dye were applied to the neurites in the SP of dFBNs. Diffusion of the dye was only detected very locally (data not shown).

4.2.4.1 Chemogenetic activation of dFBNs induces response in downstream neurons

Next, the UAS-GFP and UAS-P2X2 transgenes were combined with the R23E10-GAL4 and the R56E07-GAL4 promoter, resulting in flies that expressed GFP and P2X2 in both neuronal groups (Fig. 4.12A). Due to their clear morphological differences, the cells could easily be distinguished. ATP applications were strictly targeted to dFBN neurites, while only cell bodies immediately dorsal of the FB were patched to record from R56E07-GAL4

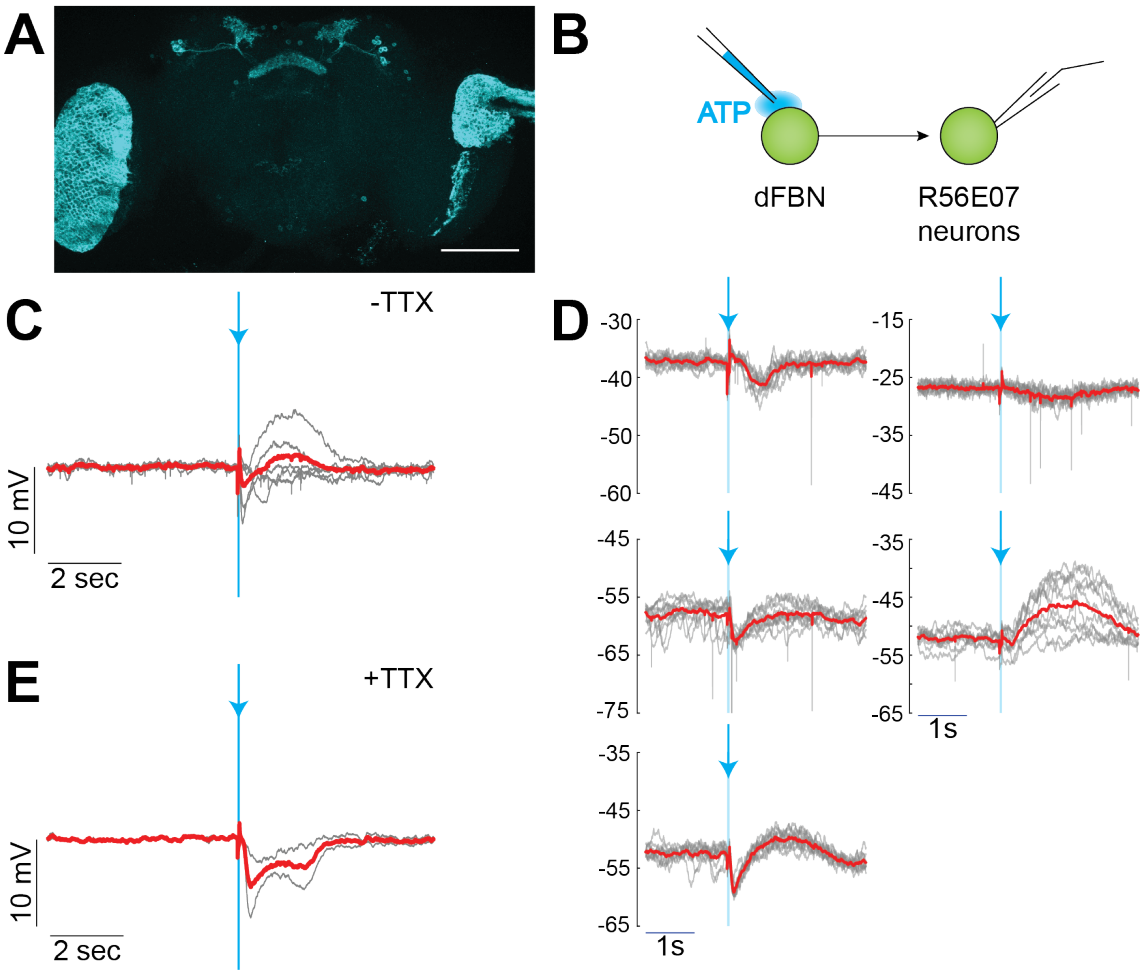

Figure 4.12: Activation of P2X2-expressing dFBNs via ATP-application elicits response in R56E07-GAL4 neurons. A) Whole brain confocal image of a *R56E07-GAL4, R23E10-GAL4 > UAS-mCD8::GFP, UAS-P2X2* animal showed expression in the two groups of neurons. Maximum intensity projection shown. Scale bar = 100 µm. B) Patch-clamp recordings of R56E07-GAL4 neurons in *R23E10-GAL4, R56E07-GAL4 > UAS-mCD8::GFP, UAS-P2X2* flies, while applying ATP to the neurites of dFBNs. C) Recordings of R56E07-GAL4 neurons during the activation of R23E10-GAL4 neurons showed a quick inhibition followed by a prolonged excitation. Traces are normalized to the first 4 seconds of recording. Grey lines indicate mean per cell, red line indicates mean of all cells. n = 5 cells. D) Recordings from individual cells are shown in subplots for easier visualization. Grey lines indicate individual stimuli, red indicates mean per cell. E) Recordings of the same neurons in the presence of TTX showed mainly an inhibitory response. Traces are normalized to the first 4 seconds of recording. Grey lines indicate mean per cell, red line indicates mean of all cells. n = 2 cells. Application of ATP is marked with blue shade (50 ms).

neurons (Fig. 4.12B). As the site of ATP application was distant to the R56E07-GAL4 neurons, diffusion of ATP and subsequent direct activation of R56E07-GAL4 neurons was not expected.

Depolarization of dFBNs with ATP elicited several different responses in R56E07-GAL4 neurons (Fig. 4.12C): cells responded with a quick inhibition and/or a slower prolonged depolarization (Fig. 4.12D). The cells had different RMPs, which was not corrected for. Adding TTX during the recordings revealed a mainly inhibitory connection, but the sample size was too low for a strong conclusion (Fig. 4.12E). Overall, it can be concluded that R56E07-GAL4 neurons receive synaptic input from dFBNs.

4.2.4.2 The function of R56E07-GAL4 neurons upstream of dFBNs

As R56E07-GAL4 neurons almost exclusively have their synaptic output in the FB (Fig. 4.5), it seemed likely that they also project onto dFBNs. To test this, transgenic flies were used that expressed CsChrimson under control of R56E07-GAL4, and GFP under control of R23E10-LexA, which allowed targeted recordings from dFBNs (Fig. 4.13A). Again, these results revealed a mix of different responses and no clear pattern was discernable when studying the mean trace of all recorded cells (Fig. 4.13B). Out of seven recorded cells, two did not respond at all (cell 2 and 5, fig. 4.13C). One cell showed a very clear excitation (cell 6), and two cells showed a clear inhibition (cell 4 and 7, fig. 4.13C). Cell 3 showed an excitation quickly followed by an inhibition and cell 1 showed a very small almost negligible inhibition (Fig. 4.13C). Overall, some, but not all cells responded to the activation of R56E07-neurons.

After adding TTX to discover monosynaptic connections that might be masked by secondary inputs, the pattern remained very similar to what could be seen in baseline

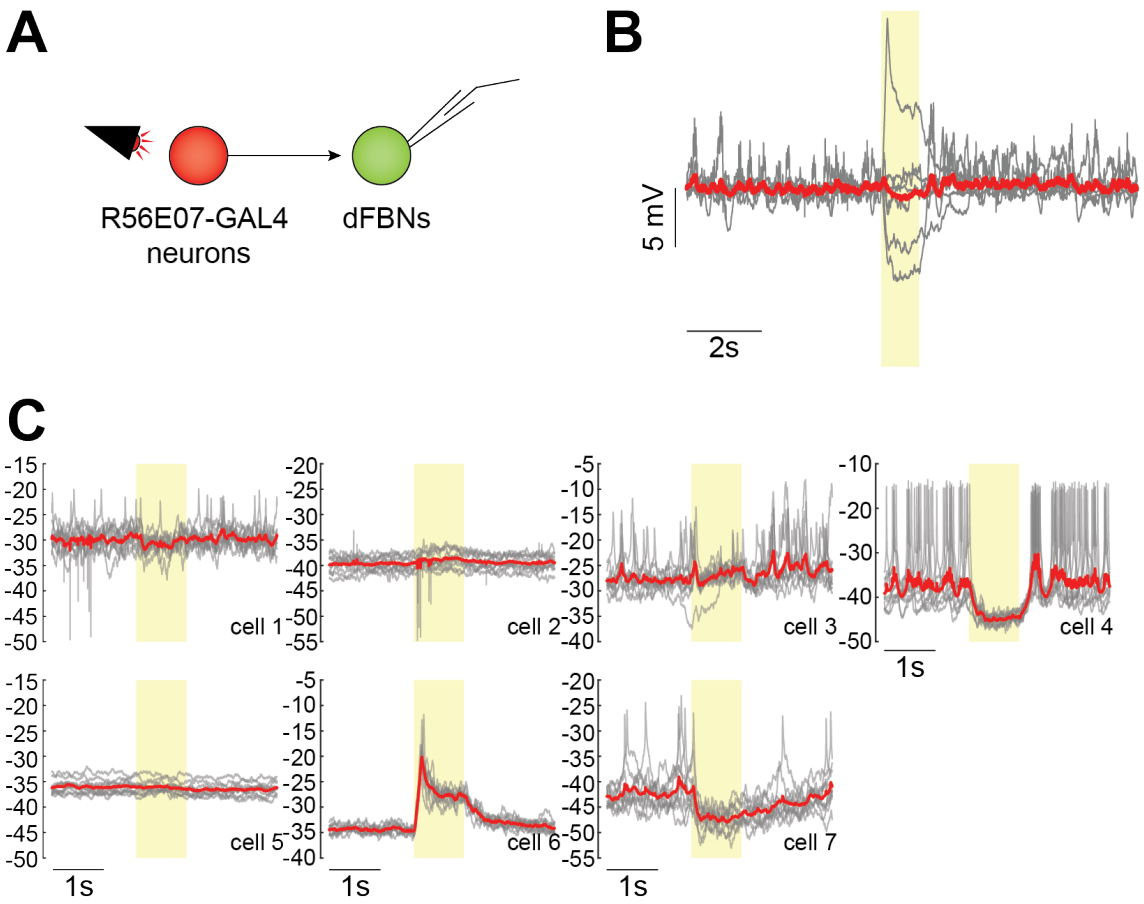

Figure 4.13: R56E07-GAL4 neurons project onto dFBNs. A) Patch-clamp recordings of dFBNs in *R23E10-LexA>LexAo-pGFP, R56E07-GAL4 > UAS-CsChrimson::tdTomato* flies during red light stimulation. B) Patch-clamp recordings reveal a response upon light activation of R56E07-GAL4 neurons. Traces are normalized to the first four seconds of the recording. n = 7 cells. Grey lines represent mean of individual cells, red line indicates mean of all cells. C) Individual plots of data in B show that the response to R56E07-GAL4 stimulation is heterogeneous. Each subplot represents the data of a single cell. Grey lines indicate individual repeats per cell. Red lines indicate mean response of the cell. Yellow shading represents light stimulation (1 sec).

conditions (Fig. 4.14A). The six recorded cells did not show a clear homogeneous pattern in their response to R56E07-GAL4 activation (Fig. 4.14B). Three out of six cells did not respond to the activation of R56E07-GAL4 neurons, one showed a sharp but short excitation (cell 3), while cell 4 showed a strong and prolonged inhibition and cell 6 showed an excitation (Fig. 4.14C). These responses were in line with their responses without TTX, suggesting that no secondary input was involved in the connection. Overall, R56E07-GAL4 projected onto roughly 50% of dFBNs, but the exact composition of the connection remains

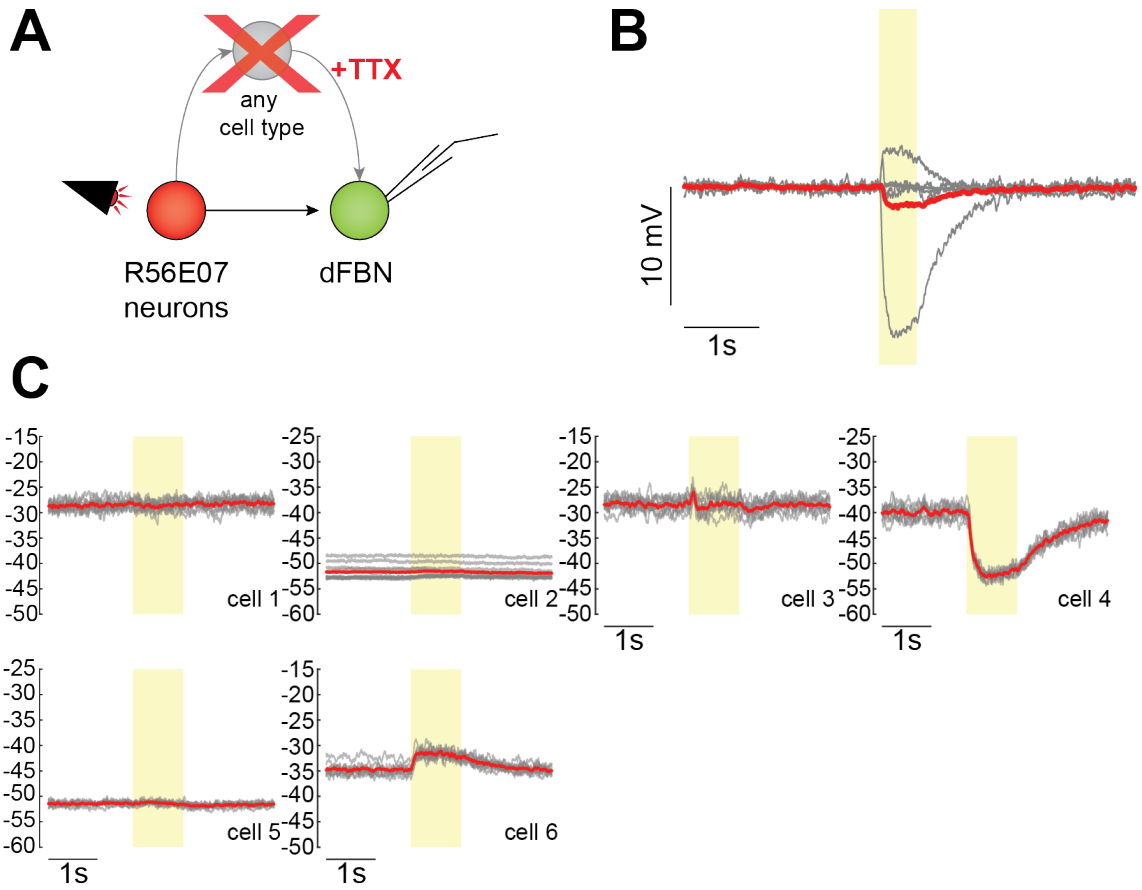

Figure 4.14: The connection of R56E07-GAL4 onto dFBNs is monosynaptic. A) Patch-clamp recordings of dFBNs in *R23E10-LexA>LexAop-GFP, R56E07-GAL4 > UAS-CsChrimson::tdTomato* flies during red light stimulation in the presence of TTX to block polysynaptic connections. B) Mean response of patch-clamp recordings of dFBNs revealed a monosynaptic connection. Traces are normalized to the first four seconds of the recording. n = 6 cells. Grey lines represent mean of individual cells, red line indicates mean of all cells. C) Individual plots of data in A showed that the response to R56E07-GAL4 stimulation is heterogeneous and only three out of six neurons responded. Each subplot represents the data of a single cell. Grey lines indicate individual repeats per cell. Red lines indicate mean response of the cell. Yellow shading represents light stimulation (1 sec). Recordings are from the same cells as in figure 4.13.

to be understood.

4.2.5 Generation of split lines to target pontine neurons more specifically

While the R56E07-GAL4 line seemed to have a restricted expression pattern in the central brain, it also showed expression in the optic lobes (Fig. 4.3). Further, when Kir2.1 was

expressed in these cells, survival seemed to be significantly impaired, potentially pointing at expression in unwanted cells (Fig. 4.2C). And last, the patch-clamp experiments performed here suggested a heterogeneous population of neurons (Fig. 4.9). One option to solve these issues might be to use a line that has a more refined expression pattern. To this end, several split-GAL4 lines were generated that would allow more precise targeting of a subpopulation of neurons in the CX.

The aim was to exclusively target expression to the neurons in the CX without expression in the optic lobes. The R56E07 GAL4-DBD were combined with several ADs that would target expression to the CX. Combination of R56E07-DBD and R72G03-AD resulted in split-GAL4 #1. During the time of this work, a new split-GAL4 line became available that used the R56E07-DBD hemidriver and combined it with R91D10-AD [55]. This line was tested as split-GAL4 #2. Another AD that specifically targets expression in the optic lobes (R65B12-AD) was used to compare whether this has an effect on the behaviour of the fly.

4.2.5.1 CX neurons in R56E07-GAL4 are responsible for the reduction in sleep

Having these more refined tools at hand allowed to test more specifically which cells were responsible for the wake promoting effect of R56E07-GAL4. As before, a thermogenetic approach was used whereby TrpA1 was expressed using the before mentioned split-GAL4 driver lines. As shown before, R56E07-GAL4 activation reduced sleep, compared to parental controls (Fig. 4.15A). The two split-GAL4 lines that target the CX both reduced sleep when activated, with a stronger effect in split-GAL4 #1. R65B12-AD;R56E07-DBD, labelling the optic lobes, did not reduce sleep, which proved that the wake promoting effect

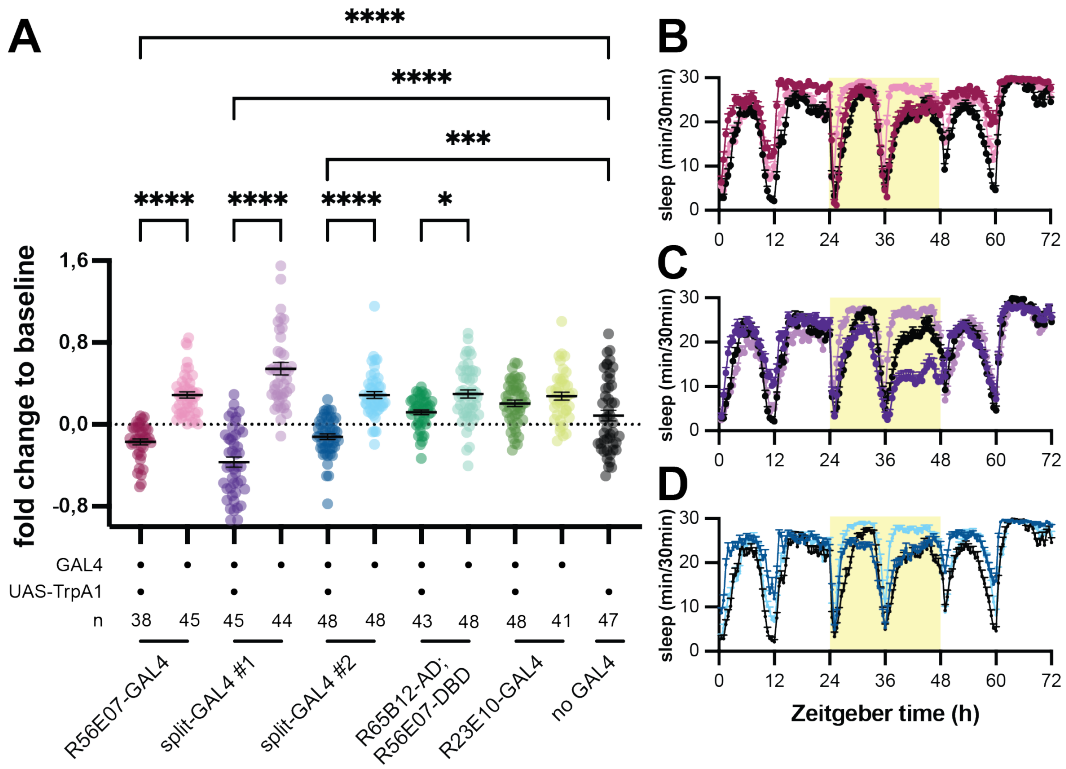

Figure 4.15: R56E07 split-GAL4 driver lines show decrease in sleep when activated. A) Fold change in sleep for *R56E07-GAL4 > UAS-TrpA1* and *split-GAL4 > UAS-TrpA1* flies and parental controls during neuronal activation via TrpA1. Fold change was calculated as heat activation day compared to baseline day. Significance was calculated with one way ANOVA with Holm-Šídák, and compared to parental controls. Stars indicate significance as follows: **** = $p < 0.0001$, *** = $p < 0.001$, ** = $p < 0.01$, * = $p < 0.05$. B) Sleep profile over 3 days for R56E07-GAL4 and its parental controls. C) Sleep profile for split-GAL4 #1 and its parental controls. D) Sleep profile for split-GAL4 #2 and its parental controls. Colours in B-D represent the same groups as in A. Yellow shading represents heat activation at 29 °C via TrpA1. split-GAL4 #1: R72G03-AD; R56E07-DBD. split-GAL4 #2: R91D10-AD; R56E07-DBD.

of R56E07-GAL4 was not due to the expression in the optic lobes. As can be seen in the sleep traces, the strongest reduction in sleep appeared during the night (Fig. 4.15B-D).

4.2.5.2 R56E07 split-GAL4 lines label different number of cells

The anatomy of these neurons was studied more closely to understand why the two split-GAL4 lines targeting the CX showed differences in the reduction of sleep. UAS-RedStinger was expressed in the neurons to label the cell bodies, which were then counted [206].

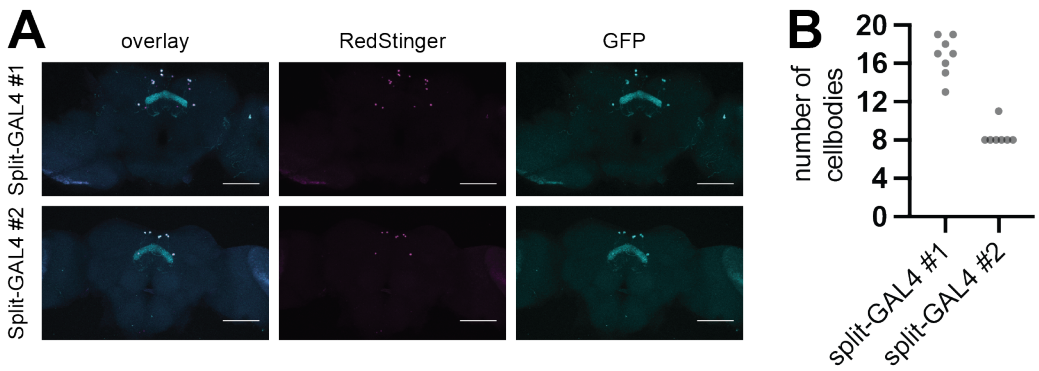

Figure 4.16: R56E07-GAL4 split-GAL4 lines label different number of cell bodies in CX. A) Confocal pictures of both split-GAL4 lines with UAS-RedStinger and UAS-GFP expression. Representative pictures are shown. Scale bars = 100 µm. B) Cell count by the RedStinger label revealed that split-GAL4 #1 labelled more cells than split-GAL4 #2. split-GAL4 #1: R72G03-AD; R56E07-DBD, n = 8 flies. split-GAL4 #2: R91D10-AD; R56E07-DBD, n = 7 flies.

No viable offspring were obtained when UAS-RedStinger was crossed to R56E07-GAL4, suggesting that this driver labelled cells that are very sensitive to genetic manipulations. The two split-GAL4 lines did produce viable offspring and could be dissected for cell body counting. The expression pattern of the two lines was very similar, with the neurites projecting to the same area in the FB (Fig. 4.16A). Counting of the cell bodies revealed that split-GAL4 #1 expressed in more cells than split-GAL4 #2, with 13-19 cell bodies and 8-11 cell bodies respectively. While split-GAL4 #1 had varying numbers of cell bodies, split-GAL4 #2 had a very consistent cell body count of 8 cells, with one exception only (Fig. 4.16B).

Interestingly, shortly after these experiments were performed, a preprint was published that described the split-GAL4 #2 to label specifically hDeltaF neurons [55].

We can conclude that the results obtained with the R56E07-GAL4 line cannot be attributed to a single cell type, but that they include hDeltaF neurons as well as others. Potentially they might be labelling some hDeltaK neurons, as expression can be detected in the EB,

and hDeltaK are the only pontine neurons with neurites outside of the FB [44].

4.3 Discussion

Many different brain regions have been implicated in the homeostatic control of sleep in the fruit fly *Drosophila melanogaster*. Neurons in the dFB have been identified as a key hub in translating sleep pressure into sleep [126, 127, 131], but how these cells act in their wider circuitry has not been studied in detail. Previous studies have identified several individual cell types that are connected [85, 129, 130, 147], but no full screen had been performed. The aim of this chapter was to understand which connections of dFBNs might be encoding relevant information for a normal sleep-wake behaviour. To this end, I performed a large behavioural screen to identify neurons that change sleep when activated or inhibited. More than 20 GAL4 lines were tested and several hits were identified that showed impaired sleep or wake (Fig. 4.1). While several hits showed significant changes in sleep, in the subsequent experiments I focussed on R56E07-GAL4 neurons. Activating these neurons increased waking time significantly compared to controls. Only one other study has been published where this driver was used as part of a big behavioural screen, and the main results suggested that activating these neurons induced jumping behaviour [207].

Several other lines also showed significant changes in sleep. These lines included lines labelling ExR1, which were not studied further as a lot of work has already covered their properties [91, 129]. Further, two lines targeting octopaminergic VPM3 neurons induced wakefulness during activation, a finding that was recently replicated and studied in detail [180]. Also R64A11-GAL4 was used in the screen but did not show changes in sleep upon

activation. Instead, it showed a sleep rebound on the day after activation, as well as an increase in sleep when inhibited with Kir2.1 (Fig. 4.1C, fig. 4.2B). A recent study has used split-GAL4 lines with the R64A11 hemidriver and found that activation of these neurons induced upwind locomotion [208], suggesting that these neurons encode a behavioural function that was outside of the scope of our behaviour recordings here.

4.3.1 GAL4 lines often target unknown additional cell types

While the GAL4 lines used in the experiments here were chosen to target specific cell types, subsequent work revealed that there is often unwanted off-target expression. R24A05-GAL4 for example likely labelled the two ExR3 neurons, but it also expressed in a plethora of other cell types in different regions of the brain (Fig. 4.3). Labelled cell bodies could be detected dorsally of the FB, but also in the suboesophageal zone, and projections could even be detected in parts of the optic lobes. For behavioural experiments, this provided a big caveat, as results were hard to map to the specific cell type. As can be seen in these results, the sleep behaviour of flies with ExR3 neuronal activation showed exactly this problem: three different GAL4 lines were chosen to target ExR3 neurons, but the observed changes in behaviour differed substantially. Only one line significantly increased sleep (compare Fig. 4.1), which questions whether the observed effect was specific to ExR3 neurons, or rather an effect of off-target expression.

Further, the unspecific labelling of neurons became obvious in the case of R56E07-GAL4. Here, Kir expression induced death within several days (Fig. 4.2). Kir2.1 expression in a few neurons in the central complex is unlikely to induce death [148], hence the observed phenotype likely resulted from off-target effects. Further, even the expression of RedStinger, a fluorophore expressed in the nucleus [206], did not produce viable offspring

(Fig. 4.16). These findings suggest that expression of R56E07-GAL4 labels a heterogeneous set of cells, but the reasons why these manipulations are lethal remain unknown.

4.3.2 Caveats of TrpA1 activation

While TrpA1 screens are widely used [55, 130] and provide an easy way to test many driver lines, there are several caveats. In order to activate TrpA1, the environmental temperature needs to be increased. While this will open the channel and allow for the neurons to be activated, an increase in temperature will have many effects on the fly's behaviour and organism. Temperature changes are known to affect the sleep pattern of flies, with an increase of sleep during the day, a reduction of sleep during the night [209–212]. While the results here were compared to a control group that underwent the same temperature shifts, it might still lead to unnatural changes in behaviour. A second problem is the activation pattern with TrpA1. While optogenetic activation allows precise control of the target cell as specific stimulation frequencies can be used, TrpA1 activation cannot be controlled specifically [213]. TrpA1 activation likely leads to tonic firing [213], which might be problematic if some neurons mainly signal via burst firing (as shown in [132] the stimulus frequency might significantly affect the resulting behaviour). Also the choice of 24 hours of heat activation can be challenged. Different studies use different lengths of TrpA1 activation, ranging from 6 [134, 140], 12 [86, 96, 130] to 24 hours [55, 214]. Different lengths and timing of heat activation will of course change the resulting behaviour, hence the obtained results might differ when heat activation is changed.

4.3.3 Synaptic connectivity testing remains difficult

Using studies of functional connectivity, I was able to show that there are synaptic connections from dFBNs onto R56E07-GAL4 neurons (Fig. 4.7, fig. 4.9, fig. 4.10). While GRASP stainings had already indicated a likely connection (Fig. 4.4), only functional testing can yield a conclusive result, whether cells are functionally connected, or only in close proximity [93]. The polarity of the connection remained surprisingly hard to understand, as the recorded cells responded differently to the same stimulus. Repeated stimulation of dFBNs always resulted in the same excitation (Fig. 4.8), suggesting that the difference must come from the downstream partner.

Differences might originate from two different sources: either recordings were from different cells, which would indicate again an unspecific labelling by the GAL4 driver. Or the cells have different responses, based on internal states/different RMPs. Importantly, the differences were mainly seen in patch-clamp recordings, but not in the calcium imaging experiments (compare figure 4.9 and figure 4.7). While calcium imaging has the advantages of being able to image a group of cells at the same time, and without changing the composition of the cytosol [215], the resolution is less precise therefore especially small inhibitions cannot be detected. A good alternative for future experiments would be voltage imaging [216], which also allows recording from several cells at the same time. New advances in the development of voltage sensors now generated constructs that can detect voltage differences as small as 1 mV [217], which would hopefully be sensitive enough to detect even small changes during synaptic events.

Overall, this chapter provides a first insight into the diversity of behavioural responses to stimulation of neurons with connections to dFBNs. Thanks to technical advances, we

now have much more precise tools available, that allow us to target individual cell types, without off-target effects. Experiments here, as well as tools developed by others, found that R56E07-GAL4 neurons mainly consist of hDeltaF neurons which can be targeted precisely with the split-GAL4 line #2 [55]. The following chapter focuses in depth on the role of these neurons, and elucidates the connection between dFBNs and hDeltaF neurons in detail.

5 | dFBNs project onto wake-promoting hDeltaF neurons

5.1 Introduction

The connectome suggests two main synaptic connections of dFBNs: hDeltaK neurons provide the strongest input and hDeltaF neurons receive the strongest output from dFBNs (see chapter 3). Further, ExR3 neurons connect dFBNs with the EB, an interesting connection as it connects two important sleep control centres [126–130]. In the following two chapters, the behaviour and the synaptic connections of these neurons are investigated (Fig. 5.1).

The strongest connected postsynaptic partners of dFBNs are hDeltaF neurons, as was shown in chapter 3. hDeltaF is one out of 13 horizontal columnar interneuron types (hDelta or hΔ) in the FB of *Drosophila* [44]. Before hDelta neurons were defined into different subtypes, they were referred to as "pontine neurons" [115, 116]. Pontine neurons are highly conserved across insects and were shown to exist in *Drosophila* [115, 218], honey bees [219], monarch butterflies [220], desert locusts [221], dung beetles [222] and cockroaches [223], amongst others, but their function has still not been well understood. Each hDelta cell type consists of 8 to 31 neurons, whose neurites are exclusively in the FB, hDeltaK form the only exception and receive synaptic input in the EB [44]. Individual neurons of these types connect two columns of the FB, with different hDelta neuron types spanning different layers of the FB [44].

Since the description of distinct pontine subtypes into hDelta neurons [44], several of these cell types have been implied to affect navigational tasks. Activation of several split-GAL4

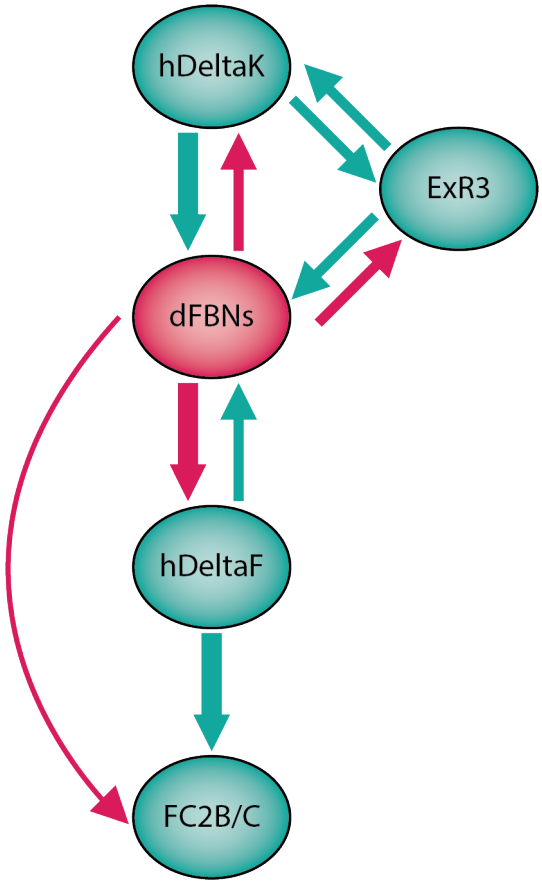

Figure 5.1: Schematic overview of the main synaptic connections of dFBNs analysed in this thesis. Additional connections are omitted for clarity. dFBNs receive direct inputs from and send direct outputs to hDeltaK, ExR3 and hDeltaF neurons. Additionally, FC2B/C neurons receive direct input from dFBNs and indirect input via hDeltaF neurons. Direct outputs from dFBNs are labelled in red.

lines labelling hDeltaB, D and E neurons induced significant upwind locomotion [208]. Further, hDeltaB alone was shown to be involved in encoding the travelling direction of the animal [94, 121] and in influencing the computations of distance approximation [224]. Another study found that hDeltaC neurons, and (or rather predominantly) hDeltaK neurons play a crucial role in wind guided olfactory navigation, as they receive input from olfactory circuits as well as neural signals encoding wind direction [124, 190, 225]. Last, hDeltaK, was predicted to be the main component of P2-GAL4. These neurons were suggested to be involved in the loss of sleep following chronic social isolation [148].

hDeltaF neurons, the neurons of interest in this chapter, comprise a group of eight neurons, whose projections are within layer 6 of the FB [44] and are predicted to be cholinergic [55, 174]. They divide the FB into six columns, which is rather unusual, as all other hDelta neuron types divide the FB into 8 or 12 columns [44]. Each hDeltaF neuron forms connections with only two, non-neighbouring columns in the FB, with one on each hemisphere [44]. So contrary to dFBNs not the whole width of the FB is covered by a single neuron, but only combined they span all columns. Each neuron connects both hemispheres, whereby input is received in both columns, but output synapses are almost exclusively located in one column per neuron [42, 45, 166, 167]. These neurons have been defined for the first time in the hemibrain dataset [43, 44] and have not yet been studied in detail. The only description of these cells was published during the preparation of this thesis, where hDeltaF neurons were shown to be potentially involved in sleep regulation, as activation of these neurons decreased sleep [55].

The lack of precise information makes it both challenging and exciting, to try to understand what these neurons might be encoding, and what the strong connection to a sleep promoting centre might represent.

To understand what signals hDeltaF neurons might receive from dFBNs, the nature of the neurotransmitter needs to be predicted, which has been a topic of debate. R23E10-GAL4 neurons have been shown to express the vesicular GABA transporter vGAT [129] and that a knock down of *Gad1*, a gene necessary for the production of GABA, blocks the sleep promoting effect of R23E10-GAL4 activation [179]. While this suggests GABA to be the relevant neurotransmitter of dFBNs, another study was not able to detect any GABA expression in these neurons [146] and no study has shown release of GABA by dFBNs.

Recent evidence suggests that non-dFBNs labelled by R23E10-GAL4 that are located in the suboesophageal zone might be expressing GABA instead [132]. Several studies further detected acetylcholine (ACh) expression in a subset of dFBNs [142, 146] that were later identified to be FB6A neurons [55], but no release of ACh could be detected using two different fluorescent sensors [132]. Interestingly, it has been shown that cholinergic transcripts are often present but not translated in many neurons [226], hence the evidence of acetylcholine transcripts in a cell might not be enough to verify that it also acts as a NT. Last, there is substantial supportive evidence for the expression of glutamate as shown by RNA expression, machine learning NT prediction and antibody staining [55, 132, 146, 174]. Glutamate was shown to be necessary in the transmission of sleep promoting signals by dFBNs [132]. Co-transmission with neuropeptides is highly present in the *Drosophila* CNS [227–229] and Allatostatin-A (AstA) and other neuropeptides have been shown to be expressed by dFBNs [129]. In the fly, glutamate can be excitatory as well as inhibitory, depending on its receptor [76, 77, 94, 230].

This chapter focuses in detail on the upstream and downstream connectivity of hDeltaF neurons, their role in sleep regulation, as well as their functional connectivity to dFBNs. The data presented here suggest that dFBNs form the main input to hDeltaF neurons and that these connect a sleep regulating centre with a navigational output circuit. Further, I found that hDeltaF neurons can shape sleep behaviour as artificial activation decreases sleep significantly, but hDeltaF neurons are unlikely to mainly encode sleep pressure. Last, hDeltaF neurons are functionally connected with dFBNs, with a surprisingly complex signalling pattern, where inhibition and excitation by glutamate can be detected between the same synaptic partners.

5.2 Results

5.2.1 Connectome analysis of hDeltaF neurons

5.2.1.1 Presynaptic connections of hDeltaF neurons are mainly formed by dFBNs

As shown in chapter 3, hDeltaF neurons are the main downstream connections of dFBNs. To understand the importance of this connection better, I wanted to see how relevant the input of dFBNs was to hDeltaF neurons. For this, I turned back to the connectome data and looked at the presynaptic connections of hDeltaF neurons.

Interestingly dFB neurons were by far the strongest input, making up more than 50 % of all incoming connections (Fig. 5.2A). At the level of cell type families, the next synaptic inputs to hDeltaF were formed by neurons in layers 7 and 6 of the FB (Fig. 5.2A). Almost 9% of inputs were coming from other hDelta neurons, and the remaining 12.5% of inputs were made up mainly by weaker connections of other FB layers, via tangential neurons and vDelta neurons (Fig. 5.2A). Examination of individual cell types revealed the same picture: dFBNs were the strongest connected neurons presynaptic of hDeltaF (with almost 25% of all connections formed by FB6A neurons), followed by neurons in layer 6 and 7 and other hDelta neurons (Fig. 5.2B). An important detail to note was that hDeltaF neurons also connect to themselves, allowing for information flow within neighbouring neurons.

To verify that the analysed data held true between connectomes, the two available datasets were compared. Here, the broad pattern remained the same: dFBNs formed by far the strongest input into hDeltaF neurons, constituting more than half of all incoming synapses in both datasets (Fig. 5.3). The observed differences between datasets in regard to input

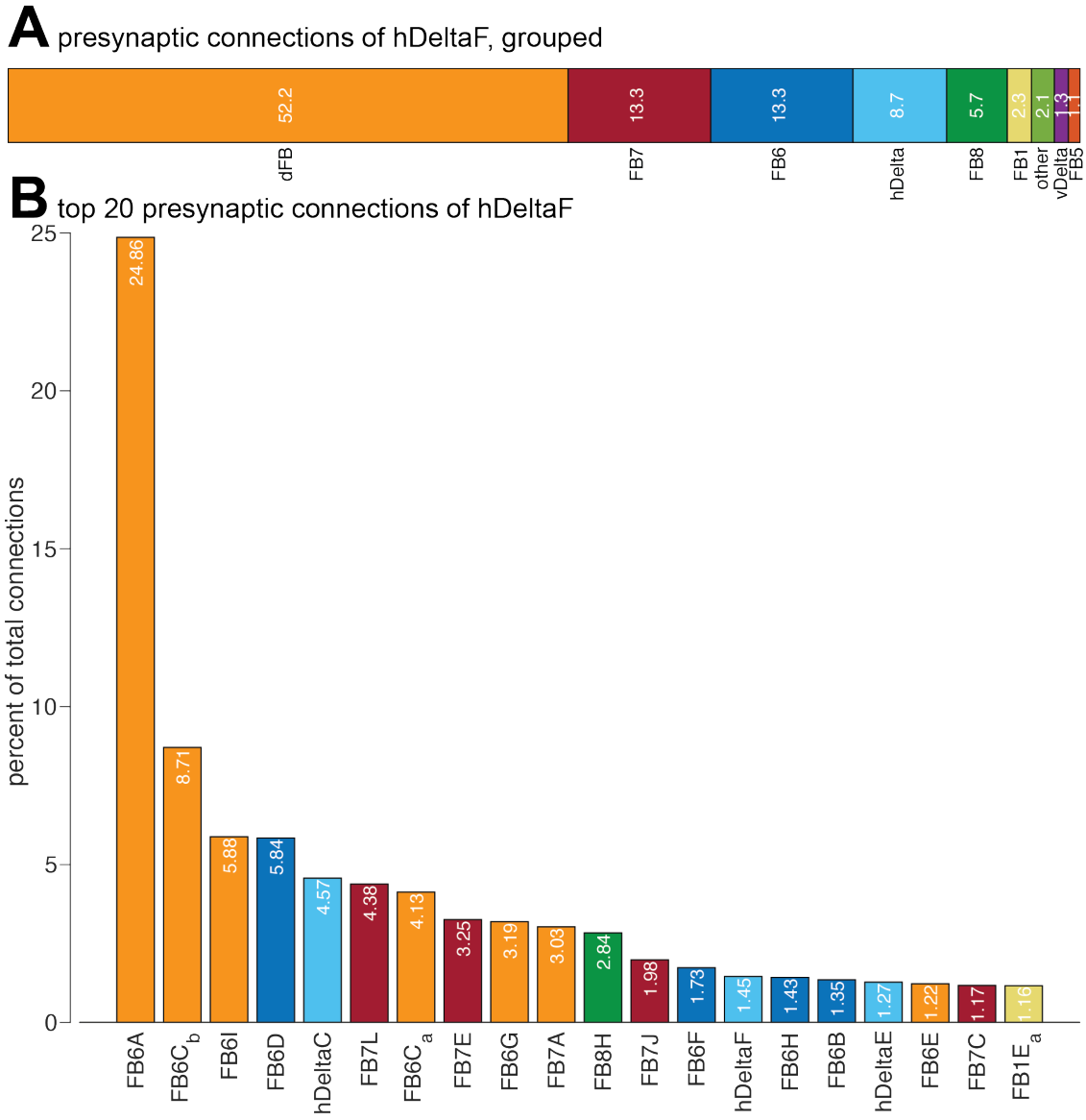

Figure 5.2: Presynaptic connections of hDeltaF neurons are mainly formed by dFBNs. A) Presynaptic connections of hDeltaF neurons, grouped by cell type families. Cell type families plotted here add up to 100%. Cell type families with a connection strength of less than 1% were summed as "other". B) The 20 strongest connected individual cell types upstream of hDeltaF. Bars are colour coded according to subgroups in figure A. Data plotted is percent of total connections of all hDeltaF neurons. Raw data obtained from Hemibrain v1.2.1 [43, 165].

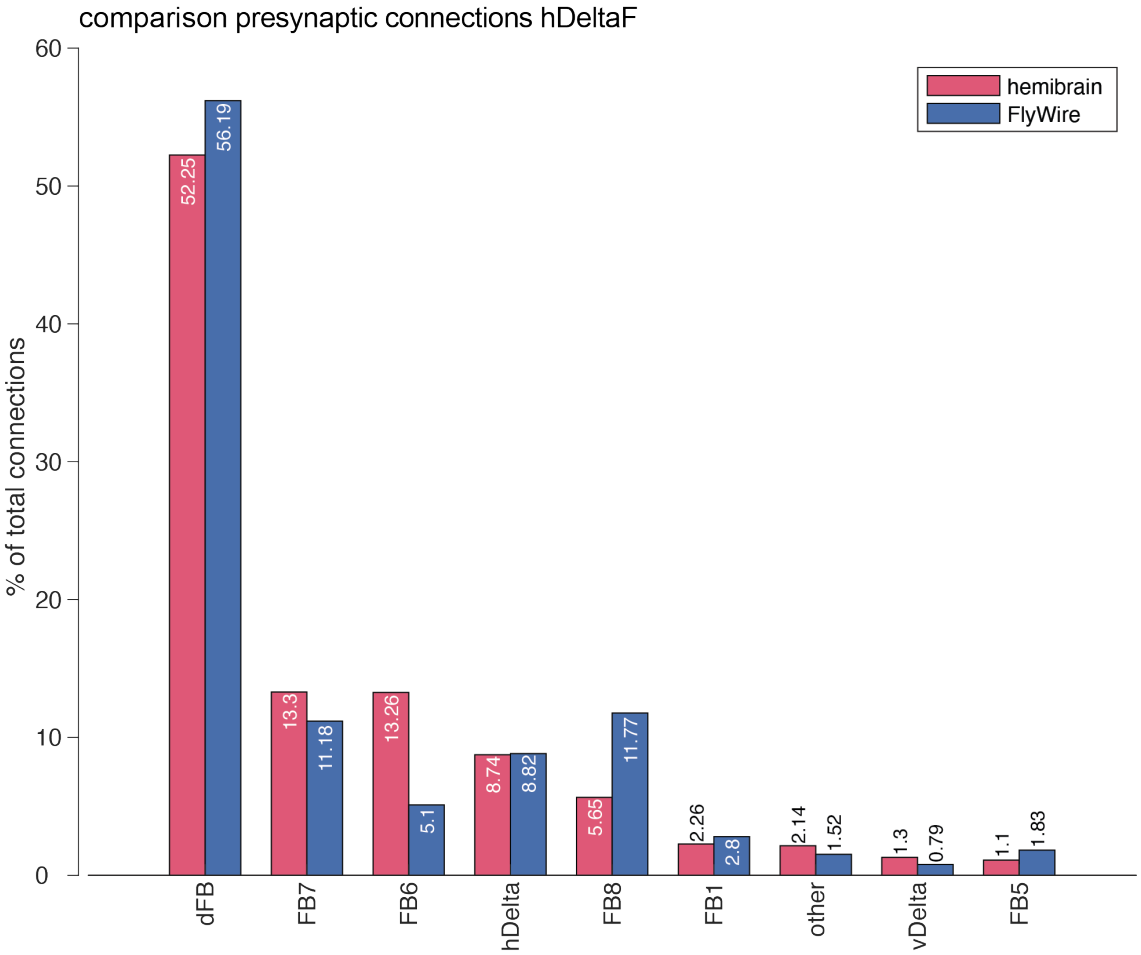

Figure 5.3: Presynaptic connections of hDeltaF neurons consist mainly of dFBNs in both connectome datasets. Connectome data was compared between hemibrain (pink) and FlyWire (blue). Connections were grouped in cell type families. Cell type families with less than 1% were summarized as 'other'.

by dFBNs and decreased input by FB6 neurons was, at least in part, due to FB6D and FB6B: these neurons have been described as individual cell types in the hemibrain dataset, and classified as non-dFB neurons. In the FlyWire dataset, these neurons could not be distinguished, hence they are included in the dFBN group. Overall, the connectome made it clear that the connection between dFBNs and hDeltaF neurons is a very strong and likely important connection.

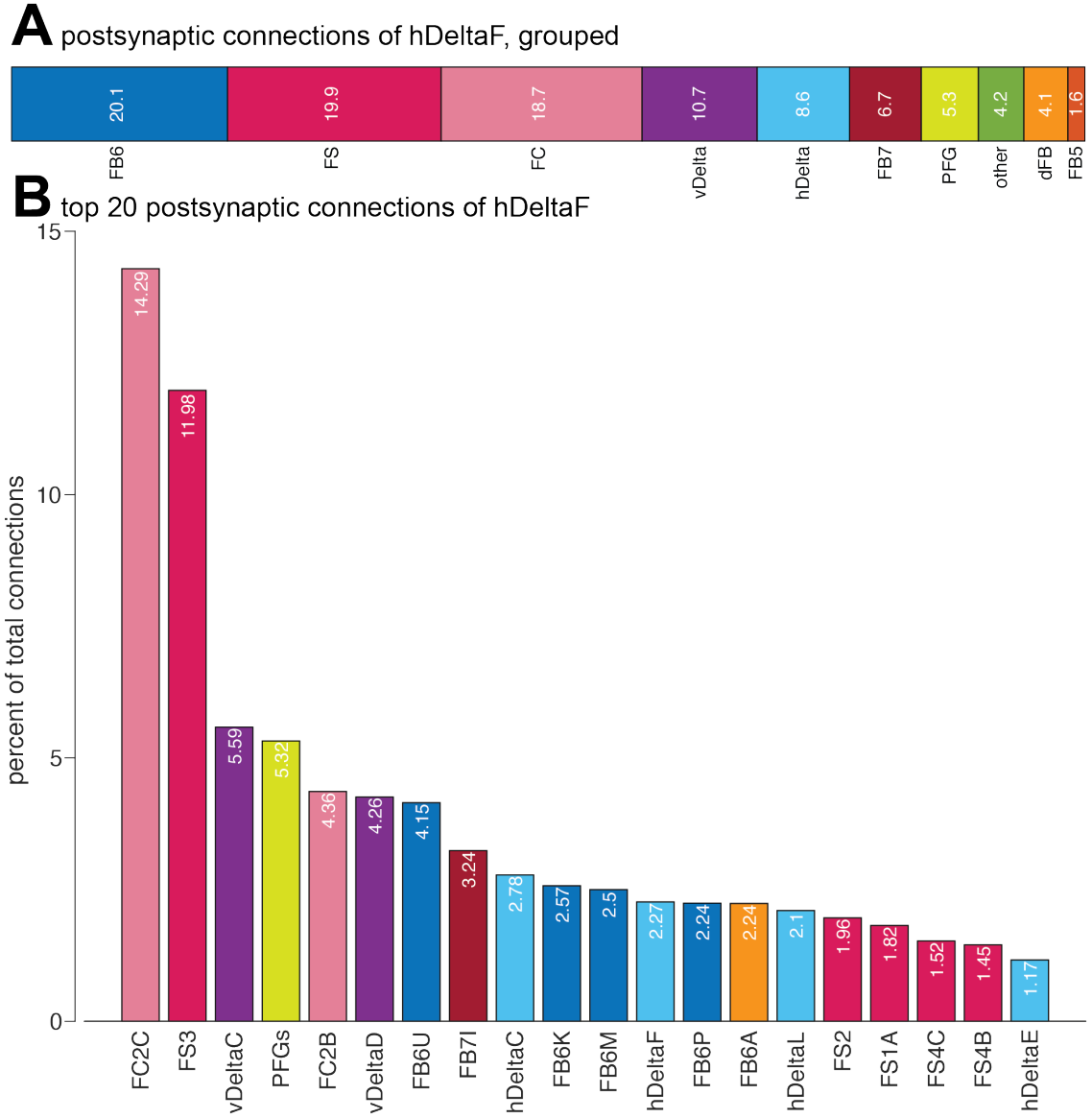

Figure 5.4: Postsynaptic connections of hDeltaF neurons target several neural circuits. A) Analysis grouped for cell type families shows the postsynaptic connections of hDeltaF neurons. Cell type families with a connection strength of less than 1% were summed as "other". B) The 20 strongest connected cell types downstream of hDeltaF, sorted by connection strength. Bars are colour coded according to subgroups in figure A. Raw data obtained from Hemibrain v1.2.1 [43, 165].

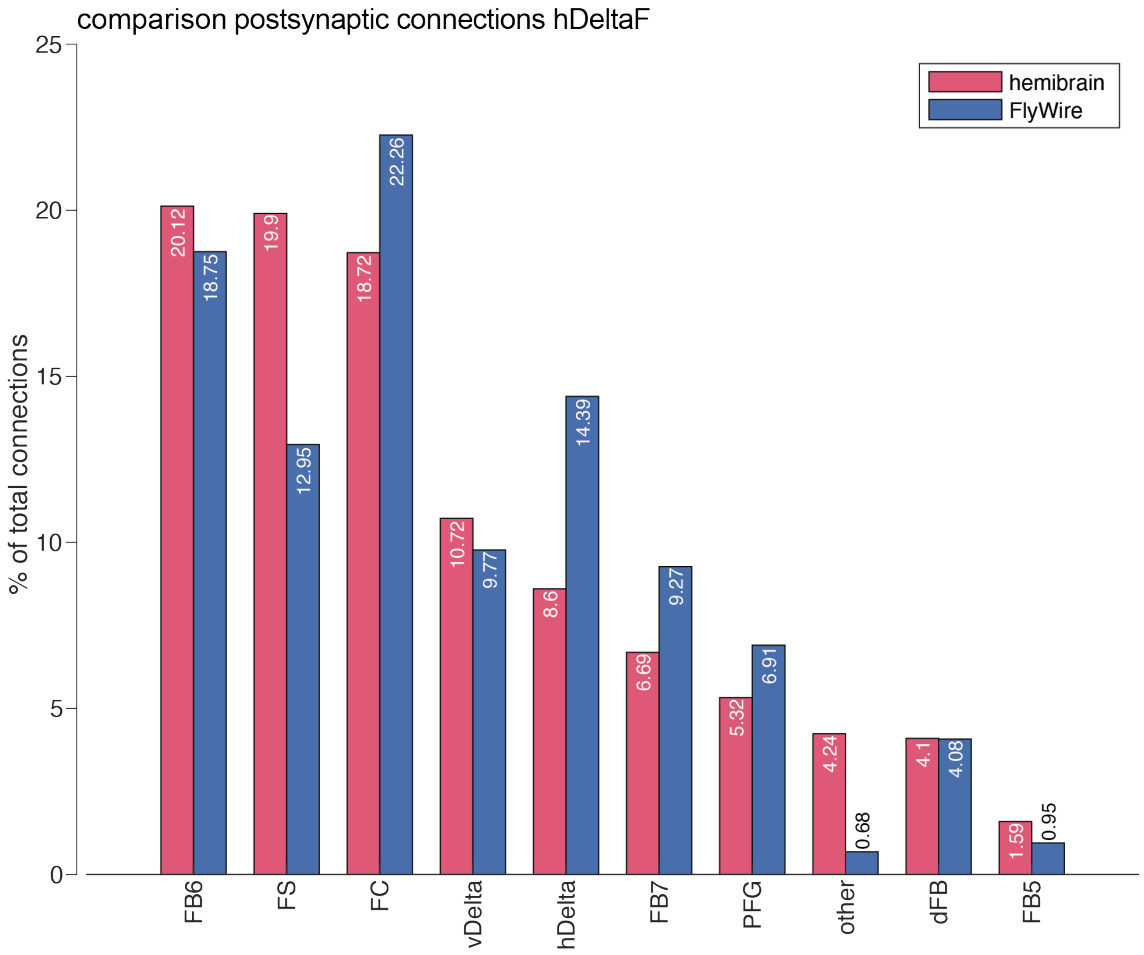

Figure 5.5: Postsynaptic connections of hDeltaF neurons reveal several differences between the two connectomes. Downstream connections of hDeltaF neurons are plotted as grouped per cell type family. Hemibrain data (pink) and FlyWire (blue). Cell type families with less than 1% were summarized as 'other'.

5.2.1.2 hDeltaF neurons target cells encoding goal angle

While the input to hDeltaF neurons was defined by few cell types, the downstream partners revealed to be much more diverse. The three strongest connected groups, all with very similar connectivity strengths, were neurons in FB layer 6, FS and FC neurons (Fig. 5.4A). Interestingly, while the connections to non-dFB neurons in layer 6 were strong, the connection to dFBNs made up only around 4% of connections, underlining the difference between dFBNs and non-dFBNs in layer 6. Examination of individual cell types revealed

that two cell types were targeted strongly by hDeltaF: FC2C and FS3 neurons (Fig. 5.4B). FC2 cells had been described to be involved in encoding the goal angle of the fly [123]. FS3 neurons have not yet been described functionally, their anatomy predicts synapses in the SP [44], which could suggest a feedback to the inputs of dFBNs.

A few differences could be seen in the FW dataset (Fig. 5.5). FS neurons showed a weaker connection than predicted by the HB data, but the connection to FC neurons, on the other hand, was even stronger. Further, the FlyWire dataset described stronger connections to hDelta, FB7 and PFG neurons. While the hemibrain dataset suggested three main output pathways, the FlyWire dataset challenged this hypothesis, and suggested several important targeted neural circuits. The strongest connected cell type remained FC2C with 18.9%, followed by vDelta neurons with 9.6% (data not shown). Overall, this confirmed the importance of the connection to FC2C, as the strongest output pathway of hDeltaF, while also highlighting other pathways.

5.2.2 Behavioural analysis of hDeltaF neurons reveals wake-promoting effect

The connectome analysis underlined the strong connection of dFBNs onto hDeltaF neurons. As the former transmit a sleep promoting signal, the next question was how this information is computed in hDeltaF neurons, and if any behavioural phenotype could be detected. To this end, hDeltaF neurons were manipulated with different tools and the resulting sleep phenotypes were studied.

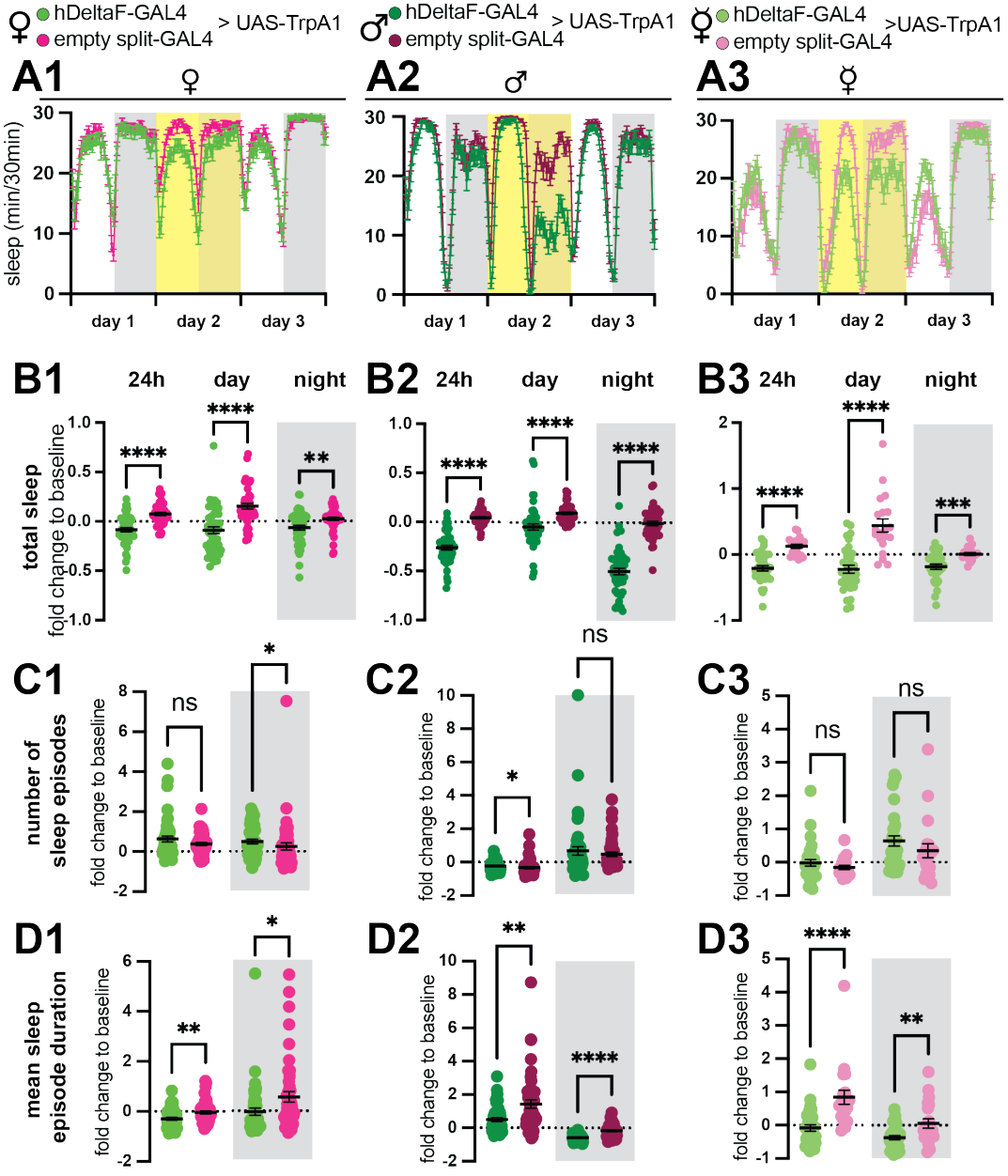

Figure 5.6: Activation of hDeltaF neurons decreases sleep. Data in the first column is from mated females, in the second column from males and in the third column from virgin females. A) Sleep profiles of *hDeltaF split-GAL4 > UAS-TrpA1* flies (green) and *empty split-GAL4 > UAS-TrpA1* flies over three consecutive days. Yellow shading indicates the day of heat activation. (Caption continued on next page.)

Figure 5.6: (Continued from previous page.) B1) Quantification of change in total sleep duration revealed a decrease in sleep in mated females during the 24h, as well as during daytime, but slightly less during nighttime. B2) Total sleep was significantly decreased in male flies upon activation of hDeltaF neurons, during 24h, daytime and nighttime. B2) Total sleep was significantly decreased in virgin female flies during 24h, daytime and nighttime. C1) The number of sleep episodes were unchanged during daytime, but increased during nighttime in mated female flies. C2) The number of sleep episodes was slightly increased during the day but unchanged during the night in male flies. C3) The number of sleep episodes was unchanged in virgin female flies during daytime and nighttime. D1) The mean length of sleep episodes was decreased during the day and night in mated female flies. D2) The mean length of sleep episodes was decreased during the day and strongly during the night in male flies. D3) The mean length of sleep episodes was decreased strongly during the day and night in virgin female flies. To obtain the fold change values, data during heat activation was compared to the same animal during baseline day. ZT = Zeitgeber time. Grey shading indicates dark period (night). Significance was calculated between experimental and control group with independent t-test for normally distributed data and Mann-Whitney U test for not-normally distributed data. Stars indicate significance as follows: **** = $p < 0.0001$, *** = $p < 0.001$, ** = $p < 0.01$, * = $p < 0.05$. n = 46 for mated females, 46 for males and 19-31 for virgin female flies. Dots represent individual flies, bars represent mean ± SEM. hDeltaF split-GAL4: R91D10-AD; R56E07-DBD.

5.2.2.1 Activation of hDeltaF neurons reduces sleep

While already studied briefly in chapter 4.15, here neuronal activation of hDeltaF neurons was examined in detail to understand exactly, what effect it had on the sleep behaviour and sleep architecture. For this, mated female, male and virgin female flies with the same genotypes were tested and analysed for their changes in sleep, during and after TrpA1 activation. Sleep behaviour in flies with TrpA1 activation in hDeltaF neurons was compared to flies with UAS-TrpA1 under control of an empty split-GAL4 control [231]. This control line was created with the same vector, used for all other split-GAL4 lines, but without an enhancer fragment, therefore it will not be expressed in any cells.

As a first note, baseline sleep already showed differences between the sexes. Male flies slept less during the night and more during the day than mated female flies (Fig. 5.6A1, A2), and virgin female flies slept much less during the day than mated females and males (Fig. 5.6A3). Activating hDeltaF neurons led to a significant decrease of sleep in all groups (Fig. 5.6B1-3). In mated and virgin female flies, the effect was strongest during the day, where

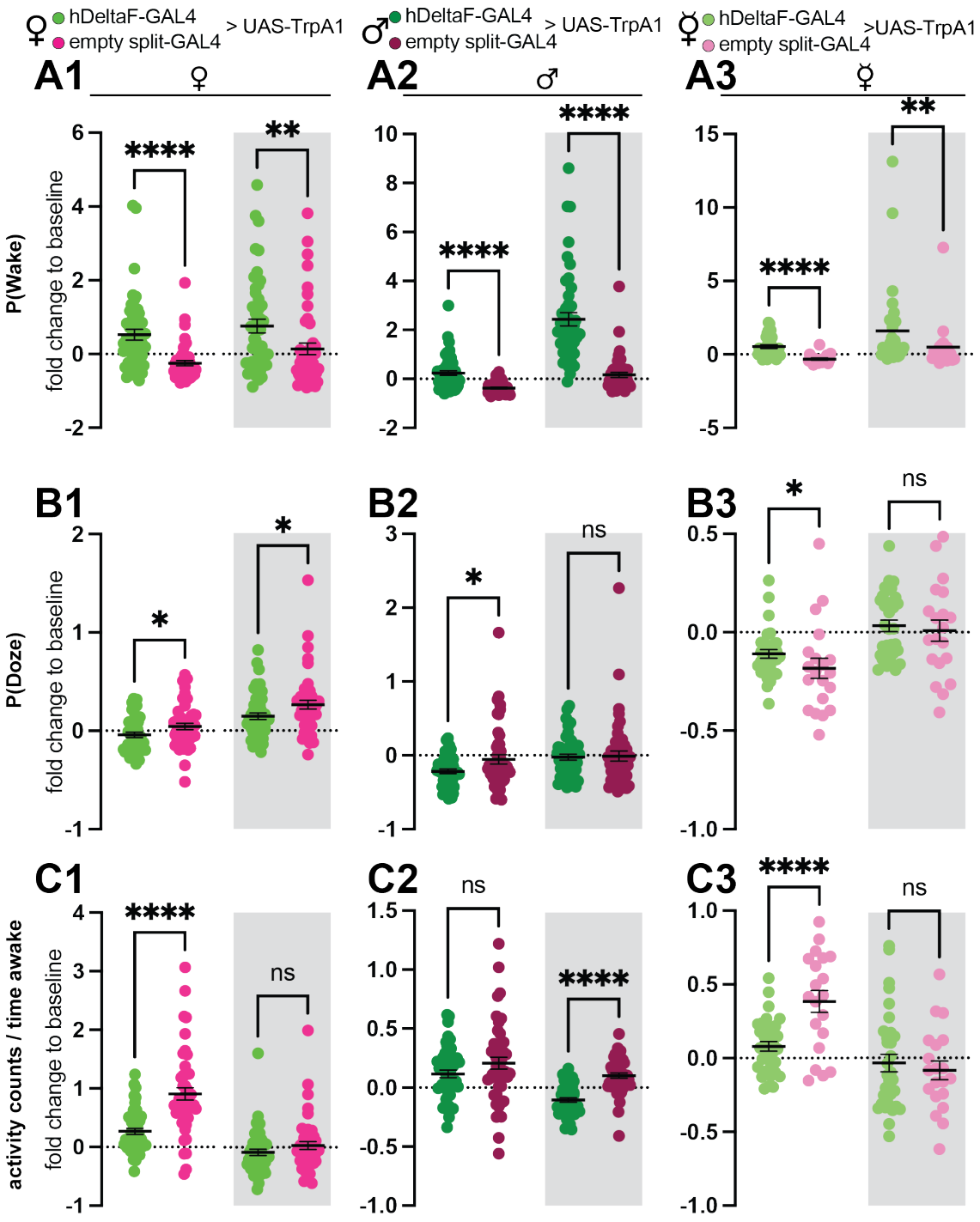

Figure 5.7: Activation of hDeltaF neurons affects sleep architecture and activity. A1) P(Wake) was increased during daytime and nighttime in mated female flies. A2) P(Wake) was strongly increased during daytime and nighttime in male flies. A3) P(Wake) was strongly increased during the day, and during the night in virgin female flies. (Caption continued on next page.)

Figure 5.7: (Continued from previous page.) B1) P(Doze) was slightly decreased during the day and night in mated female flies. B2) P(Doze) was slightly decreased during the day, but not during the night in male flies. B3) P(Doze) was slightly increased during the day, but unchanged during the night in virgin female flies. C1) Activity was strongly decreased during the day, but not during the night in mated female flies. C2) Activity was unchanged during the day, and strongly decreased during the night in male flies. C3) Activity was strongly decreased during the day, but unchanged during the night in virgin female flies. Grey shading indicates dark period (night). Significance was calculated between experimental and control group with independent t-test for normally distributed data and Mann-Whitney U test for not-normally distributed data. Stars indicate significance as follows: **** = $p < 0.0001$, *** = $p < 0.001$, ** = $p < 0.01$, * = $p < 0.05$. n = 46 for mated females, 46 for males and 19-31 for virgin female flies. Individual dots represent individual flies, bars represent mean ± SEM. Dark shading indicates nighttime. hDeltaF split-GAL4: R91D10-AD; R56E07-DBD.

they lost 0.8 and 1.4 hours of sleep respectively (compared to a respective increase of 1.1h and 1.7h in control animals) (Fig. 5.6B1, B3). Male flies lost 0.6 hours of sleep during the day but 3.8 hours during the night, which decreased their nighttime sleep by roughly 50% (Fig. 5.6B2).

To understand where the differences in sleep came from, the changes of the sleep architecture of these flies was analysed more closely. The number of sleep episodes remained unchanged in most cases, with some minor increase during the night in mated female flies and during the day in male flies (Fig. 5.6C1-3). The second sleep architecture parameter analysed was the length of sleep episodes, which was reduced in all groups during day and night (Fig. 5.6D). Therefore the decrease in total sleep stemmed mainly from a decrease in sleep bout length, rather than a reduction of number of sleep bouts.

P(Wake) and P(Doze) were analysed for all three groups as a measure for the stability of sleep. These two measures are based on the transition probabilities between an active and an inactive state of the fly. P(Wake) describes the probability for a fly to start moving after a period of inactivity, which can be related to the sleep depth of the animal [110]. P(Doze) is the probability for the fly to transition from an active state to an inactive state, which is correlated to the sleep pressure of the animal [110]. All three groups showed a strongly

significant increase in P(Wake) when hDeltaF neurons were activated, as compared to the empty split-GAL4 control (Fig. 5.7A). This effect was strongest during the daytime in mated and virgin female flies, which was also the time when these animals lost most sleep (Fig. 5.7A1, A3). Male flies showed a strong increase in P(Wake) during day and night, which also aligned with their strong reduction in sleep during these times (Fig. 5.7A2). The increase in P(Wake) indicated a higher probability for the animals to wake up, which led to a decrease in total sleep, as well as sleep bout length. P(Doze), on the other hand, showed much smaller changes, with a slight reduction during day and night in mated female flies, as well as during the day for male flies (Fig. 5.7B1, B2). This decrease in P(Doze) signalled a decrease in sleep pressure, hence the reduction in sleep. Surprisingly, in virgin female flies P(Doze) was increased during the daytime, which signalled a higher sleep pressure during this time (Fig. 5.7B3). Interestingly, this group of flies were also the only ones that showed rebound sleep on day three of the experiment, indicating that there was indeed higher sleep pressure that could only be dissipated during the next day (Fig. 5.6A3).

Last, to verify that the flies did not harbour a locomotor defect that might indicate movement artefacts rather than sleep changes, the activity of the flies was analysed. Activation of hDeltaF neurons did not lead to hyperactivity of the flies, but rather decreased their activity significantly, as compared to the control animals (Fig. 5.7C). Notably in two cases the strong differences were mainly driven by the strong increase in activity by the control animals compared to the baseline day, that almost doubled their activity in mated female flies, whereas experimental animals remained the same levels of activity during heat activation (Fig. 5.7C1).

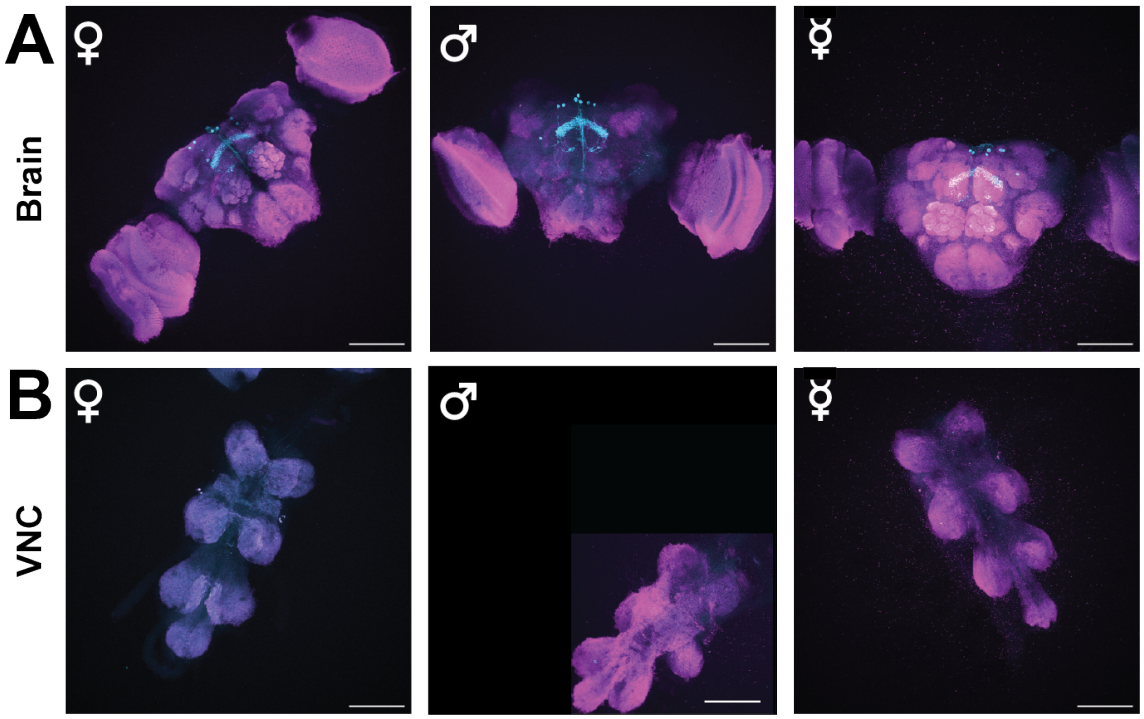

Figure 5.8: The hDeltaF split-GAL4 driver has the same expression pattern independent of sex and mating status. A) Expression pattern of *hDeltaF split-GAL4 > UAS-mCD8::GFP* in the brains of mated females, males and virgin female flies. Several cell bodies dorsal of the FB and a layer in the FB were labelled. Expression pattern did not differ between sex and mating status. B) Expression pattern of *hDeltaF split-GAL4 > UAS-mCD8::GFP* in the VNC of mated females, males and virgin female flies. No cells in the VNC were labelled by the hDeltaF split-GAL4 driver. Maximum intensity projections of representative images are shown. At least 5 animals were dissected per condition. GFP signal in cyan, nc82 staining in magenta. Scale bars indicate 100 µm. hDeltaF split-GAL4: R91D10-AD; R56E07-DBD.

While differences in sleep pattern between the sexes, and also between mated and virgin females are known [102–104, 232], it was surprising that activating the same neuronal cell type would present with such different effect sizes between these groups. In the quest to understand where these differences might come from, the expression patterns of the GAL4 line were studied. Flies expressing GFP in hDeltaF neurons were dissected, and their brain as well as their VNC were imaged (Fig. 5.8). All dissected brains showed the same expression pattern: with roughly eight cell bodies, six of them located more dorsal to the FB, and two were close to the FB, one on either side (Fig. 5.8A). No other cell bodies were labelled in the whole brain, nor in the VNC (Fig. 5.8B). Overall, the GAL4

line used for the experiments labelled the same number and type of cells independent of sex and mating status. Another explanation might be that these neurons are part of a sexually dimorphic neuronal circuitry, which therefore affects the sexes differently. At the time of writing this thesis, the male connectome of the *Drosophila* brain had not yet been published, and the data could therefore not be compared between the sexes. The known connections of hDeltaF neurons do not point to known sexual dimorphisms.

5.2.2.2 Inhibiting synaptic output from hDeltaF neurons does not affect sleep

To test if hDeltaF neurons are necessary for a physiological sleep pattern, their neuronal signalling was blocked and sleep behaviour was studied. To this end, *shibire^{ts}* was expressed in hDeltaF neurons to block synaptic transmission. This transgene encodes a temperature sensitive version of *shibire*, which encodes dynamin, a protein necessary for vesicular recycling [233]. *Shibire^{ts}* is a mutated version of dynamin that cannot recycle at high temperatures and hence blocks synaptic output [233]. Increasing the environmental temperature above permissive temperature induces synaptic blocking that can be temporally controlled [233]. To control for the effect of increased environmental temperature, flies expressing *shibire^{ts}* under control of the hDeltaF split-GAL4 were compared to flies carrying *shibire^{ts}* under control of empty split-GAL4. During the heat activation day, both groups slept more than during the baseline day, with *hDeltaF>UAS-TrpA1* flies sleeping slightly more, but no significant difference could be detected (Fig. 5.9B). While the overall amount of sleep did not change between genotypes, the sleep architecture differed quite strongly during the day. Flies with blocked synaptic transmission in hDeltaF neurons had more consolidated sleep, which manifested itself in a lower number of sleep bouts but a strong increase in the length of these sleep bouts (Fig.

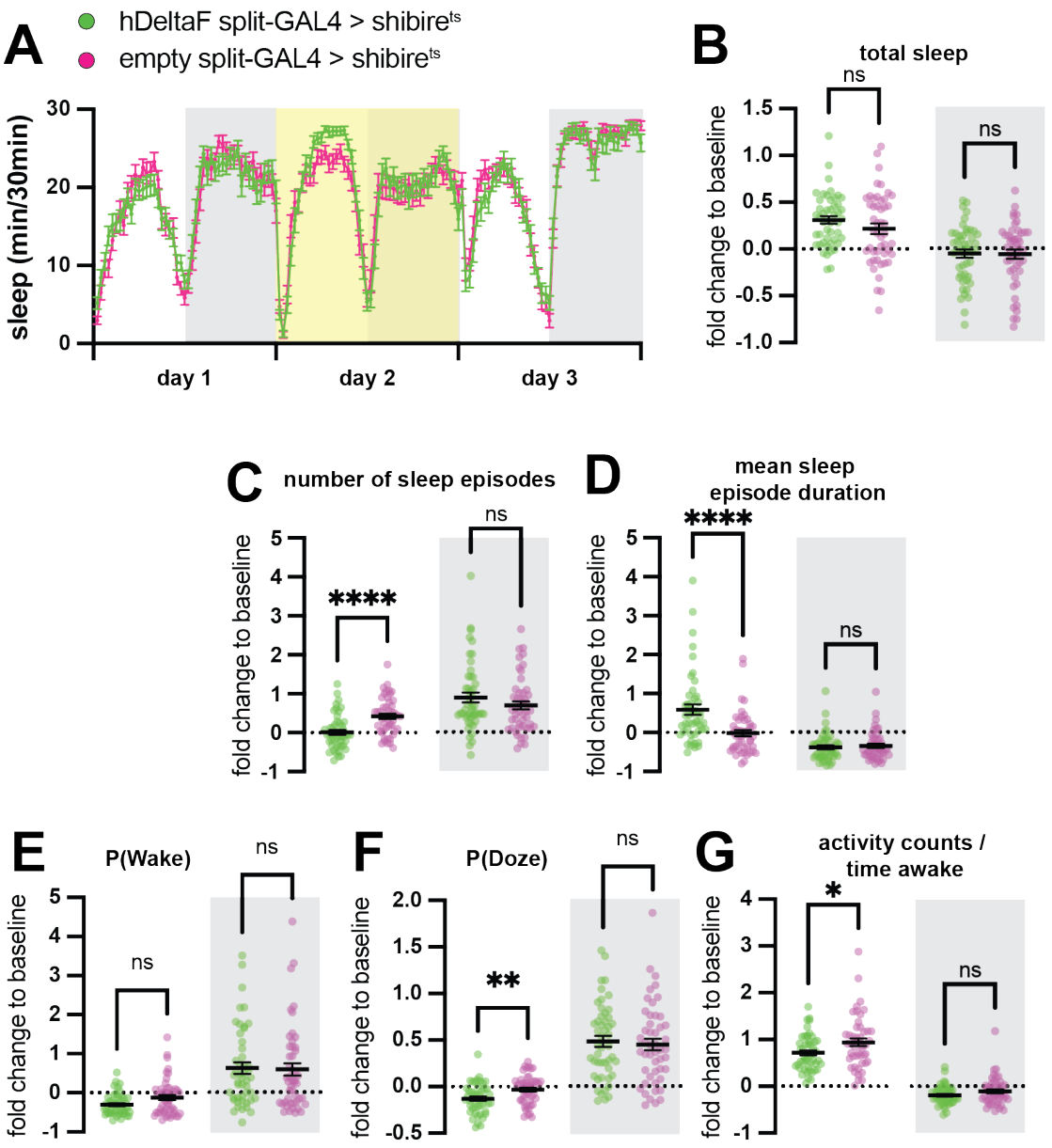

Figure 5.9: Blocking of hDeltaF neurons' synaptic release changes sleep architecture during the day. A) Sleep profile over three consecutive days of *hDeltaF split-GAL4 > UAS-shibire^{ts}* and *empty split-GAL4 > UAS-shibire^{ts}*. Yellow background indicates 24h of heat induction and activation of shibire^{ts} at 31 °C. B) Fold changes in total sleep during day and night showed no differences between groups. C) Number of sleep episodes were significantly reduced during the day, but unchanged during the night. D) Mean length of sleep episodes were significantly prolonged during daytime, but unchanged during nighttime. E) P(Wake) remained unchanged during day and night. F) P(Doze) was significantly decreased during the day, but not the night. (Caption continued on next page)

Figure 5.9: (Continued from previous page.) G) Decrease in movement during the day, but no fold change in movement between the groups during the night. Significance was calculated between experimental and control group with independent t-test for normally distributed data and Mann-Whitney U test for not-normally distributed data. Stars indicate significance as follows: **** = $p < 0.0001$, *** = $p < 0.001$, ** = $p < 0.01$, * = $p < 0.05$. n = 48 flies in both groups. Individual dots represent individual flies. Bars represent mean ± SEM. Grey shading represents nighttime. hDeltaF split-GAL4: R91D10-AD; R56E07-DBD.

5.9C, D). P(Wake) as a marker of the probability to wake up was unchanged in these flies, which was in line with a consolidated sleep pattern (Fig. 5.9E). The flies' probability to fall asleep on the other hand was reduced during the day, indicating lower sleep pressure, which might be due to the more consolidated sleep when asleep (Fig. 5.9F). Activity was slightly reduced in these flies during the day, which could indicate an involvement of hDeltaF neurons in locomotor activity, although this was unlikely as the activity during the night was unchanged (Fig. 5.9G).

A second approach to decrease synaptic transmission while studying behaviour is through expression of the EKO channel, which hyperpolarizes the cells [234]. This channel is a modified version of the Shaker potassium channel that was genetically engineered to prevent excitability when expressed [234]. Expression of EKO continuously inhibits depolarization of the cells that express the channel and can therefore be used to study behaviour with a lack of neuronal signals from a specific cell type. Here, EKO was expressed in hDeltaF neurons, and the flies' sleep behaviour was analysed and compared to flies that carry the EKO transgene under the empty split-GAL4 promoter.

In mated female flies, expression of the EKO channel did not have any significant effect on the sleep behaviour of the flies (Fig. 5.10). The flies' total sleep during the whole day, as well as during daytime and nighttime did not show any significant differences (Fig. 5.10A,B). The sleep architecture also remained unchanged: the number of sleep bouts did

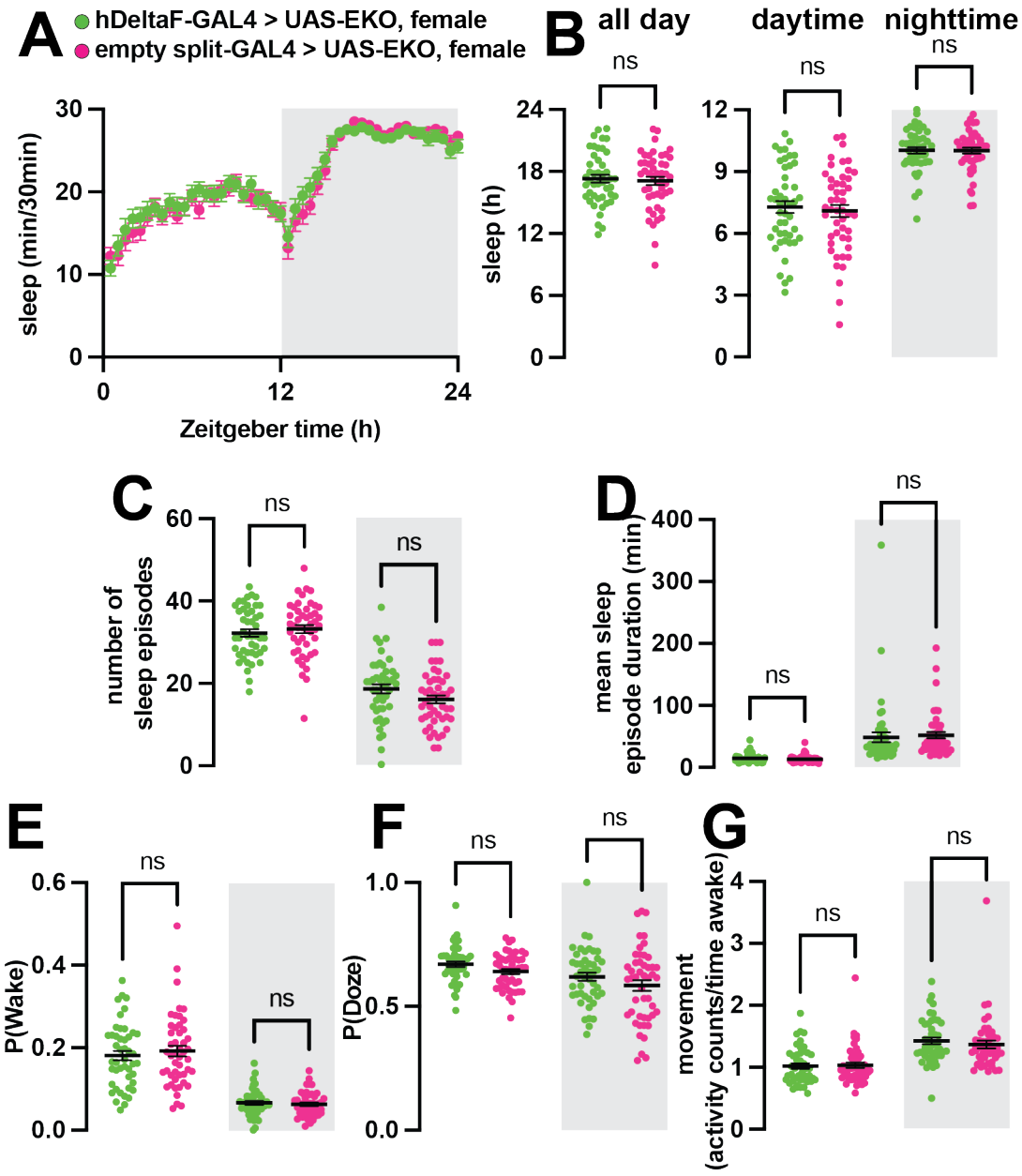

Figure 5.10: Inhibition of hDeltaF neurons with EKO female flies does not change their sleep behaviour. A) Sleep profile over 24h hours of *hDeltaF split-GAL4 > UAS-EKO* flies and *empty split-GAL4 > UAS-EKO* flies. B) No change in total sleep between groups. C) Number of sleep episodes remained unchanged, D) as well as the mean length of the sleep episodes. E) No differences observed in P(Wake) F) and P(Doze). G) Movement activity was unchanged between groups. Significance was calculated between experimental and control group with independent t-test for normally distributed data and Mann-Whitney U test for not-normally distributed data. Stars indicate significance as follows: **** = $p < 0.0001$, *** = $p < 0.001$, ** = $p < 0.01$, * = $p < 0.05$. n = 46-48 flies in both groups. Individual dots represent individual flies. Bars represent mean ± SEM. hDeltaF split-GAL4: R91D10-AD; R56E07-DBD.

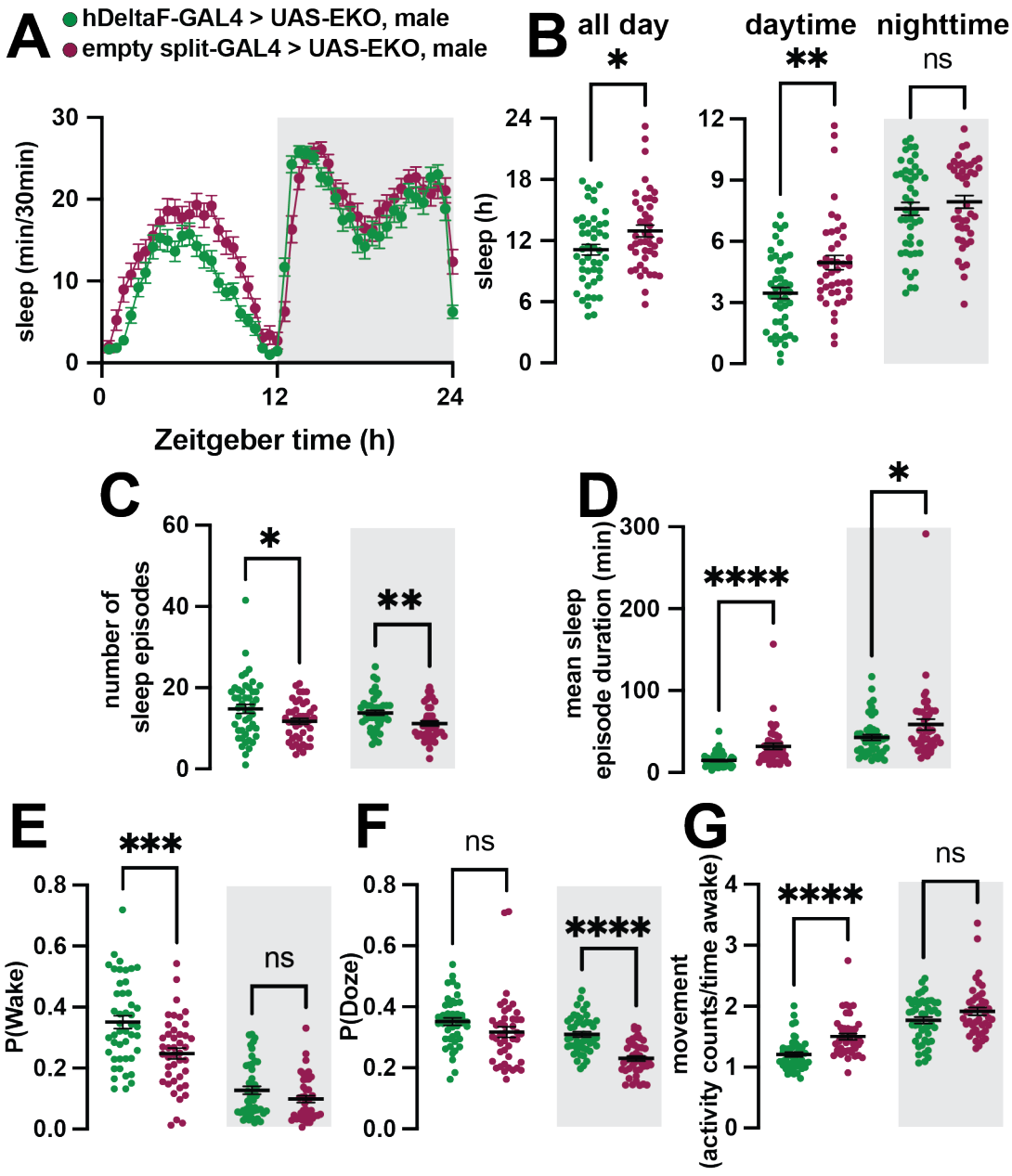

Figure 5.11: Depolarization of hDeltaF neurons in male flies decreases sleep during the day. A) Sleep profile over 24h of *hDeltaF split-GAL4 > UAS-EKO* and *empty split-GAL4 > UAS-EKO* flies. B) Total sleep was reduced when hDeltaF neurons were hyperpolarized. The effect could be seen during the day only. C) Number of sleep episodes were increased compared to control flies, in both daytime and nighttime. D) Sleep episodes were reduced in flies when hDeltaF neurons were inhibited with a strong effect during the day and a smaller effect during the night. E) P(Wake) was increased during the day, but not during the night. F) P(Doze) did not show any differences during the day, but a strong increase during the night. (Caption continued on next page)

Figure 5.11: (Continued from previous page.) G) Movement activity was strongly decreased during the day, but unchanged during the night. Significance was calculated between experimental and control group with independent t-test for normally distributed data and Mann-Whitney U test for not-normally distributed data. Stars indicate significance as follows: **** = $p < 0.0001$, *** = $p < 0.001$, ** = $p < 0.01$, * = $p < 0.05$. n = 43-46 flies in both groups. Individual dots represent individual flies. Bars represent mean ± SEM. Grey shading represents nighttime. hDeltaF split-GAL4: R91D10-AD; R56E07-DBD.

not differ during the day and night (Fig. 5.10C), nor did the average length of the sleep bouts (Fig. 5.10D). Also no changes were observed in the probabilities to change from activity to inactivity or vice versa, as well as in the movement during the waking time (Fig. 5.10E-G). Overall, expression of EKO in hDeltaF neurons did not change the sleep behaviour of mated female flies as compared to control flies (Fig. 5.10).

As TrpA1 activation of hDeltaF neurons differed between the sexes, EKO inhibition was also tested in male flies. Indeed, male flies that express EKO in hDeltaF neurons slept less than control flies, with the main effect during the daytime (Fig. 5.11A). Overall, flies lost almost 2 hours of sleep, with 1.5 hours during the light period (Fig. 5.11B). The overall sleep seemed to be more fragmented, as shown in an increased number of sleep bouts during light and dark (Fig. 5.11C) and a strongly decreased average length of sleep bouts, which was decreased by half during the daytime (Fig. 5.11D). The instability of sleep especially during the day could also be seen in the P(Wake) measurements: the probability to wake up was significantly increased during the day, indicating a less consolidated sleep pattern (Fig. 5.11E). P(Doze) was strongly increased during the night, which indicated higher sleep pressure, potentially due to the fragmented sleep during the night, which might lead to a build-up in sleep pressure (Fig. 5.11F). Further, activity of these flies was strongly reduced during the day (Fig. 5.11G) as was also the case in female flies with shibire inhibition of hDeltaF neurons.

5.2.3 Electrophysiological analysis of the connection from dFBNs to hDeltaF neurons

The connectomic analysis clearly described a strong connection from dFBNs onto hDeltaF neurons, but the nature of the connection remained unknown until now. As previous experiments with the R56E07-GAL4 line had shown that the connection might be diverse based on the RMP of the cell, this time the cells were held at certain membrane voltages. Besides studying the native response of the cells to the activation of dFBNs, different toxins were added in order to block neurotransmitter receptors to verify the neurotransmitter and -receptor responsible for the connection.

5.2.3.1 Optogenetic stimulation of dFBNs elicits response in hDeltaF neurons

As a first approach, CsChrimson was expressed in dFB neurons and red light flashes were used to depolarize these neurons in the same setup as before. hDeltaF neurons were labelled with GFP and patched during the light stimulus, to detect responses to the activation of dFBNs. Cells were held at -30 mV and -60 mV to have two different conditions and to detect any changes in response based on the RMP of the cell.

When cells were held at -30 mV, an activation of dFBNs mainly led to a hyperpolarization of hDeltaF neurons (Fig. 5.12A). Analysis of individual cells revealed a heterogeneous pattern: one cell showed a very sharp inhibition, followed by an excitation, while the majority of cells showed a clear inhibition, with a clear hyperpolarization of the membrane and a lack of action potentials (5 out of 8), and one cell showed a slight excitation, or no change to baseline (Fig. 5.12B). TTX was added to distinguish monosynaptic from secondary inputs. The responses became smaller and predominantly inhibitory, with the

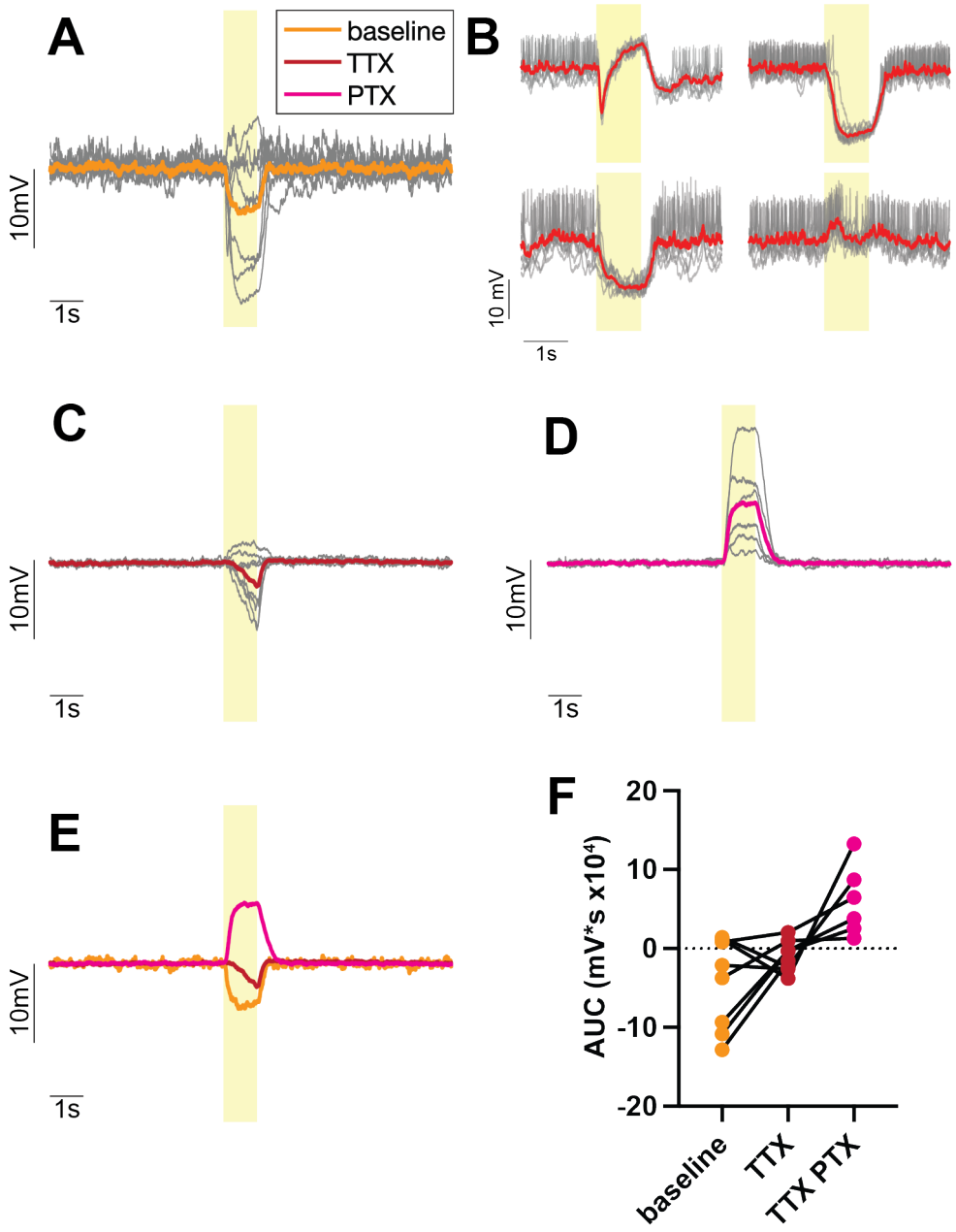

Figure 5.12: Optogenetic activation of dFBNs elicits diverse responses in hDeltaF neurons when held at -30 mV. A) Patch-clamp recordings of hDeltaF neurons showed an overall inhibitory response to the activation of dFBNs. n = 8 cells. B) Representative recordings of hDeltaF neurons during dFBN stimulation. 4 out of 8 recordings from A) plotted. Grey lines indicate individual trials of light stimulation, red line indicates mean per fly. C) Reduced response of hDeltaF neurons to the stimulation of dFBNs in the presence of TTX. n = 8 cells. D) Adding PTX to the bath turned the response into a depolarization. n = 6 cells. (Caption continued on next page)

Figure 5.12: (Continued from previous page.) E) Overlay of mean responses of A), C) and D). F) Quantification of area under the curve. Individual points represent individual cells. Yellow shading indicates light stimulation. Individual traces shown in grey represent an average of 10 repeated stimulations per cell. Mean of all recorded cells is plotted in bold, coloured. Flies were fed with ATR.

inhibition becoming stronger during the duration of the stimulus (Fig. 5.12C). As dFBNs are expected to be mainly glutamatergic [132] and the main inhibitory glutamate receptor is the glutamate-gated chloride channel, picrotoxin (PTX, 100 µM) was added to the bath to block this receptor [72, 76]. Surprisingly, the response was not removed, but instead became a strong depolarizing response (Fig. 5.12D,E).

Recording from hDeltaF neurons while holding them at -60 mV and activating dFBNs resulted in an excitatory response (Fig. 5.13A). All neurons except one showed a depolarization that lasted the entire duration of the stimulus. Adding TTX revealed that the cells are indeed connected monosynaptically, but the resulting excitation was much smaller than without TTX (Fig. 5.13B). Finally, PTX was added which increased the response to levels above baseline (Fig. 5.13C, D). When looking at the changes in single cells, it became clear that all cells decreased the intensity of their response in the presence of TTX, and all cells increased their response above baseline levels when PTX was added (Fig. 5.13E).

A potential explanation of the excitation might be leaky expression of the CsChrimson transgene in hDeltaF neurons [235]. Therefore, we recorded from hDeltaF neurons upon light stimulation in flies that carried the LexAop-CsChrimson transgene, but no LexA driver to drive its expression [236]. Recordings in these flies showed no response to the light stimulus in hDeltaF neurons. This held true under all tested experimental conditions: holding the cells at -60 mV showed no detectable response, also not when TTX or PTX

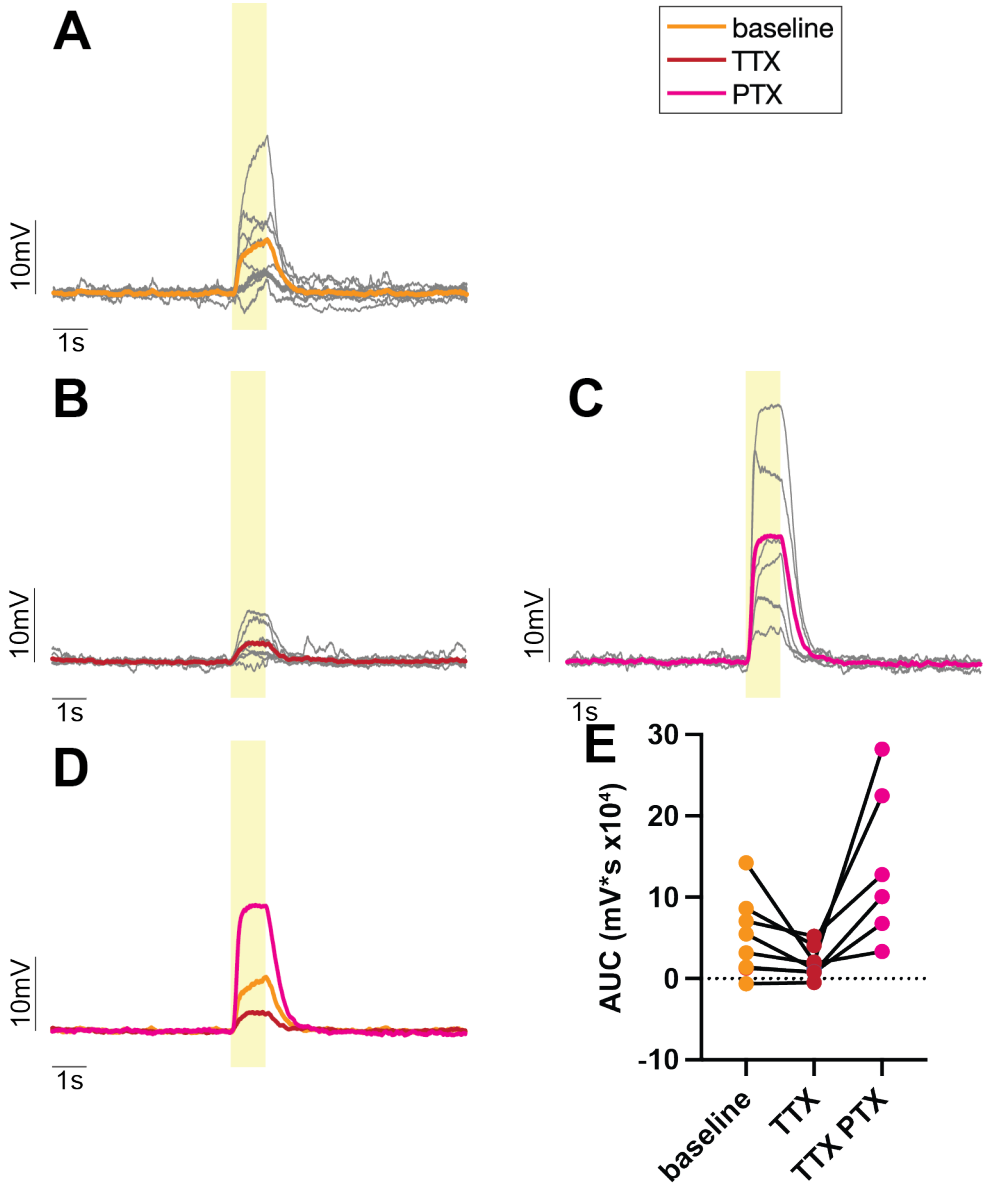

Figure 5.13: Optogenetic activation of dFBNs elicits an excitatory response in hDeltaF neurons, when held at -60 mV. A) Patch-clamp recordings of hDeltaF neurons revealed a depolarization in response to dFBN stimulation. n = 8 cells. B) Depolarization remained present in the presence of TTX. n = 8 cells. C) Light stimulation of dFBNs with further addition of PTX (with TTX) elicited a strong depolarizing response. n = 6 cells. D) Comparison of the mean traces of the different conditions from A, B and C. E) Quantification of the area under the curve (AUC) during light stimulation. Individual points represent mean of 10 repeated stimuli of one cell. Yellow shading indicated light stimulation. Individual traces shown in grey represent an average per cell. Mean of all recorded cells is plotted in bold, coloured. Flies were fed with ATR.

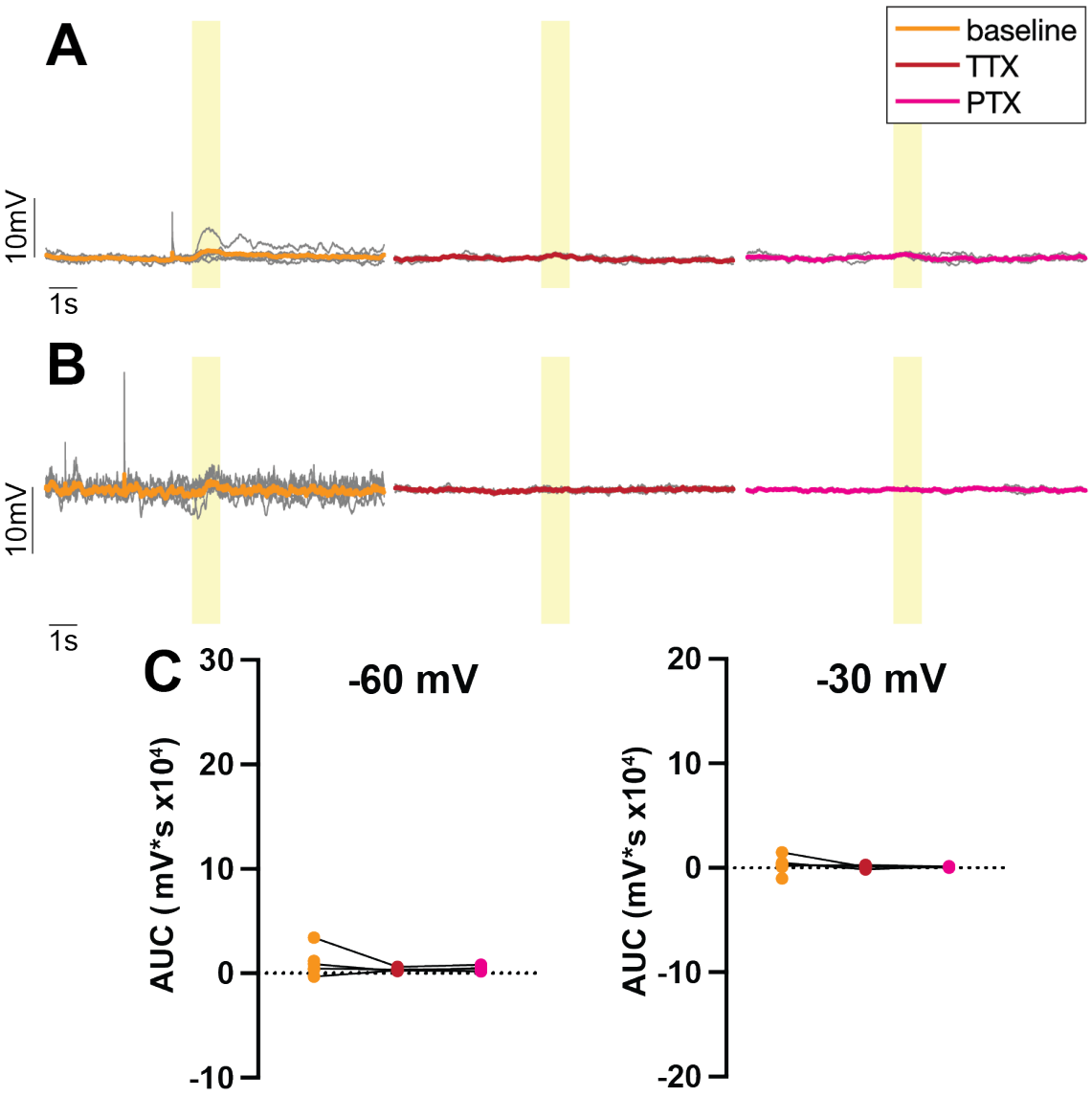

Figure 5.14: Light stimulation does not elicit a response in hDeltaF neurons. Recordings of *+ > LexAop-CsChrimson, hDeltaF split-GAL4 > UAS-GFP* neurons did not respond to light when A) held at -60 mV, neither after the application of TTX and PTX (n baseline = 7 cells, n TTX = 4 cells, n PTX = 4 cells.) B) Recordings of the same cells as in A), when held at -30 mV verified that light stimulation did not elicit a response. (n baseline = 6 cells, n TTX = 4 cells. n PTX = 3 cells) C) Quantification of area under the curve during the 1 second of light stimulation of cells in A) and B). Individual points represent mean of individual cells. Lines connect same cells with added toxins. Yellow shading represents light stimulation. Flies were fed with ATR.

were added (Fig. 5.14A,C). The same results were observed when the cells were held at -30 mV, to verify that the RMP did not mask any underlying response. During the second half of the stimulation, a very small depolarization could be seen, but addition of TTX fully abolished this response, proving that it is not due to CsChrimson expression in hDeltaF neurons (Fig. 5.14B, C). The small depolarization might hint at a light response arriving at hDeltaF neurons via certain inputs or leaky expression in other neurons in the upstream circuitry. Due to the small size of the signal, this effect was negligible for the previously presented experiments and the observed effect could indeed be attributed to the biological characteristics of the circuit.

The experiments described here showed that dFBNs form functional monosynaptic connections with hDeltaF neurons, but the polarity of the signal depends on the RMP of the postsynaptic cell. When the cells are hyperpolarized the signal will be predominantly excitatory, but when the cells are already depolarized, the signal will be mainly inhibitory as transmitted via GluCl channels. Further, there is a second, excitatory signal acting in this synapse which becomes especially apparent when the inhibitory signal is blocked.

5.2.3.2 The connection between dFBNs and hDeltaF neurons is driven by glutamate

The connection between dFBNs and hDeltaF neurons is made up by two different elements: either two neurotransmitters, dFBNs are likely glutamatergic [132], but might be co-transmitting acetylcholine [55] and AstA [129], or by, at least, two different sets of receptors on hDeltaF neurons. To disentangle these options, optogenetic activation of dFBNs was replaced by direct pressure ejection of glutamate onto hDeltaF neurons. This setup allowed the study of glutamate-specific changes in the membrane potential of

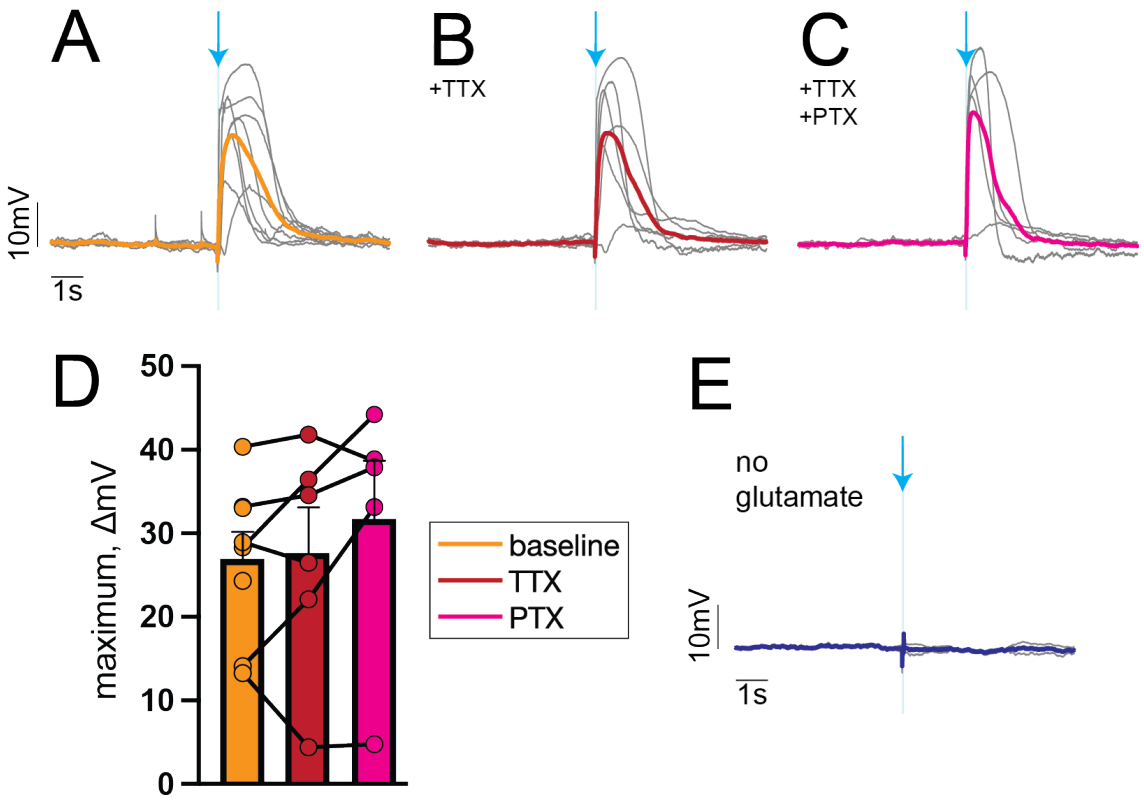

Figure 5.15: Glutamate elicits depolarization when applied onto hDeltaF neurons held at -60 mV. A) Pressure ejections of 1 mM glutamate directly onto hDeltaF neurons led to strong membrane depolarization. n = 10 cells. B) Depolarization by glutamate remained present throughout the addition of TTX. n = 6 cells. C) hDeltaF neurons showed depolarization upon glutamate application also in the presence of TTX and PTX. n = 5 cells. D) Quantification of the maximum change in membrane voltage as a measurement of depolarization. Individual points represent individual cells. Lines connect the same cell during experimental conditions. E) Pressure ejection onto hDeltaF neurons without glutamate did not elicit any change in membrane potential. n = 2 cells. Blue shading and arrow represent 50 ms of glutamate pressure ejection. Grey lines indicate mean per cell. Coloured, bold lines indicate mean of all cells.

hDeltaF neurons, without the potential of confounding effects by a secondary signalling molecule.

In line with the previous experiments, patch-clamp recordings were performed from GFP-labelled hDeltaF neurons while holding the cells at -60 mV. Short puffs of glutamate were applied directly onto the fan-shaped body, where it binds to receptors on hDeltaF neurons, amongst others. Glutamate elicited a strong depolarization in all recorded cells (Fig. 5.15A). The shape and timing of the depolarization differed between cells, likely due

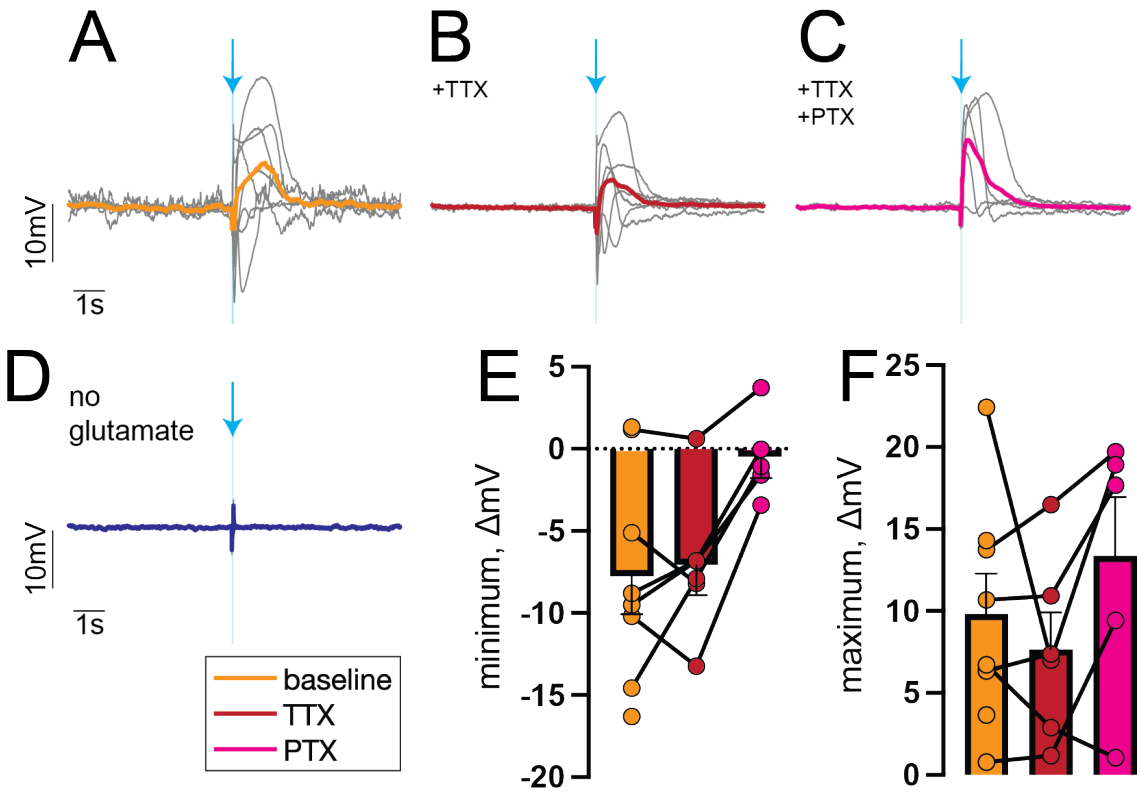

Figure 5.16: Glutamate elicits several responses in hDeltaF neurons when held at -30 mV. A) Pressure ejection of glutamate on hDeltaF neurons elicited a mix of hyper- and depolarizing currents. n = 8 cells. B) Glutamate application in the presence of TTX showed a decreased response in hDeltaF neurons. n = 6 cells. C) Further addition of PTX eliminated any inhibitory response in hDeltaF neurons. n = 5 cells. D) Pressure ejection without glutamate did not change the membrane voltage of hDeltaF neurons. n = 2 cells. E) Quantification of maximal negative deflection in membrane voltage in hDeltaF neurons upon glutamate application. F) Quantification of maximal positive deflection in membrane voltage in hDeltaF neurons upon glutamate application. Individual points represent individual cells, data from A, B and C. Blue shading and arrow represent 50 ms glutamate application. Grey lines indicate mean per cell. Coloured, bold lines indicate mean of all cells.

to the placement of the ejection pipette. TTX was added, which did not change the cells' response to glutamate, supporting the conclusion that glutamate acts directly on these cells (Fig. 5.15B). Last, PTX was added to replicate the previous experiments, which also did not change the response significantly (Fig. 5.15C, D). Importantly, no change in membrane potential was detected, when pressure ejection was performed with extracellular solution only (Fig. 5.15E), supporting the claim that the depolarization was specifically due to the effect of glutamate.

Next, the cells were held at -30 mV to see how glutamate would act on a more depolarized membrane potential. Here, a striking picture could be seen: glutamate application elicited a quick hyperpolarization, followed by a depolarizing effect (Fig. 5.16A), suggesting that glutamate could inhibit and excite a cell at the same time. The effects differed slightly between cells, again likely due to the positioning of the ejection pipette. In the presence of TTX, the effect remained consistent, only with a slightly decreased amplitude, which verified that the observed effect was a direct effect of glutamate on hDeltaF neurons (Fig. 5.16B). Finally, addition of PTX blocked the hyperpolarizing effect, verifying that it was indeed gated via GluCl channels (Fig. 5.16C, E, F). These experiments nicely replicated the findings obtained when dFBNs were stimulated optogenetically, suggesting that the synaptic connection between these two cell types is mainly, or exclusively, maintained by glutamate.

Last, now that GluCl was shown to be one of the receptors connecting dFBNs and hDeltaF neurons, the effects of the receptor on sleep behaviour was tested. Using two RNAis and a CRISPR/Cas9 knockout (KO) approach, GluCl expression was reduced or abolished in hDeltaF neurons. The three approaches revealed different results, hence interpretation of

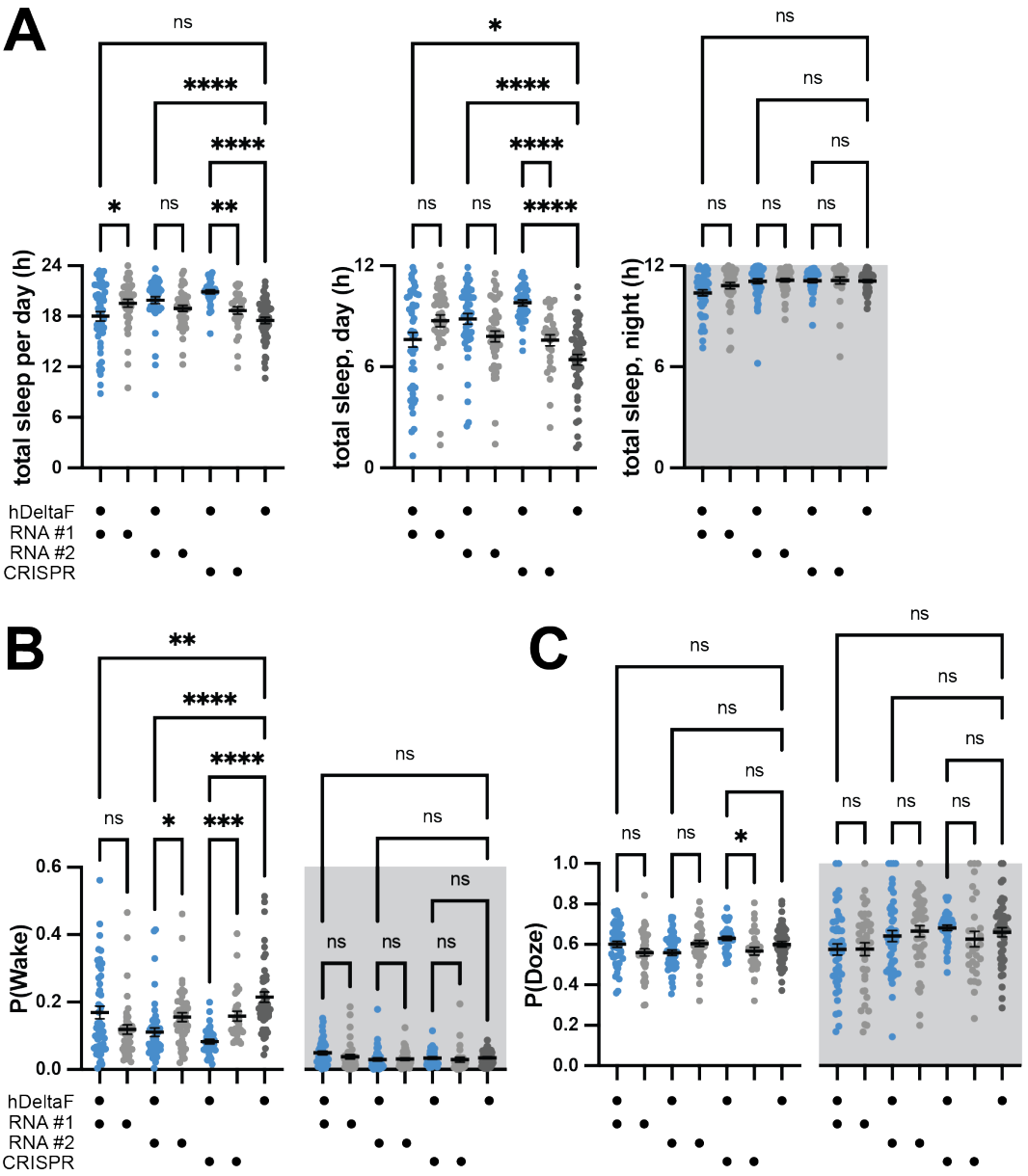

Figure 5.17: Knockdown of the glutamate receptor in hDeltaF neurons has equivocal effect on the sleep behaviour. A) Total sleep in flies with a knockdown of GluCl was unchanged with both RNAi lines and increase with by CRISPR/Cas9 knockout. (Caption continued on next page)

Figure 5.17: (Continued from previous page.) B) P(Wake) was decreased for RNAi #2 and CRISPR KO during the day. No change in P(Wake) during the night. C) P(Doze) remained unchanged during day and night for all groups. RNA #1: 107971KK RNA #2: 105754KK CRISPR: UAS-GluCl gRNA, UAS-Cas9. Significance was calculated between the experimental group and their two parental controls. **** = $p < 0.0001$, *** = $p < 0.001$, ** = $p < 0.01$, * = $p < 0.05$, ns = $p > 0.05$ n = 29-47 flies. Individual dots represent individual flies, bars represent mean ± SEM.

the results remained difficult. Total sleep was significantly increased in the CRISPR KO flies, with the change only during the daytime (Fig. 5.17A). The two RNAi lines changed sleep only compared to one parental control, hence no judgements about the significance can be made (Fig. 5.17A). P(Wake) was significantly reduced with RNAi #2 and CRISPR KO during daytime only, no change in RNAi #1 (Fig. 5.17B). P(Doze) on the other hand remained unchanged in all groups (Fig. 5.17C). Sleep architecture remained mainly unchanged, only RNAi #2 presented a strong decrease in number of sleep episodes during the day (Fig. 5.18A) and an increase in the mean sleep episode duration (Fig. 5.18B). Last, all groups showed slight differences in their mean activity counts compared to their controls, which might be driven by the *hDeltaF>CS* control that showed very little activity in general, hence all other groups seemed to have an increase in activity levels (Fig. 5.18C). Overall, the manipulations did not affect sleep strongly, but the efficiency of the RNAi KD and the CRISPR KO need to be verified.

5.3 Discussion

This chapter is the first work to date that studies hDeltaF neurons in detail. I first studied their neuronal connections based on the published connectome data, followed by a dissection of sleep behaviour based on different manipulations of hDeltaF neurons, and finished with studies of functional connectivity between dFBNs and hDeltaF neurons.

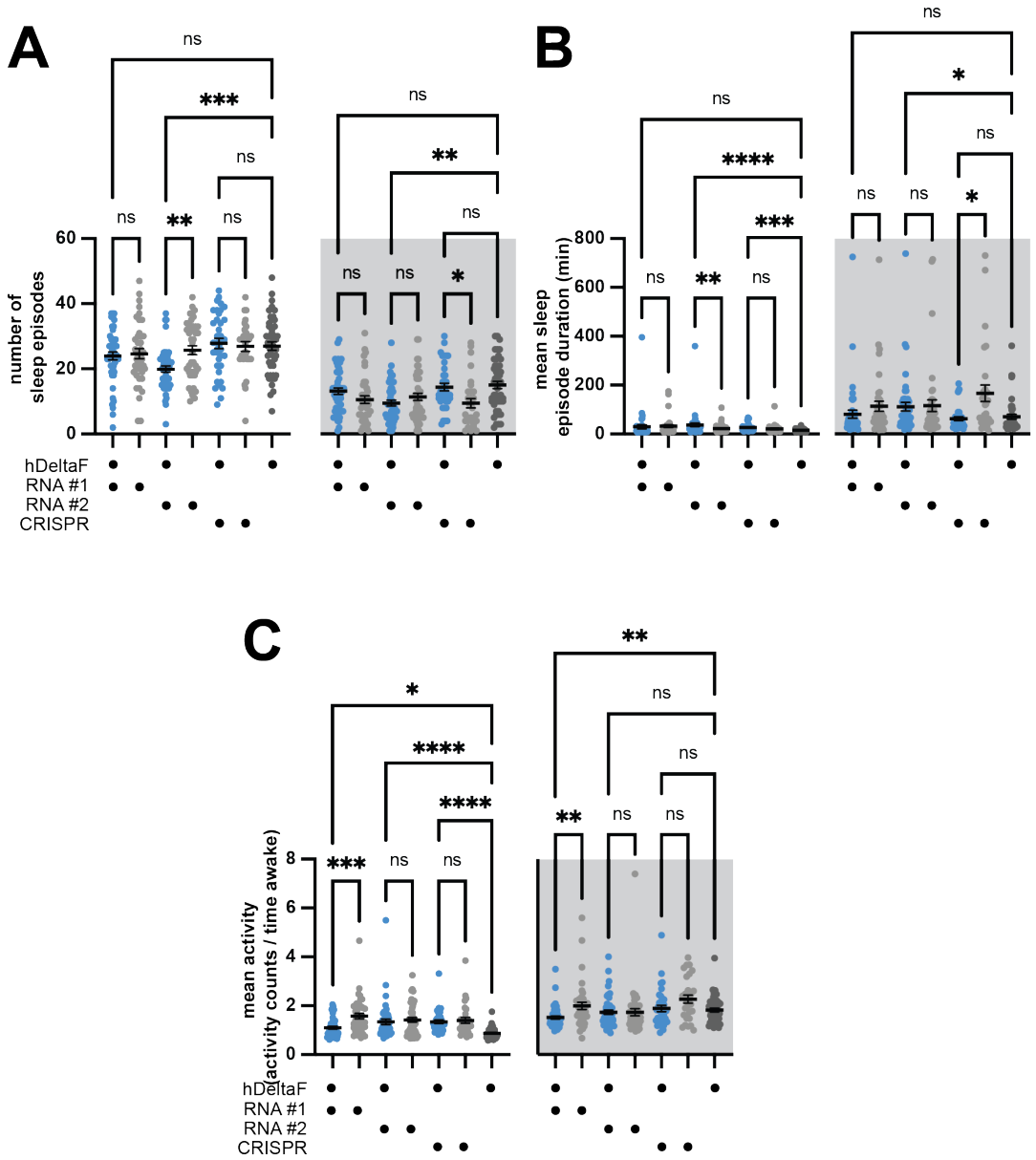

Figure 5.18: Removal of GluCl in hDeltaF neurons induce only minor changes in sleep architecture. A) The number of sleep episodes was significantly reduced only with RNAi #2 during the day, but no changes during the night for any group. B) Mean sleep episode duration remained unchanged with RNAi #1 and CRISPR KO. RNAi #2 significantly decreased sleep episode duration during the day.

Figure 5.18: (Continued from previous page.) C) Mean activity counts in all groups were different to one parental group, but not the other during the day. During the night, KD of GluCl with RNAi #1 decreased the flies' activity. RNAi #2 and CRISPR KO did not affect activity levels at night (Kruskal-Wallis test). RNA #1: 107971KK RNA #2: 105754KK CRISPR: UAS-GluCl gRNA, UAS-Cas9. Significance was calculated between the experimental group and their two parental controls. **** = $p < 0.0001$, *** = $p < 0.001$, ** = $p < 0.01$, * = $p < 0.05$, ns = $p > 0.05$ n = 29-47 flies. Individual dots represent individual flies, bars represent mean ± SEM.

5.3.1 hDeltaF neurons connect a sleep centre with neurons encoding goal angle representation

The connectome presents a clear picture for the hDeltaF circuitry: these neurons form an intermediary step that integrates sleep promoting information from dFBNs, feeds this information forward to a navigational circuit, and back to several other groups of neurons. Overall the downstream targets can be described in four groups: first, input to FC2 cells, which will be discussed below, second, a potential feedback loop to dFBNs, via FS3 cells and the superior protocerebrum, third, a connection to non-dFBN FB6 neurons and last, connections to other columnar neurons in the FB (hDelta and vDelta neurons) (Fig. 5.4, fig. 5.5).

The strongest output of hDeltaF neurons is onto a navigational circuit via FC2C neurons (Fig. 5.4, [123]). FC2 cells have been shown to encode the goal angle of the fly and artificially changing the location of the calcium activity bump in FC2 cells can induce a change in the walking direction [123]. FC2 cells project onto PFL2 and PFL3 cells, which are integrating incoming information about heading direction and goal angle, and compute the directional movement cues of the animal through output onto locomotor circuits [122, 123]. Interestingly, dFBNs also form direct connections to FC2 cells (Fig. 3.2), suggesting that there is a direct and an indirect pathway from the sleep circuit onto the navigational centre. The interaction of a sleep circuitry with the navigational circuitry will be discussed

in detail in chapter 7.

The feedback onto non-dFB neurons in layer 6 is interesting, as it actually suggests a differential role of at least two groups of neurons in layer 6 of the FB. dFBNs are not targeted very strongly by hDeltaF neurons, while the non-dFBNs in layer 6 are. What the intrinsic and functional differences between these two cell types are, needs to be studied in more detail, but they do not seem to be distinguished based on known neurotransmitter expressions [55]. Heterogeneity within neurons that are anatomically similar to R23E10-GAL4 neurons, and therefore likely in layer 6, have been shown on a behavioural and pharmacological level: activation of different sets of dFB-like neurons resulted in different effects on sleep induction (sometimes none or even wake promoting) [55, 134]. Further, dopamine as well as serotonin receptors have been shown to be expressed only in a subset of dFBNs and layer 6 neurons [134, 135], and some neurons in layer 6 of the FB can influence food choice [237, 238]. Whether these neurons overlap with dFBNs or not needs to be verified. Thus it is likely that not all layer 6 neurons encode sleep relevant signals and hDeltaF neurons target the neuronal group with unknown function.

One strong single cell type connection by hDeltaF neurons is onto PFG neurons, a cell type that also presents very strong bidirectional connections to dFBNs (compare figure 5.4, fig. 3.1 and fig. 3.2). Only very recently have these cells been studied, with one study not detecting a sleep phenotype during activation [160], while another study tested four different split-GAL4 lines and found a strong sleep promoting effect during activation in two out of four lines in females, but not in males [55]. Further, these cells will be interesting to study, due to their signalling molecules: they were shown to express the neurotransmitter tyramine, as well as the neuropeptides Mip and Dh31 [55].

An unusual feature of hDeltaF neurons that results from the EM data, is the way they divide the FB into 6 columns [44]. hDeltaF neurons are the only hDelta neurons that have this division, all other hDelta neurons divide the FB into 8 or 12 columns [44]. Interestingly, this division does not seem to be conserved in the neurons' downstream circuits, as all their main postsynaptic partners (FC, FS3 and PFG neurons) divide the FB into 9 columns [44].

5.3.2 The role of hDeltaF neurons in the control of sleep

I was able to show that activation of hDeltaF neurons decreased sleep, which was validated by a recent paper [55]. Surprisingly this effect presented differently depending on the sex and mating status of the fly (Fig. 5.6). Interestingly, also the behaviour upon inhibition of hDeltaF neurons differed between the sexes (compare figure 5.10 and 5.11). Based on stainings of expression patterns of *fruitless* and *doublesex*, hDeltaF neurons are unlikely to be sexually dimorphic intrinsically [239–241], but differences in the circuitry can only be identified once the male connectome becomes available. Differences in baseline sleep behaviour between male and female flies are known [102–104], as well as the effect of mating on female flies [232]. Interestingly, a recent study found a similar sex difference in sleep behaviour upon TrpA1 stimulation: When activating OA-VPM3 neurons male flies showed a much stronger decrease in sleep than female flies [180]. Also in this example, no differences in expression pattern by the GAL4 line could be detected [180], which resembles the results obtained here with hDeltaF neurons. Activation of OA-VPM3 neurons was shown to induce courtship behaviour in males, but not in female flies [180], suggesting that hDeltaF neurons might also encode further behavioural information that might differ between the sexes and lead to differences in sleeping behaviour.

To test if hDeltaF neurons form a relevant sleep control centre or if they primarily fine

tune the behaviour, the effect of a lack of signalling from hDeltaF was tested. In mated female flies, no significant change in sleep amount could be observed (Fig. 5.10, fig. 5.9), suggesting that hDeltaF neurons encode a signal that can be wake promoting, but in itself is not necessary for the induction of wakefulness. hDeltaF neurons are likely not the main sleep control centre of the fly, but rather a population whose activity can shape the waking time of the fly if necessary.

On the other hand, hyperpolarizing hDeltaF neurons in male flies reduced and fragmented sleep (Fig. 5.11). This effect is surprising, as it suggests that activation as well as inhibition of the same population of neurons could have the same effect on the sleep behaviour of the animal (compare figs. 5.11 and 5.6). Analysing the details revealed that the two manipulations did no have the exact same effects: activation of hDeltaF neurons decreased sleep mainly during the night while inhibiting hDeltaF neurons decreased sleep mainly during the day. To understand this phenomenon better, it would be interesting to study spontaneous hDeltaF activity during day and night. Are there intrinsic differences that could explain the effects of the manipulations? Does light or zeitgeber time play a role? To further verify this result, inhibition of hDeltaF neurons should be performed under temporal control, e.g. with shibire^{ts}. This would exclude any potential developmental effect of the manipulation.

A second relevant finding in these experiments is the decrease in movement in male and female flies during the day but not during the night, when activity of hDeltaF neurons was changed (Fig. 5.7, fig. 5.9 and fig. 5.11). This might suggest an involvement of hDeltaF in navigational strategies of the fly. Inhibiting a navigational signal might lead to lack of orientation of the fly. A potential consequence might be that the overall movement of the

fly is reduced, as it does not have a direction to navigate to. As most studies only look at changes during the whole day, rather then separating findings into day and night, changes in activity levels cannot be compared [55, 160].

5.3.3 Functional connection of dFBNs onto hDeltaF neurons

As had been suggested by the connectome, we can verify that hDeltaF neurons form a functional connection with dFBNs. This connection proved to be much more diverse than expected, with the signal from dFBNs eliciting different responses in hDeltaF neurons. Interestingly, the results obtained here resemble the results obtained with the R56E07-GAL4 line in the previous chapter (Fig. 4.9), which underlines the reliability of these findings.

Holding the cells at two different membrane potentials revealed striking differences: holding the cells at -30 mV results in an overall inhibition, while holding the cells at -60 mV makes the synaptic input from dFBNs excitatory (Fig. 5.12, fig. 5.13). These changes suggest chloride to be a driving force in this connection, as chloride channels have been shown to have different polarities at different membrane voltages [242]. Further, several studies proved how in the fly applications of GABA can elicit currents of different polarity based on the membrane voltage of the cell [72, 243]. The exact reversal potential of chloride depends on the solutions used in the experiment. The solutions used in this thesis contain the same chloride concentrations as used by other labs [122–124, 138, 139, 162, 244–247], differences only occur in the sugar concentration used in the extracellular solutions. Even lower intracellular chloride concentrations are used by [208], which drive the reversal potential to more negative values. The composition of these solutions was chosen to have a GABA reversal potential near the chloride reversal potential and the spike threshold close to -40

mV, as was proven experimentally [248].

Considering that chloride could be a driving force in the connection, and that dFBNs are likely glutamatergic [132], the glutamate-gated chloride channel GluCl was a likely candidate to facilitate the connection. Blocking GluCl by applying PTX in high concentrations [72, 76] led to surprising results: it did not block the connection as would have been expected, but revealed a strong excitatory response (Fig. 5.12, fig. 5.13). This suggests that GluCl was blocked, but there is a secondary excitatory signal in the same synapse. These two signals might be encoded in two ways: either via the use of two signalling molecules in dFBNs, or via two different receptor types in hDeltaF neurons.

Direct applications of glutamate replicated the findings obtained by optogenetic stimulation of dFBNs, hence the connection between dFBNs and hDeltaF neurons only relies on one NT to transmit this diverse signal. This data presents a surprising finding: at the same synapse, glutamate is responsible for two different types of responses: an inhibitory response via GluCl, and an excitatory response. The receptor for the latter still needs to be identified, but likely candidates would be AMPA or NMDA receptors [77, 249]. While this data does not argue that glutamate is the sole neurotransmitter used by dFBNs, it does imply that glutamate is likely the main transmitter used by dFBNs to target hDeltaF neurons. Other downstream targets might be connected via different transmitters [129].

The data here cannot yet be compared to other synapses in the FB, because no other group has analysed such a connection in this amount of detail. Most studies of hDelta neurons in the FB have relied on calcium imaging methods [94, 121, 124, 191], which miss out of the fine tuned details of the synapse. The calcium imaging approach here (Fig. 4.7) also did not resolve the details that appeared in patch-clamp recordings (Fig. 4.9, 4.12, 5.12,

5.16).

6 | Connections between the EB and the dFB

6.1 Introduction

In the previous chapter, hDeltaF neurons were studied in detail, as they present the strongest synaptic connection downstream of dFBNs. Although important, it is not the only cell type that exhibits significant connections with dFBNs. Many other cells types could be identified that convey relevant information onto dFBNs or receive information from dFBNs and transmit it downstream to the wider circuitry.

In this chapter, hDeltaK and ExR3 neurons were analysed more closely. These cells are of special interest, as they form a connection between the EB and dFBNs. The connection of these two neuropils is especially important, as both regions have been implied in the regulation of sleep [126, 127, 129, 130, 157].

hDeltaK neurons form the main synaptic input to dFBNs, but also receive synaptic input from dFBNs themselves. Anatomically, these neurons are especially interesting, as they are the only type of hDelta neurons that receive input not only in the FB, but also in the EB [44]. Behaviourally, these neurons have been suggested to partake a role in olfactory navigation [124, 190, 191], and in sleep regulation during social isolation [148].

The second group of neurons studied here are ExR3 neurons [44, 250]. While their connections to dFBNs are not as strong as the ones formed by hDeltaK neurons, they also connect bilaterally to dFBNs. There is only one ExR3 neuron per hemisphere, each with extensive neurites in several brain areas: including the SMP, FB and EB [250]. ExR3 neurons are expected to be serotonergic [250], which is interesting as the serotonin receptor

5-HT2B has been implicated in sleep regulation on a subset of dFBNs [135], but the source of serotonin has not been mapped to a specific neuron.

A recent study has analysed similar parameters, confirming some of the results obtained here [55]. In this chapter, both cell types were studied during acute neuronal activation via TrpA1 as well as during blocking of synaptic signalling via *shibire*^{ts}. Both manipulations revealed a wake-promoting effect in these neurons. I then performed functional connectivity experiments, verifying the synaptic input from hDeltaK onto dFBNs.

6.2 Results

6.2.1 Manipulation of hDeltaK neurons increases wake

hDeltaK neurons receive the majority of their synapses from PFG neurons, followed by hDeltaB, ExR3 and FB6A neurons (Fig. 6.1A). Downstream, they target mainly FB6A and PFG neurons, together forming almost 75% of all their output connections (Fig. 6.1B). Unlike hDeltaF neurons, hDeltaK neurons appear to focus their synaptic output onto very few pathways, underlining the importance of their connection with dFBNs, in the form of their connection with FB6A.

hDeltaK neurons can be labelled with several split-GAL4 lines, two of which were used for the following experiments: SS63089 and SS54676 [55]. Both lines label the same neurons, hence this should confirm the specificity of the observed behavioural results to the targeted neurons.

To get a first idea whether hDeltaK neurons might be relevant for the regulation of sleep, as was suggested previously [148], sleep behaviour was analysed during artificial activation

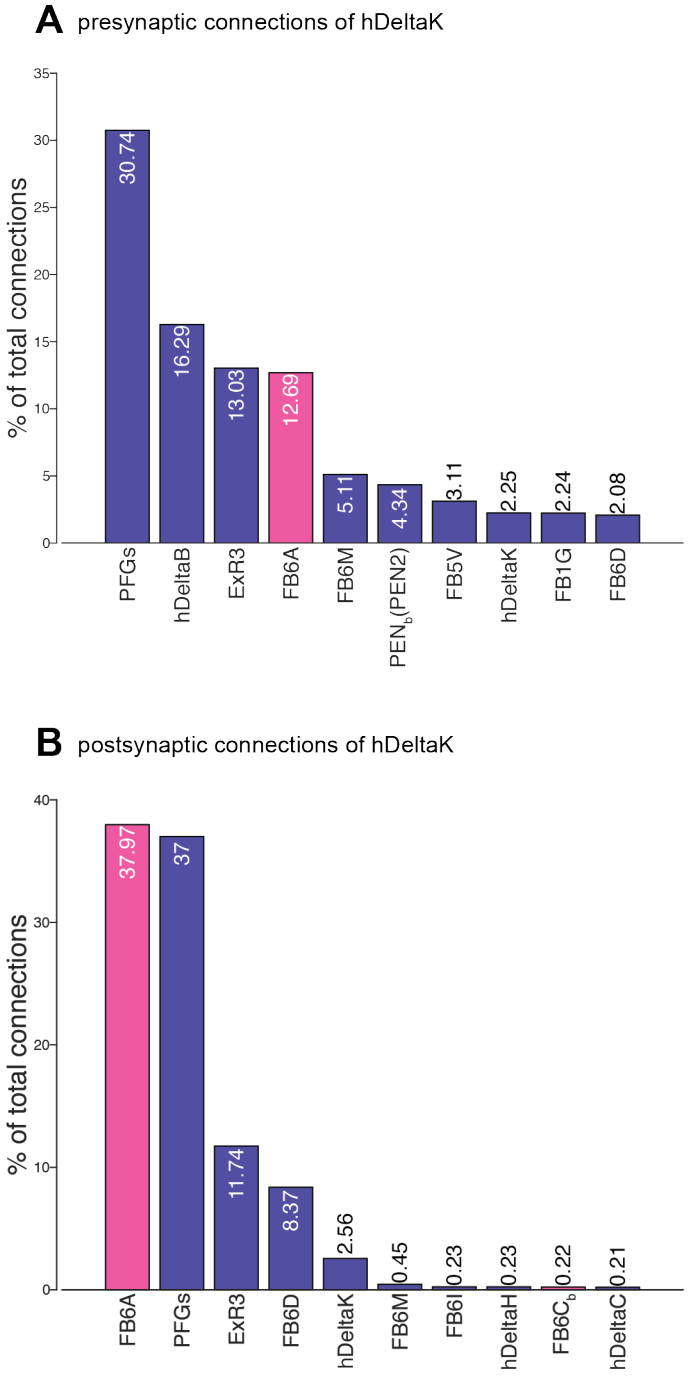

Figure 6.1: hDeltaK neurons are strongly connected to dFBNs. A) Top 10 presynaptic connections of hDeltaK neurons. B) Top 10 postsynaptic connections of hDeltaK neurons. dFBNs are labelled in pink. Unannotated connections were removed from the analysis. Raw data obtained from Hemibrain v1.2.1 [43, 165].

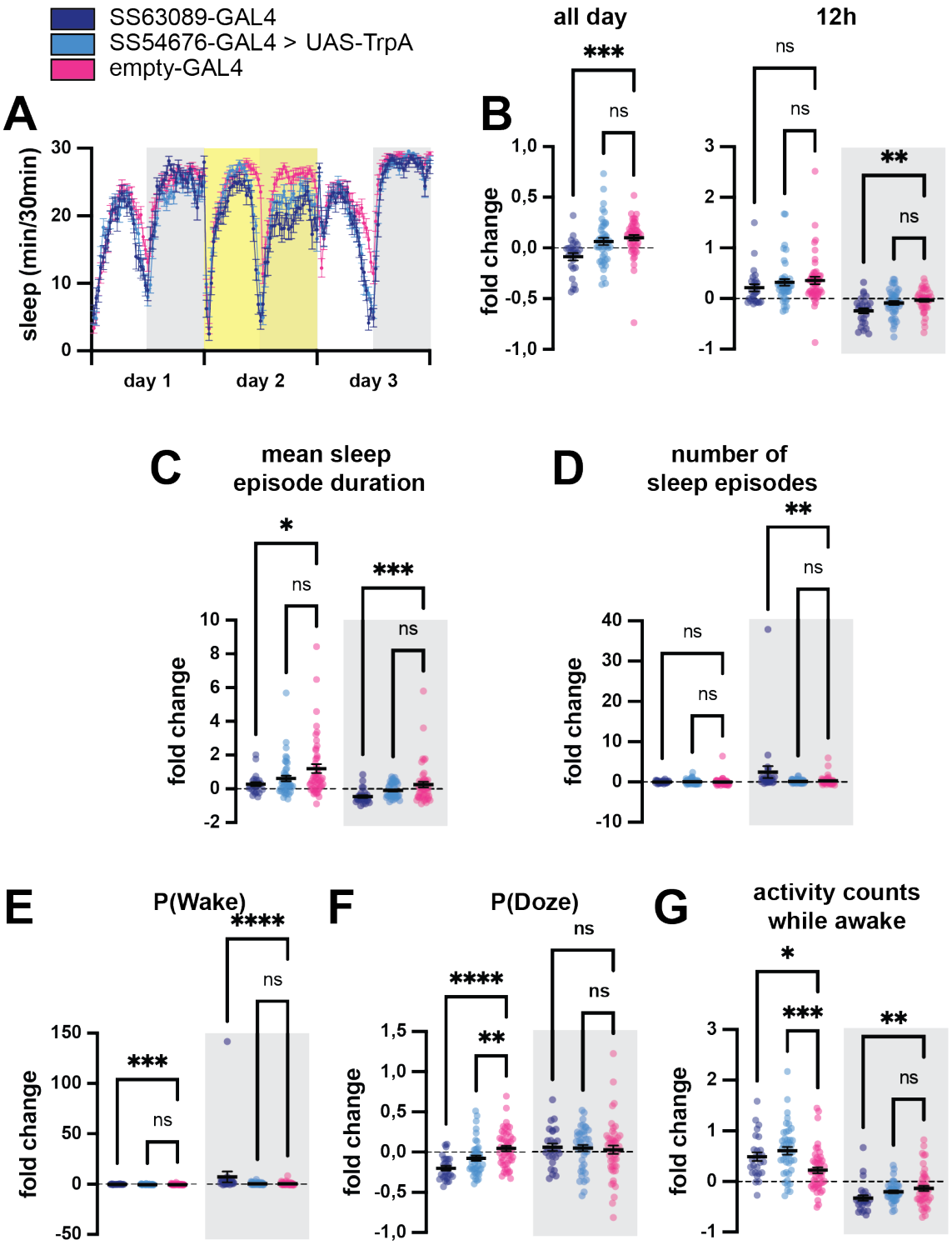

Figure 6.2: Activation of hDeltaK neurons decreases sleep. A) Sleep profile over three consecutive days in flies that express UAS-TrpA1 in hDeltaK neurons, with day two as the heat activation day (indicated in yellow). B) Only SS63089 decreased total sleep compared to the baseline day, during the whole day, as well as during nighttime only. (Caption continued on next page)

Figure 6.2: (Continued from previous page.) C) Mean sleep episode duration was reduced in SS63089 during day and night, but unchanged in SS54676. D) Only SS63089 showed a significant increase in number of sleep episodes during the night time. E) P(Wake) was significantly increased during day and night in flies with SS63089 neurons activated. F) P(Doze) was significantly decreased during the day when hDeltaK neurons were activated with both lines, but no change during nighttime. G) Activity of the fly was increased during the daytime of hDeltaK activation. During the nighttime SS63089 showed a significant decrease while SS54676 remained unchanged. Grey shading indicates night time. All data indicates the fold change from heat activation day (day 2) compared to baseline day (day 1). Significance was calculated between the experimental groups and the empty GAL4 control. One-way ANOVA with Holm-Šídák correction was used for normal distributed data, Kruskal-Wallis test with Dunn's post hoc test was used for data without normal distribution. **** = $p < 0.0001$, *** = $p < 0.001$, ** = $p < 0.01$, * = $p < 0.05$, ns = $p > 0.05$. n *SS63089 > UAS-TrpA1* = 26 flies, n *SS54676 > UAS-TrpA1* = 43 flies, n *empty GAL4 > UAS-TrpA1* = 47 flies. Dots represent individual flies, bars represent mean ± SEM.

of hDeltaK neurons with TrpA1. Surprisingly, the results obtained from the two lines were not identical, but differed quite substantially in a range of measurements. While SS54676 showed barely any changes upon activation, SS63089 showed changes in a variety of measurements (Fig. 6.2). Activation of SS63089 decreased sleep, with the main effect at nighttime (Fig. 6.2B). The reduction of sleep seemed to be due to fragmentation of sleep during the night, as indicated by a decrease of the mean sleep bout duration, and an increase in the number of sleep episodes (Fig. 6.2C, D). Further, P(Wake) was strongly increased during day and night, indicating lighter sleep (Fig. 6.2E), as suggested by the changes in sleep architecture. Interestingly, P(Doze) was reduced during the day with both split lines, indicating a decreased probability of the flies to fall asleep (Fig. 6.2F). While this difference did not translate into a change of total sleep during the day, it indicated that activation of hDeltaK might indeed induce changes in the fly's efficiency to translate increasing sleep pressure into sleep. Last, the manipulations performed here did change the activity levels of the flies: activation of SS63089 increased activity during the day, but decreased activity during the night, while SS54676 increased activity during the day, but did not cause any changes during the night (Fig. 6.2G). The contrasting changes in activity observed with SS63089 activation make a movement impairment that might be

disguising a sleep phenotype unlikely, but the reasons for these changes should be studied further.

To understand if the signals from hDeltaK neurons are necessary for a normal sleep behaviour, synaptic output from hDeltaK neurons was blocked with *shibire*^{ts} using the same two split-GAL4 lines. SS63089 also showed a stronger phenotype in these experiments, as was the case in the activation experiments. Inhibition of hDeltaK neurons decreased sleep, with a strong effect during the light period of the day. At night, no change could be observed (Fig. 6.3B). While the mean sleep episode duration was only slightly reduced (only significant in one group), the number of sleep episodes was strongly reduced in both lines (Fig. 6.3C, D). In line with the reduction in sleep, both lines showed a strong increase in P(Wake), underlining the increased waking probability (Fig. 6.3E). P(Doze) was significantly reduced during the day with both lines, again adding to the increased wakefulness during this time period. Interestingly, both lines showed an increase in P(Doze) during the night, suggesting that sleep pressure was higher than controls, potentially trying to compensate for the accumulated sleep loss during the day (Fig. 5.9F). Last, activity of the flies was increased during the day with SS63089, but decreased during the night with both lines (Fig. 6.3F). Comparing this experiment with the activation of hDeltaK neurons revealed a surprising result: both experiments showed the almost identical behavioural outcome, as seen in the changes in total sleep, sleep architecture, as well as P(Wake) and P(Doze). On top, even the changes in activity (increase during the day, as well as decrease during the night) were identical. This indicates, assuming that the manipulations worked as expected, that activating and inhibiting hDeltaK neurons had the same informational value.

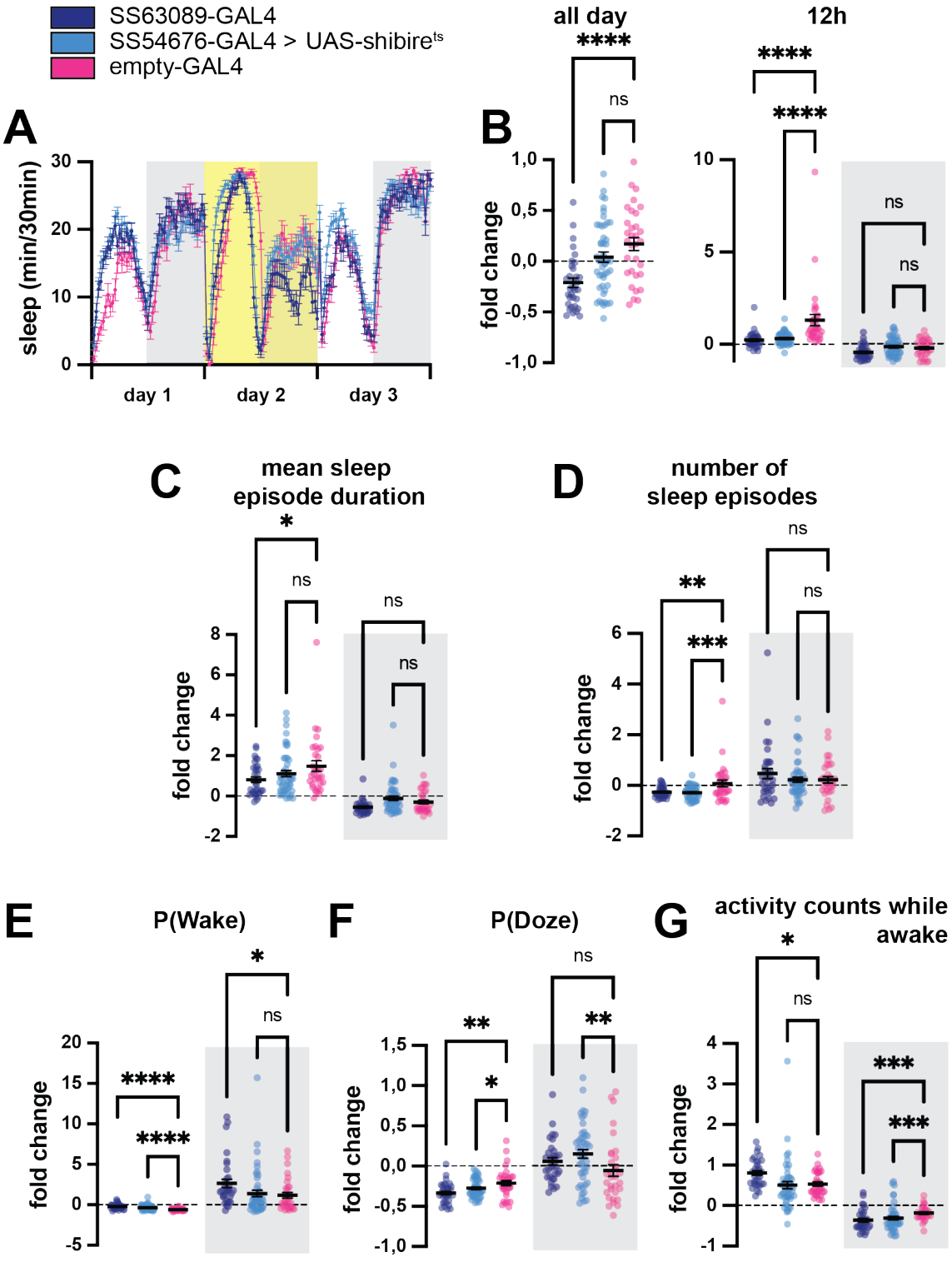

Figure 6.3: Blocking hDeltaK neuronal output decreases total sleep as well as sleep depth. A) Sleep profile of flies that express *shibire^{ts}* in hDeltaK neurons over three consecutive days, with day two as the heat activation day (indicated in yellow). B) SS63089 decreased total sleep compared to the baseline day, during the whole day, while both groups show a significant reduction in sleep during the daytime. (Caption continued on next page)

Figure 6.3: (Continued from previous page.) C) Mean sleep episode duration was slightly reduced in SS63089 during the day, otherwise all groups unchanged. D) Blocking synaptic output in hDeltaK neurons decreased the number of sleep episodes with both drivers during the day, but not during the night. E) P(Wake) was significantly increased during the day for both groups, and during the night for SS63089 only. F) P(Doze) was significantly reduced in both groups during the day, but significantly increased for SS54676 at night. G) Activity counts were slightly increased in SS63089 during the day, but significantly reduced in both groups during the night. Grey shading indicates night time. All data indicates the fold change form day 2 (heat activation day) compared to baseline day (day 1). Significance was calculated between the experimental groups and the empty GAL4 control. One-way ANOVA with Holm-Šídák correction was used for normal distributed data, Kruskal-Wallis test with Dunn's post hoc test was used for data without normal distribution. **** = $p < 0.0001$, *** = $p < 0.001$, ** = $p < 0.01$, * = $p < 0.05$, ns = $p > 0.05$. n *SS63089 > UAS-shibire^{ts}* = 33 flies, n *SS54676 > UAS-shibire^{ts}* = 48 flies, n *empty GAL4 > UAS-shibire^{ts}* = 32 flies. Individual dots represent individual flies, bars represent mean ± SEM.

Next, the connection between hDeltaK and dFBNs was analysed functionally. hDeltaK neurons form the main input onto dFBNs (Fig. 3.1) and dFBNs form the main output connection of hDeltaK neurons (Fig. 6.1B), hence a strong connection was expected.

For this, CsChrimson was expressed in hDeltaK neurons while changes in the membrane potential of GFP-labelled dFBNs were recorded (Fig. 6.4A, B). Optogenetic activation of hDeltaK neurons induced a depolarization in dFBNs, confirming the cells were connected (Fig. 6.4C). The depolarization persisted in the presence of TTX, verifying that hDeltaK neurons indeed form a monosynaptic connection with dFBNs (Fig. 6.4D).

According to the connectome, hDeltaK neurons do not only provide input to, but also receive information from dFBNs (Fig. 6.1A). Therefore, I next tested if this connection could also be verified functionally. In line with the previous experiment, CsChrimson was expressed in dFBNs (using the R23E10-LexA driver) and changes in membrane voltage were recorded from hDeltaK neurons (Fig. 6.5A). No clear response could be detected in hDeltaK neurons in response to activation of dFBNs (Fig. 6.5B). During the recordings, the membrane potential was unstable, which confounded the results slightly. TTX was added, but also in this condition, no response to dFBN activation could be detected (Fig.

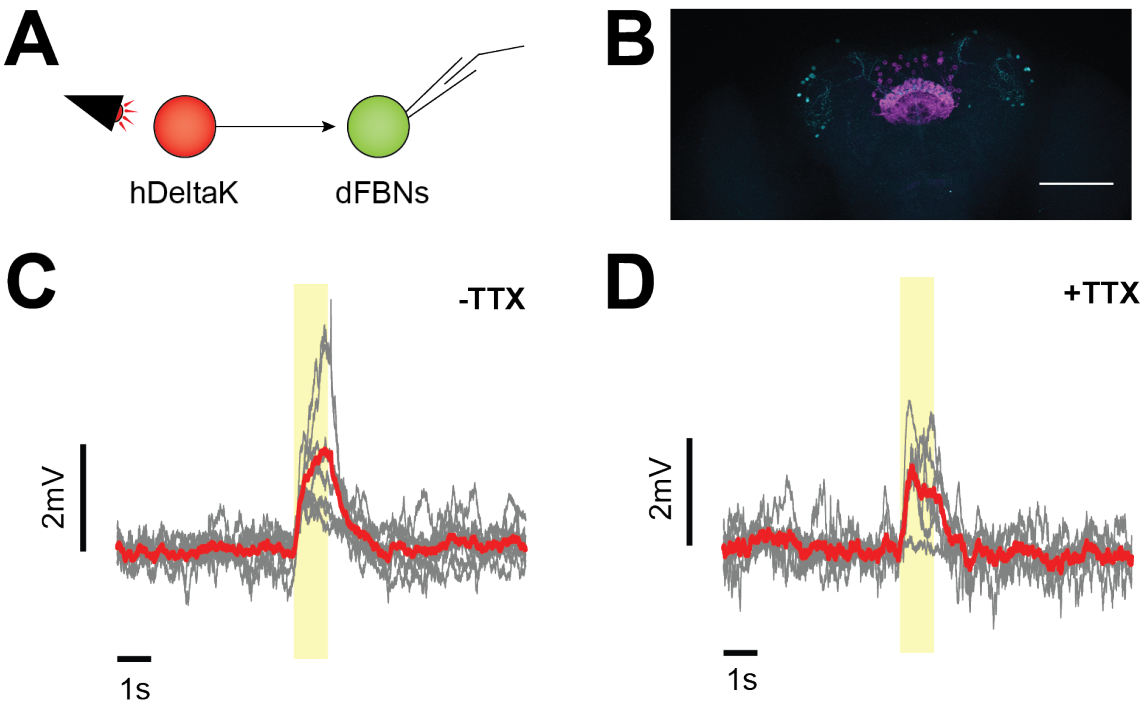

Figure 6.4: hDeltaK neurons form monosynaptic functional connection with dFBNs. A) Schematic description of the experimental setup: CsChrimson expressing hDeltaK neurons are activated by light while activity is recorded from dFBNs. B) Confocal image of the whole brain of a *SS63089-GAL4 > UAS-CsChrimson::tdTomato, R23E10-LexA > LexAop-GFP* fly. GFP signal in cyan, CsChrimson signal in magenta. Scale bar = 100 µm. C) Patch-clamp recordings from dFBNs in *SS63089-GAL4 > UAS-CsChrimson::tdTomato, R23E10-LexA > LexAop-GFP* flies revealed a depolarization when hDeltaK neurons are activated optogenetically. n = 8 cells. D) Depolarization sustained in the presence of TTX. n = 6 cells. Yellow shading represents light stimuli to activate hDeltaK neurons for 1 sec. Cells were held at -60 mV. Grey lines represent mean one cell. Red line represents mean of all recorded cells.

6.5C).

The connection from dFBNs onto hDeltaK neurons is almost exclusively formed by one subtype of dFBNs: FB6A neurons (Fig. 6.1A). The R23E10-LexA driver that was used to express CsChrimson in the previous experiment does not label all dFBNs and potentially excludes FB6A neurons, hence it might miss the connection. Therefore, in line with experiments performed to detect the input to R56E07-GAL4 neurons by dFBNs (Fig. 4.12), UAS-P2X2 was used and expressed under control of R23E10-GAL4. This should allow a stronger input from dFBNs, including FB6A neurons, to hDeltaK neurons. ATP

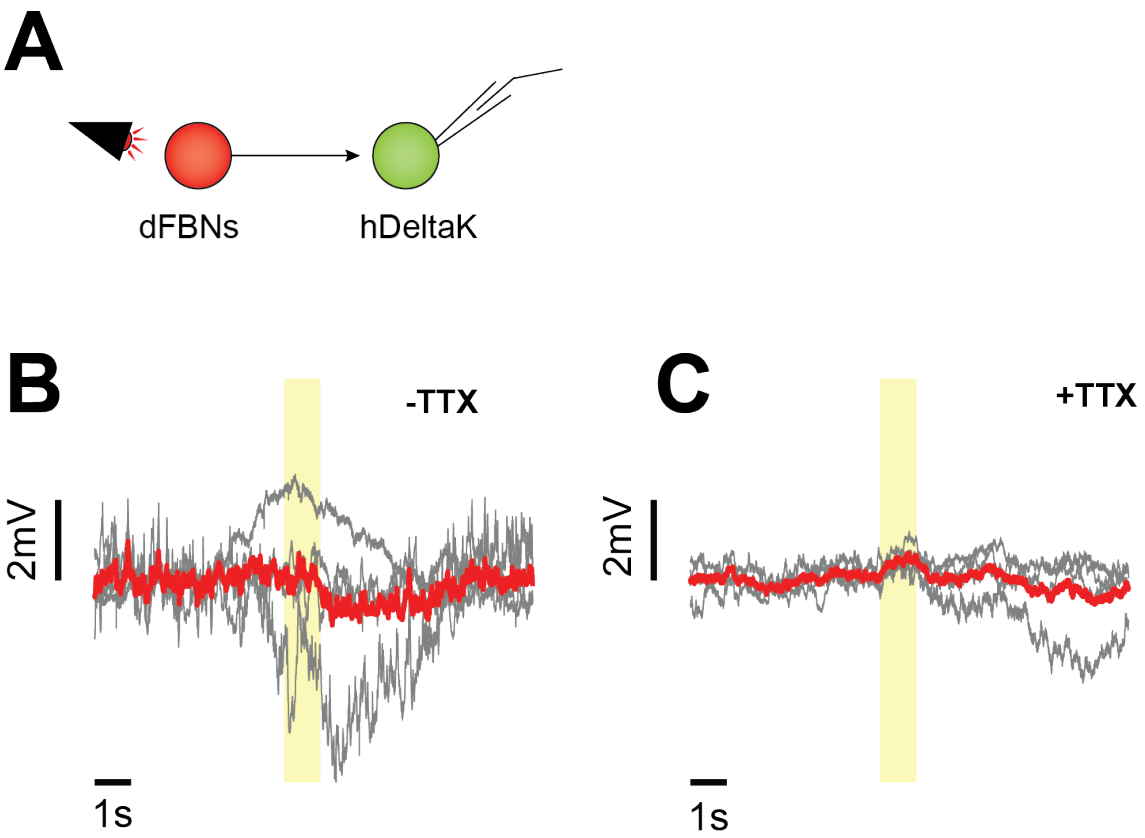

Figure 6.5: dFBNs connection onto hDeltaK neurons remains unclear. A) Schematic description of the experimental setup: CsChrimson expressing dFBNs are activated by light while activity is recorded from hDeltaK neurons. B) Patch-clamp recordings in hDeltaK neurons in *R23E10-LexA > LexAop-CsChrimson::tdTomato, SS63089-GAL4 > UAS-mCD8::GFP* flies did not reveal a clear change upon dFBN activation. n = 4 cells. C) Adding TTX did not reveal a connection either. n = 4 cells. Yellow shading indicates light stimuli to activate dFBNs for 1 sec. Grey lines represent mean per cell. Red line represents mean of all recorded cells.

ejection was targeted to the neurites of dFBNs in the SP, while patch-clamp recordings were performed from hDeltaK neurons (Fig. 6.6A, B). Activating dFBNs with ATP did not elicit a response in hDeltaK neurons (Fig. 6.6C). A small artefact during the ATP application could be seen, due to the movement or the electric noise during pressure ejection. But no changes in membrane voltage were detected that could be attributed to the depolarization of dFBNs. TTX was added to the preparation to verify that there is no underlying effect that is masked by secondary signals. But also here, no response to the depolarization of dFBNs was detected (Fig. 6.6D).

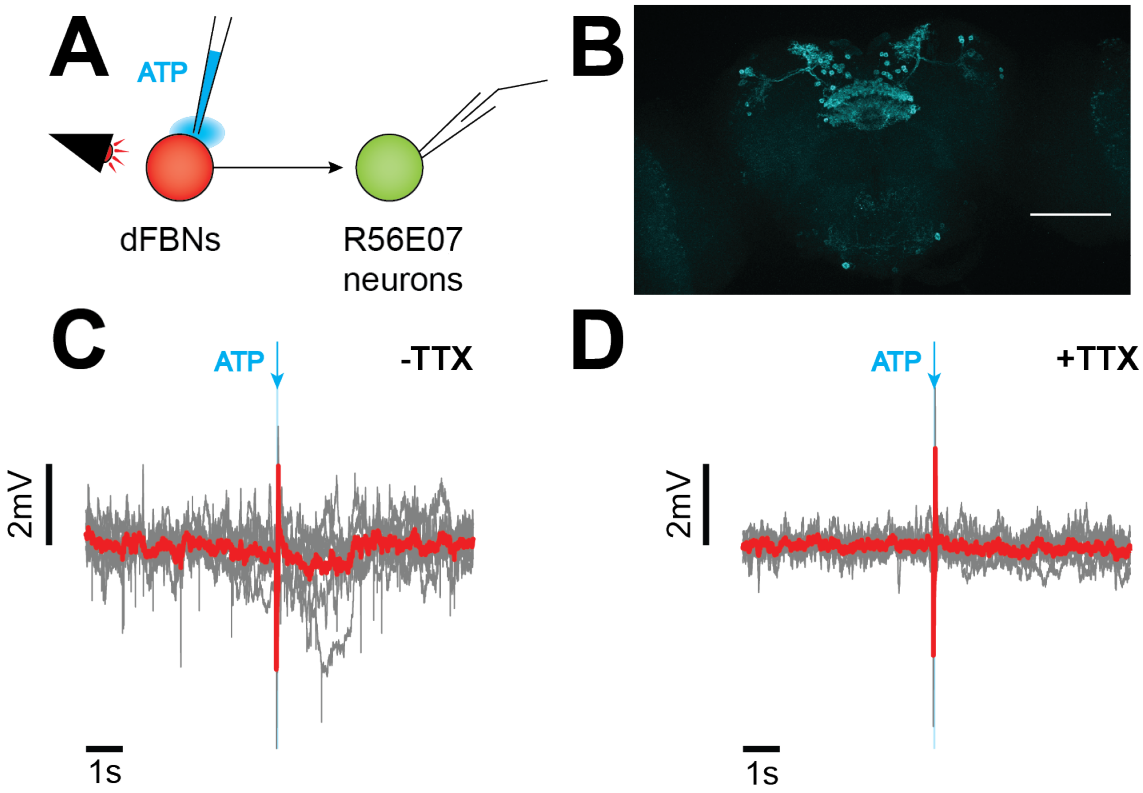

Figure 6.6: dFBNs connection onto hDeltaK cannot be detected. A) Schematic description of experimental setup. ATP ejection onto dFBNs, while recording from hDeltaK neurons. B) Confocal picture of the brain of a *R23E10-GAL4, SS63089-GAL4 > UAS-P2X2, UAS-cDB8::GFP* fly. anti-GFP in cyan. Scale bar = 100 µm. C) Pressure ejection of ATP onto the dendritic tree of dFBNs in *R23E10-GAL4, SS63089-GAL4 > UAS-P2X2, UAS-mCD8::GFP* flies did not cause a response in hDeltaK neurons. n = 8 cells. D) Adding TTX did not reveal any underlying response. n = 7 cells. Blue shading and arrow indicates pressure ejection of ATP. Grey lines represent mean per cell. Red line represents mean of all recorded cells.

To summarize, there is a clear functional monosynaptic connection from hDeltaK neurons onto dFBNs but the reverse connection could not be detected.

6.2.2 Inhibition of serotonergic ExR3 neurons increases wake

ExR3 neurons connect the two sleep centres, EB and FB [44, 126, 127, 130]. As described in chapter 3, they connect pre- and postsynaptically to dFBNs.

To test the role of ExR3 neurons in the regulation of sleep, ExR3 neurons were activated and the subsequent changes in sleep were recorded. Again, two different split-GAL4 driver lines

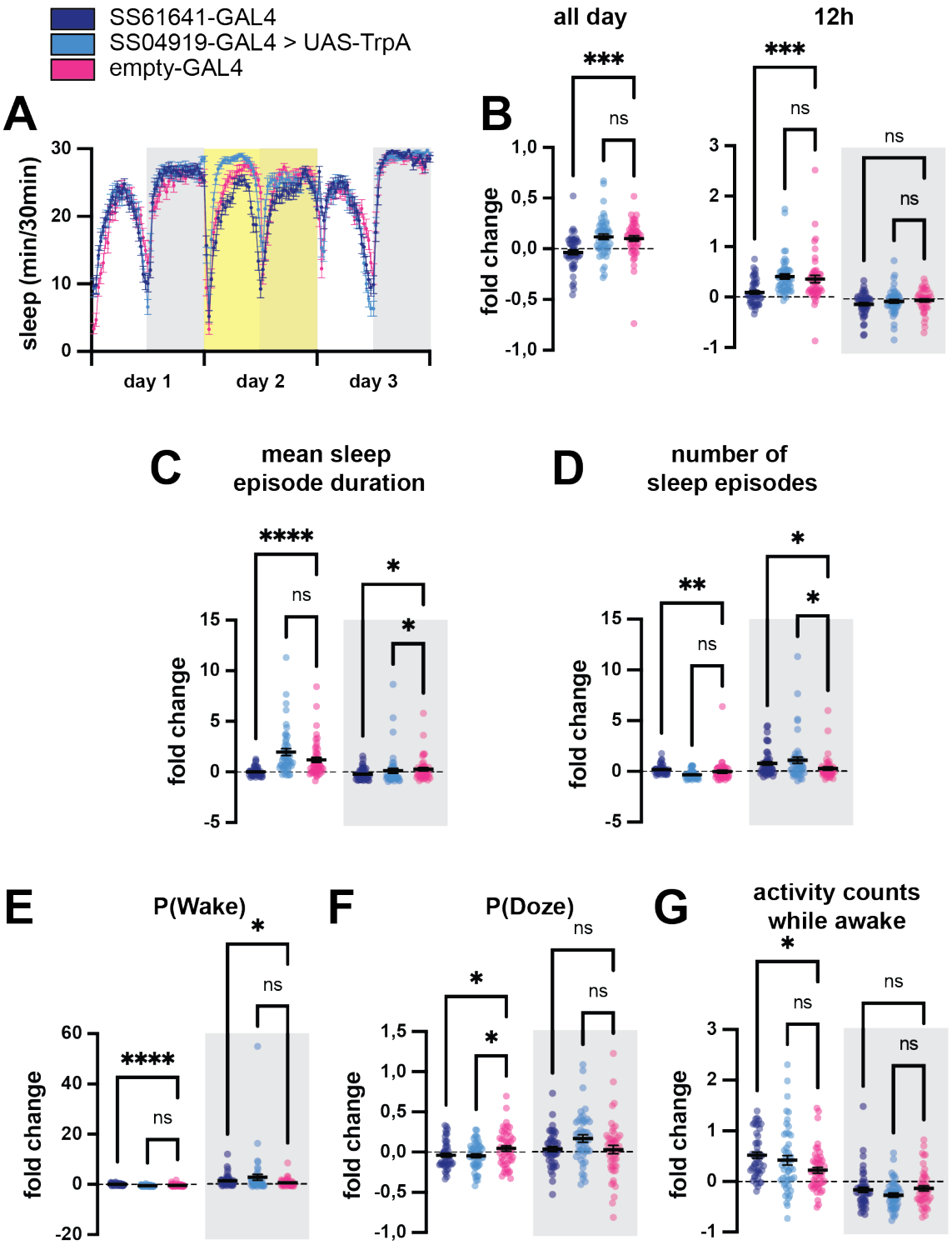

Figure 6.7: Activation of ExR3 neurons fragments sleep A) Sleep profile of flies that express TrpA1 in ExR3 neurons over three consecutive days, with day two as the heat activation day (indicated in yellow). B) Only SS61641 decreased total sleep compared to the baseline day, during the whole day, as well as during daytime, but not during nighttime. (Caption continued on next page)

Figure 6.7: (Continued from previous page.) C) SS61641 decreased mean sleep episode duration during the day and night, while SS04919 only reduced the duration during the night. D) Only SS6164 increased the number of sleep episodes during the day, while both line increased the number of sleep episodes during the night. E) P(Wake) was increased in SS61641 day and night, but not in SS04919. F) P(Doze) was reduced with both lines during the day, but not during the night. G) Flies with activated ExR3 neurons via SS61641 showed an increase in activity during the day, but not during the night. SS04919 did not induce changes in activity. Grey shading indicates night time. All data indicates the fold change form day 2 (heat activation day) compared to baseline day (day 1). Significance was calculated between the experimental groups and the empty GAL4 control. One-way ANOVA with Holm-Šídák correction was used for normal distributed data, Kruskal-Wallis test with Dunn's post hoc test was used for data without normal distribution. **** = $p < 0.0001$, *** = $p < 0.001$, ** = $p < 0.01$, * = $p < 0.05$, ns = $p > 0.05$. n *SS61641* > *UAS-TrpA1* = 48 flies, n *SS04919* > *UAS-TrpA1* = 48 flies, n *empty GAL4* > *UAS-TrpA1* = 47 flies. Individual dots represent single flies, bars represent mean ± SEM.

were used for TrpA1 activation, SS61641 and SS04919. Only one of these lines changed the amount of sleep when activated: activation of SS61641 decreased sleep significantly during the day, but did not affect the duration of sleep at night, while the activation of SS04919 did not change the amount of sleep (Fig. 6.7B). The mean sleep episode duration was significantly decreased during day and night with the SS61641 line, while the other line caused only a slight decrease at night (Fig. 6.8C). The number of sleep episodes on the other hand was increased during day and night with SS61641 and only during the night with SS04919 (Fig. 6.8D). P(Wake) was increased during day and night with SS61641, but not with SS04919 (Fig. 6.8E). P(Doze) was decreased during the day with both lines, but remained unchanged during the night (Fig. 6.8F). Further, activation of ExR3 neurons via SS61641 induced a minor increase of activity during the day (Fig. 6.8G).

Next, it was tested if blocking ExR3 output by shibire^{ts} would affect the control of sleep. Indeed, sleep was significantly decreased during the day, as well as slightly during the night (Fig. 6.8B). Interestingly, the two split GAL4 lines seemed to affect different aspects of sleep architecture: while blocking SS61641 decreased the mean sleep episode duration during the day, it did not change the number of sleep episodes (Fig. 6.8C, D). SS04919

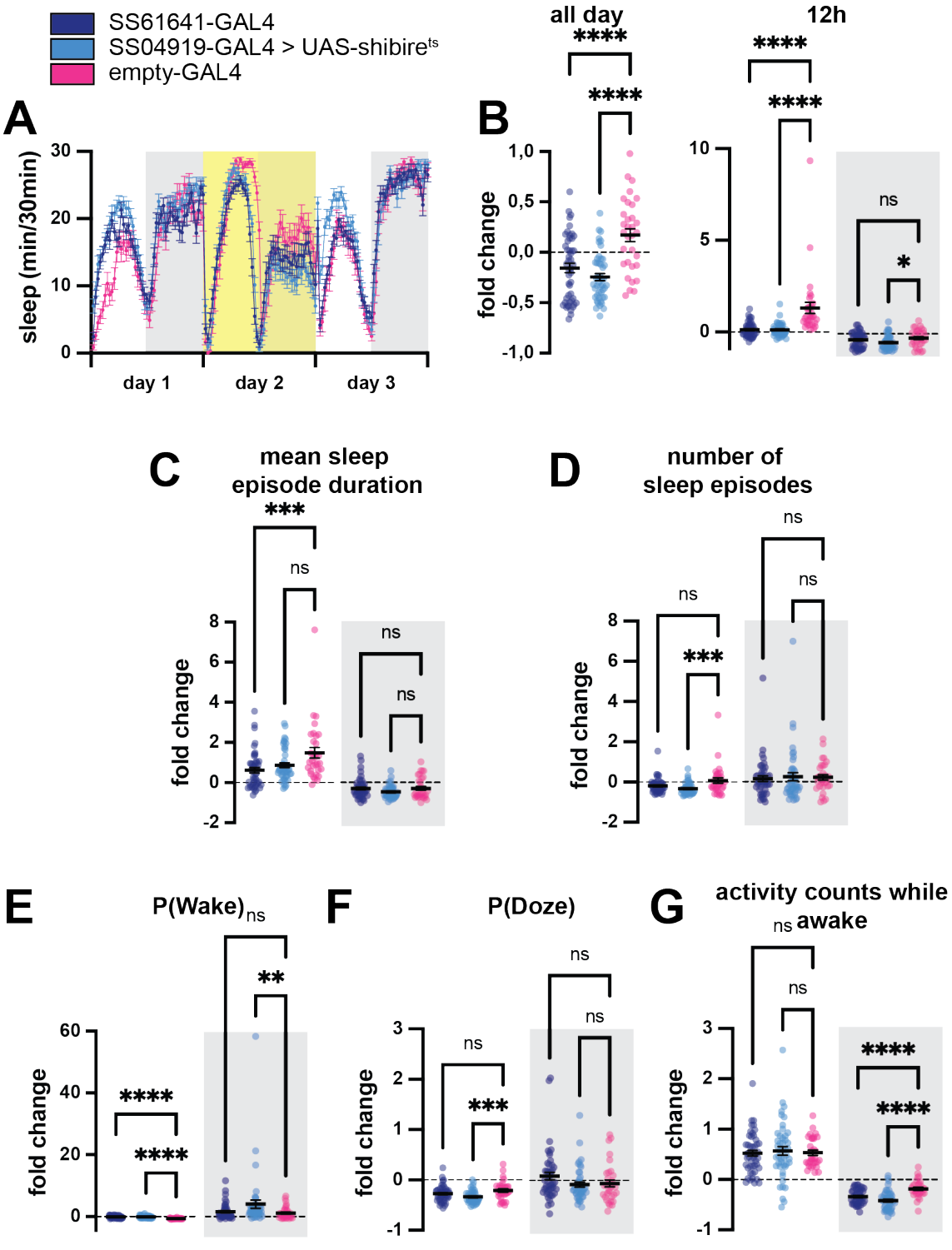

Figure 6.8: Blocking synaptic output in ExR3 neurons decreases sleep. A) Sleep profile of flies that express *shibire*^{ts} in ExR3 neurons over three consecutive days, with day two as the heat activation day (indicated in yellow). B) The total amount of sleep was strongly reduced in flies that express UAS-shibire^{ts} with two different driver lines. Both line strongly decreased sleep during the day, with one line also decreased sleep during the night. (Caption continued on next page)

Figure 6.8: (Continued from previous page.) C) Mean sleep episode duration was decreased with one line during the day, unchanged during the night. D) The number of sleep episodes was reduced with one line during the day, but not with the other. Neither line changed the number of sleep episodes during the night. E) P(Wake) was strongly increased during the day with both lines, and during the night with one line. F) P(Doze) was decreased with one line during the day, no change at night. G) Activity was unchanged during the day, but decreased during the night. Grey shading indicates night time. All data indicates the fold change from heat activation day (day 2) compared to baseline day (day 1). Significance was calculated between the experimental groups and the empty GAL4 control. one-way ANOVA with Holm-Šídák correction was used for normal distributed data, Kruskal-Wallis test with Dunn's post hoc test was used for data without normal distribution. **** = $p < 0.0001$, *** = $p < 0.001$, ** = $p < 0.01$, * = $p < 0.05$, ns = $p > 0.05$. n *SS61641* > *UAS-shibire^{ts}* = 48 flies, n *SS04919* > *UAS-shibire^{ts}* = 46 flies, n *empty GAL4* > *UAS-shibire^{ts}* = 32 flies. Individual dots represent single flies, bars represent mean ± SEM.

on the other hand did not significantly change the mean sleep episode duration, but did decrease the number of sleep episodes (Fig. 6.8C, D). P(Wake) was significantly increased in both lines, and also during the night in one line (Fig. 6.8E). P(Doze) was decreased in one of the lines during the day, but not during the night (Fig. 6.8F). Interestingly, blocking synaptic output from ExR3 neurons did not change activity levels during the day, but it did significantly decrease activity during the night (Fig. 6.8G).

ExR3 neurons have been predicted to use serotonin as a neurotransmitter [55, 174], but this has not been verified experimentally. To test this, brains expressing GFP in ExR3 neurons were stained with an anti-serotonin antibody, to detect any potential overlap in signals. While the antibody clearly stained several neurites and cell bodies, a clear overlap of the serotonin staining could be detected with the two ExR3 cell bodies (Fig. 6.9).

Figure 6.9: ExR3 neurons are serotonergic. Immunohistochemistry stainings of *SS16969 > 20x-UAS-GFP* animals with anti-GFP (cyan) and anti serotonin (magenta). White arrows indicate localization of ExR3 cell bodies. Scale bar = 100 µm.

6.3 Discussion

6.3.1 Opposing manipulations of hDeltaK lead to the same behavioural output

The study of hDeltaK neurons in sleep revealed several interesting findings: first, while two different split-GAL4 lines label the same group of neurons, manipulating these neurons did not cause identical changes in sleep behaviour. Either, the lines have off-target effects that were not noticed before, or the split-GAL4 lines used here have different expression levels [56]. While age can affect the expression levels [251], it should not be the case here as all animals were age-matched for the experiments. Focussing on the behaviour of SS63089, the line that showed changes in sleep behaviour during TrpA1 activation and shibire^{ts} blocking, a really unexpected finding became apparent: activation and inhibition had the same effect (compare fig. 6.2 and fig. 6.3). In both cases there was a reduction of sleep and P(Doze) during daytime. Further there was an increase in P(Wake), and activity was increased during the day, but decreased during the night. The similarity of the behavioural output of the two manipulations is very surprising. If we consider that hDeltaK transmit information in the form of an activity bump, as suggested by pervious

work [124, 190, 191], activation and inhibition of the neurons will destroy the bump signal and cause a homogeneous activity of the neurons. If information lies in the location of the bump, destruction of the bump would have the same informational value. Interestingly, a similar phenomenon can be observed in a different cell type: EPG neurons, best known for their role in head direction [152, 153, 252], were recently shown to increase sleep when activated [96, 160]. Another group further tested inhibition of EPG neurons and found that it strongly induced immobility in these flies [91]. Navigational information is also encoded as an activity bump in EPG neurons [152], suggesting that in both cases, loss of a meaningful bump has the same behavioural outcome. To gain a deeper understanding of the encoded information, future studies should activate only a subpopulation of neurons within hDeltaK or titrate the activation patters provided to these cells and study the behavioural outcome.

A striking second feature were the changes in activity levels that differ during day and night. Both manipulations increased activity during the day, and decreased activity during the night. Considering that hDeltaK neurons might transmit information about odour and wind guided navigation [124, 191], a lack of this information might explain the changes in activity: having no clear navigational cues might increase the fly's activity during the day, as it cannot look for food in a precise manner and might therefore spend more time searching. During the night, less cues might be transmitted to the fly, and therefore there is less incentive to move.

hDeltaK neurons have also been implicated in the reduction of sleep following social isolation [148]. Surprisingly, in that study activation or inhibition of hDeltaK neurons did not change the levels of sleep in group housed flies. In this study here, flies were group

housed prior to the sleep measurements, hence the differences in the results are surprising. The most obvious difference lies in the driver lines used. While the lines used here are believed to be highly specific [55], the line used in the previous study labels P2-neurons, whose main component was suggested to be hDeltaK neurons [148]. P2 neurons though are a group of 20 interneurons (and the driver line used only labels 80-90% of these) [253], while hDeltaK neurons are a group of 31 neurons [44]. Hence the driver line used labels only a subset of hDeltaK neurons and this difference is likely responsible for the difference in behavioural outcome.

6.3.2 hDeltaK neurons target dFBNs

The data presented here shows that hDeltaK neurons excite dFBNs, likely via acetylcholine [174]. Interestingly, there is a likely second connection between these two groups of neurons, namely via Allatostatin-A. AstA gene expression has been detected in hDeltaK neurons [55] and dFBNs are expected to express the AstA receptor, as R23E10-GAL4 uses the AstA-R1 enhancer [52]. Application of AstA reduced activity in dFBNs [134], which is opposite to the results obtained here (Fig. 6.4). Thus, the results here are likely gated by a fast-acting neurotransmitter. The actions of AstA though would need further investigation, as they are likely to take place at the same time, but might be harder to detect. In the context of food choice, AstA signalling onto dFBNs has been described, although here no direct source of AstA had been identified [237]. One could hypothesize, that sleep and food signals are transmitted via two different signals onto dFBNs.

There are two interpretations to the negative result of the connection from dFBNs onto hDeltaK neurons: either the connection is wrongly predicted by the connectome, and the synapses might be misattributed (e.g. the directionality of these synapses was predicted

wrong and actually the only information flow is from hDeltaK onto dFBNs). Or the connection is functional but cannot be resolved with the methods used here. The first option is unlikely, as now two different connectomes have provided evidence for this connection [42–45], but a previous study did imply that only functional connectivity experiments are able to fully prove a connection [93]. The second option therefore seems more likely, that the methods here do not allow the resolution that might be necessary to detect this connection. Patch clamp in *Drosophila* has a big caveat that might be a problem for the experiments here: the spatial resolution. Neurons in the fly brain have an unusual shape compared to vertebrate neurons: cell bodies are localized at the brain's periphery, while the neurites of these neurons are in the centre of the brain, often at quite a distance [43]. Often, neural signals that occur at distant neuropils do not propagate (fully) back to the soma and might therefore not be detected when recording there [246]. While it is possible in some neurons to detect EPSPs, in other neurons action potential firing cannot even be blocked by hyperpolarizing the soma to -70 mV, as the patch electrode might not offer enough control over the rest of the neuron [96, 246]. Maybe dFBNs input very locally onto hDeltaK neurons in form of axo-axonic connections that do not propagate back to the soma, but shape the synaptic output of hDeltaK neurons locally.

The connection of ExR3 and dFBNs was only briefly examined here, and much more research would be needed to understand its significance. Serotonin has long been hypothesized to be involved in the control of sleep, but with different suggested functions, sometimes sleep promoting [135, 254, 255], sometimes rather wake promoting [156]. While activation of ExR3 neurons decreased sleep in one out of two lines, blocking their synaptic output decreased sleep significantly for both split-GAL4 lines used here, in both cases accompanied with an increase in P(Wake) and a decrease in P(Doze) (both mainly or only

during day time). Again, just like hDeltaK neurons, both manipulations decrease sleep, rather than one causing an increase in sleep. This result is in line with the serotonin receptor 2b knockdown in dFBNs, that also caused a decrease in sleep [135]. The 5HT2B receptor induces calcium release from intracellular stores [256], which might increase the dFBN's firing rate and therefore increase sleep [127]. The same receptor in dFBNs has also been involved in an autism-like phenotype, where KD of the receptor in dFBNs increases social distancing [257]. While there is no proof yet that ExR3 is the only serotonergic input into dFBNs (recently it was suggested that FB6H neurons co-express serotonin [55]), it is likely that these neurons do form one of the main signals, based on their connectivity. hDeltaK neurons were also predicted to express serotonin, but this revealed to be a wrong prediction [174], and also serotonin staining in these neurons did not show any expression (data not shown). It seems unlikely that serotonin would be encoding a sleep pressure signal, but rather a signal that needs to be at the correct levels, and either a loss or excess signal to the fly that it should stay awake to correct for the mismatch. Activation of serotonergic neurons in the fly brain in general has been shown to fragment sleep by increasing the number of sleep episodes (although with an unclear change of total sleep) [156]. The data here suggests that ExR3 neurons alone can induce this fragmentation when activated, but the increase of P(Doze) observed when activating all serotonergic neurons could not be replicated here, suggesting that other 5-HT neurons are responsible for this effect [156]. 5-HT7-GAL4 neurons, which mainly express in the EB, were shown to fragment sleep, but knocking down the actual receptor in these neurons should tell us more specifically if this is transmitted directly via 5-HT signalling. On the other hand, increases in serotonin [254] as well as impairments in the serotonin reuptake [255] have been linked to an increase in sleep. This would suggest, that the sleep promoting effect of

serotonin happens at different synapses than the ExR3-dFBN connection examined here.

7 | Discussion

7.1 Main findings

This work is the first effort to date to understand the synaptic connections of dFBNs in detail, on a theoretical, behavioural, and functional level.

I showed that dFBNs receive inputs in the SP and the FB with the strongest connections from hDelta interneurons as well as tangential neurons. The main postsynaptic targets of dFBNs were all within the FB, mainly hDelta interneurons, as well as FC2 goal angel cells (see chapter 3).

hDeltaF neurons were identified as the strongest postsynaptic partner of dFBNs and their activation decreased sleep. Further, the synaptic connection between dFBNs and hDeltaF neurons was analysed in detail, revealing a surprising synapse: while the synapse is neither clearly inhibitory nor excitatory, it appears to be both. The same synapse, and more specifically the same neurotransmitter, was able to encode excitatory as well as inhibitory input at the same time (see chapter 4 and chapter 5).

Last, two other important connections of dFBNs that both form connections to the EB, hDeltaK as well as ExR3 neurons, were analysed. All manipulations in these neurons increased wake, suggesting that any changes to natural activity will be sleep disruptive. Overall, it shed light on the plethora of synaptic partners of dFBNs that might affect sleep regulation (see chapter 6).

Importantly, this study is the first work to date that performed patch-clamp recordings in a specific subset of hDelta neurons and studied their synaptic connectivity. While previous

studies have recorded calcium activity from hDelta neurons [90, 94, 121, 124, 191], none of these studies have recorded their electrical activity via patch-clamp electrophysiology. As shown here, there is a wide range of details in a simple synaptic connection that cannot be uncovered by calcium imaging. The significance of the details revealed here will need to be uncovered in future experiments.

7.2 Limitations

The results obtained in any experiment can only be as good as the tools that were used. This problem becomes evident throughout this thesis in light of the different GAL4 lines. Many of the results obtained here, as well as by others, reveal that GAL4 lines label either a heterogeneous population of neurons [90, 148, 190, 258], as is the case for the R23E10-GAL4 driver [44, 132, 134, 146], and/or unwanted off-targets outside of the population of interest, as shown here in the example of the R56E07-GAL4 line and also with the R23E10-GAL4 driver [140, 142, 155]. Further, and likely because of these reasons, behavioural observations of several GAL4 driver lines labelling a specific cell type often result in different behaviours, as could be seen in the sleep behavioural screen performed in chapter 4 and in other studies [86, 155]. Strikingly, while the generation of split-GAL4 lines should aid with this problem and label only specific cell-types [53–56, 259], there are still clear differences between experimental groups, as observed in chapter 6 and by others [55]. The differences between individual split-GAL4 drivers that label the same populations will need to be uncovered to gain a reliable understanding of the function of individual cell types. Differences in expression strength or undetected off-targets might be potential explanations.

Another noteworthy limitation is the focus on one behaviour only, which will miss out on

any behaviour that is not sleep related. While hDeltaK neurons in this study decreased sleep when manipulated, other studies suggest they are involved in olfactory navigation [124, 191]. Even dFB neurons themselves have been implicated in other behaviours, such as feeding and encoding of food preferences [141, 237, 238]. Further, while KD of the 5-HT2B receptor in dFBNs decreased sleep, another group suggests that it also impairs social interaction [135, 257]. Hence, while the behavioural screen performed here did lead to the discovery of hDeltaF neurons as wake promoting, no tests were conducted to see whether these, or any other neurons, controlled any other relevant behaviour.

Optogenetic stimulation and patch-clamp recordings with added TTX were used to verify the connection between dFBNs and hDeltaF neurons as monosynaptic. While TTX prevents polysynaptic transmission, it does not isolate the synapse in any other way. Hence in cases of excessive neural stimulation with high neurotransmitter release, transmitters from neighbouring synapses might diffuse and target receptors they would not reach under physiological conditions. This cannot be fully ruled out under the present conditions and further experiments using shorter stimulation times and physiologic stimulation frequencies [132] to reduce the amount of NT release from dFBNs will help exclude this possibility. While mammalian studies would use dual patch-clamp recordings to verify a monosynaptic connection based on the latency between stimulation and response, this is not normally done in *Drosophila* due to the differences in signal propagation within the neurons and the technical difficulties [93, 246].

While this effort tried to delineate the most important connections, many connected neurons were not studied but might still harbour important information. Helicon cells nicely represent these connections, as their connection strength to dFBNs is low, but their

behavioural importance has been studied thoroughly [91, 129]. Further, one potentially important participant in the circuitry of sleep homeostasis in *Drosophila* are glia cells whose changes in calcium levels have recently been shown to describe a sleep homeostat [141, 260]. As the connectome does not provide enough data about glia, they were not analysed here [44, 45, 173].

7.3 Implications

The results obtained here open up new insights into the neural circuitry of dFBNs. In the following sections I will discuss some of the key implications and open questions that result from this work.

7.3.1 The connection between a sleep control centre and a navigational centre

The connectomics described in the various chapters suggest that sleep-promoting dFBNs connect strongly to two cell types that are implicated in the encoding of navigational strategies: first, they directly connect to goal angle encoding FC2 cells [123], as well as indirectly via hDeltaF neurons. Second, they receive the majority of their inputs from hDeltaK neurons, which have been implicated in olfactory navigation [124, 190, 191].

The idea of a connection between a sleep circuit and a navigational hub is not completely new: a number of studies in recent years have suggested connections between similar circuitries, and many neurons involved in navigational control have been shown to affect sleep [90, 91, 96, 129, 160, 214, 261].

A central sleep regulatory centre in the brain of *Drosophila* is formed by R5 neurons in

the EB [130, 157]. They were shown to encode sleep pressure and artificial activation induced sleep during as well as after the stimulation [130]. R5 neurons project indirectly via helicon cells, but functionally onto dFBNs, which is believed to induce sleep in the animal [91, 129, 130]. Recent evidence has further shown that increased sleep pressure enhances their synaptic connectivity to downstream neurons [96, 156]. These postsynaptic partners were identified as EPG neurons, which are mainly known for their function as head direction (HD) cells, as they encode the interaction of external visual landmarks and internal representation of location, and are necessary for goal directed behaviours [152–154, 252]. Spatial encoding in EPG neurons happens in the form of an activity bump, as identified in calcium activity recordings, with one bump in the EB and two bumps in the PB [152, 154, 262]. Interestingly, artificial activation of EPG neurons strongly induces sleep [96, 160], and inhibition of EPG neurons also induces immobility [91], suggesting that any deviation from a physiological signal induces a decrease in mobility and likely an increase in sleep.

EPG neurons further project to neurons in the PB, where they transmit their HD information onto several cell types, such as PFN neurons. Some of these direct synaptic connections have been implied in sleep regulation: PFN neurons, for example, are wake promoting upon activation, but also transmit locomotor information further to the FB [44, 94, 121, 214]. PFN neurons also receive inputs from SpsP neurons that transmit egocentric travelling information, but at the same time have been described as sleep-promoting [94, 121, 160, 214]. The FB combines information from HD cells in the EB as well as locomotor information from PFN neurons and computes the current travelling direction in relation to the external world, as encoded in hDeltaB neurons, a subtype of pontine neurons [94, 121]. Other types of pontine neurons, such as hDeltaC/K are necessary for olfactory navigation

and again, pontine neurons have been shown to decrease sleep, in the present study as well as by others [90, 148]. Further, the goal angle is encoded as an activity bump in FC2 cells [123, 263]. While these neurons have not been studied for their involvement in sleep, the work presented here describes the substantial inputs they receive from dFBNs, hence likely sleep promoting input. Overall, the data provided here suggests that the known navigational circuitry in *Drosophila* is playing a big role in the encoding of sleep and arousal signals. No study to date has combined these findings in such a manner, but as more information is gathered, this connection needs to be analysed further.

The main distinction that needs to be made, in light of the information just presented, is whether the neurons actually encode sleep signals and are responsible for sleep control, or if the resulting changes in sleep are side effects of the manipulation. For example, if activating a neuron induces hunger in the animal, it will likely induce wake as a result, as starvation is known to promote wakefulness [264], but the neuron itself would not be involved in the control of sleep. A fine distinction between these cases is needed in order to better understand the dual function of many neurons.

While dFBNs have never been described in a navigational context, but mainly during sleep and feeding, it will be especially interesting to understand how they compute incoming navigational information. In the downstream circuit, I would suggest that an increased sleep signal would decrease the valence of navigational cues, making the fly prioritise sleep over navigation in times of high sleep pressure.

This hypothesis of course needs much more evidence, and detailed studies in the future will help to understand the precise mechanism of this circuitry. First, the role of hDeltaF neurons needs to be delineated further. Understanding if they encode an activity

bump, just like hDeltaB [94, 121], and hDeltaC/K [124, 190, 191], will help understand if they encode directional cues. Further, the function of FC2 cells needs much more information. While first studies have shown that they encode the goal angle and that artificial manipulation of the encoded bump can change the flies' locomotor direction, it is not yet known how the incoming information is computed into a meaningful signal [123, 263]. And last, studying the activity of FC2 cells in sleep deprived animals, compared to rested animals, should help understand differences in their activity. Together, this will help to understand how sleep pressure shapes the navigational behaviour of the fly.

7.3.2 The synaptic connections of dFBNs

This thesis further focussed on the detailed analysis of functional synapses of dFBNs and their connections to verify predicted synapses [93]. The input synapse from hDeltaK onto dFBNs was clearly excitatory, but the synapse from dFBNs onto hDeltaF neurons remains hard to understand. While glutamate seems to be the sole NT involved in this connection, but not necessarily the only signalling molecule used by dFBNs [55, 129], it is performing dual functions: It can inhibit or depolarize the postsynaptic cells, depending on their resting membrane potential. Based on the data obtained here, depolarized cells are mainly inhibited by dFBNs, whereas hyperpolarized cells become more depolarized. This could play an important role if hDeltaF neurons are naturally at different RMPs. For instance, hDeltaK and hDeltaB neurons have been shown to encode an activity bump, hence neurons of these types exhibit different RMP states and only a subset are active at any given time [94, 121, 124, 190]. Based on the similarities in connectivity among these neuron types, hDeltaF neurons might also encode their information via an activity bump [44]. If this is the case, the input from dFBNs would prevent this information from being transmitted:

depolarizing the more hyperpolarized cells and inhibiting the more depolarized cells will align them at a similar RMP and hence lose the informational value that was transmitted with the activity bump.

This, undoubtedly, elicits many new questions, which will need further investigation. First of all, the RMP for hDeltaF neurons as well as their naturally occurring dynamic range need to be clearly analysed. Further, it should be tested if hDeltaF neurons encode an activity bump under physiological conditions, and what information this encodes. Next, it should be tested how the connectivity between dFB and hDeltaF neurons changes with increasing sleep debt: Does an increase in sleep pressure increase the signalling onto hDeltaF, hence does high sleep pressure inhibit hDeltaF signalling? Or does higher sleep pressure actually reduce glutamatergic action on hDeltaF neurons (as suggested in [132]), which would release the signal stored in hDeltaF neurons during these conditions. Ideally we would analyse the synaptic connection in spontaneous conditions, e.g. using two voltage imaging sensors [91]. Finally, the structure of the fan-shaped body is conserved across layers, with many glutamatergic tangential neurons providing input onto several types of pontine neurons within the FB, suggesting the same type of connectivity might be present at other synapses [44, 174]. It would be interesting to test how glutamate acts on those synapses and if the same inhibition-excitation pattern can be detected.

These results were unexpected and might easily be overlooked in any calcium imaging studies. The field mainly uses GCaMP measurements to infer neural activity, which can nicely represent population dynamics [94, 121, 124], but it cannot resolve these precise dynamics uncovered in this single synapse.

7.4 Future directions

While this thesis has generated insights into the synaptic connectivity within the FB, a lot more needs to be elucidated. dFBNs are only one group of tangential neurons, and we cannot yet state how representative the data obtained here is. NT predictions suggest that the vast majority of, if not all, tangential neurons are glutamatergic [174], suggesting that synaptic connectivity patterns from tangential neurons to other hDelta neurons could be similar. Understanding the connection from tangential neurons onto other neurons in the FB will help to understand the integration of sensory signals in the navigational context.

Further, more evidence is accumulating that cells in layer 6 of the FB are also encoding non-sleep related information [141, 237, 238, 257]. As recent tools have enabled us to identify single cell types within dFBNs [44, 55], these techniques need to be leveraged further to delineate sleep function as well as other behaviour to individual subtypes, if possible. This will aid also in the understanding of the encoding of sleep, as once a sleep-specific subpopulation is identified, any confounding signals can be excluded.

The FB, while central to the brain of insects, is a hugely complex structure whose computations we are only beginning to understand. In this work, I provided a small contribution to the field that will help to understand the complexity in the FB better, and hopefully one day solve the mystery of how sleep is controlled.

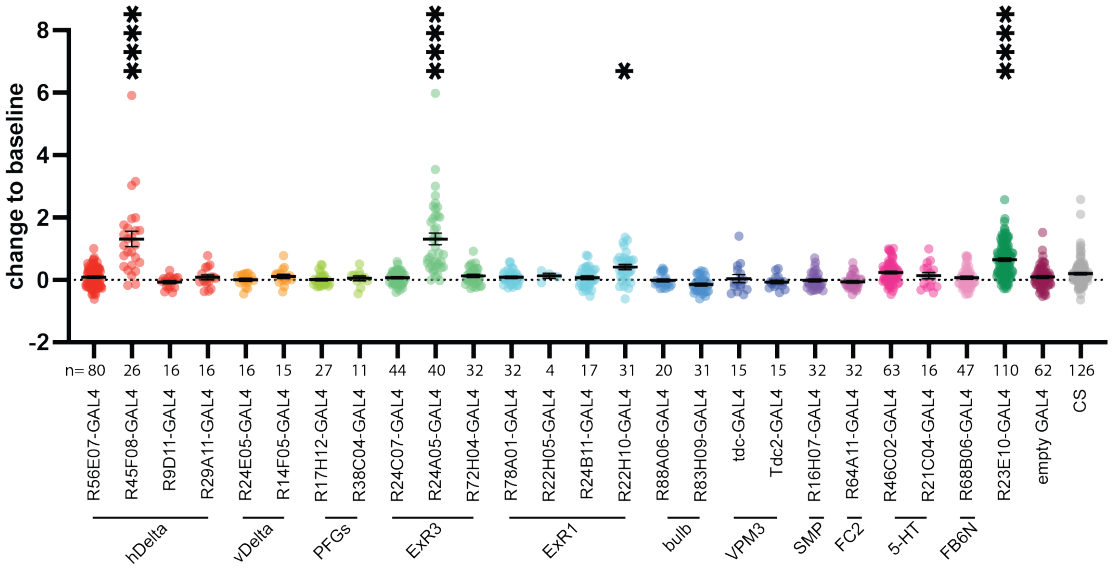

Figure S1: Movement during thermogenetic screen.
Stars indicate significant differences, compared to the empty GAL4 control group. One way ANOVA with Holm-Šídák. **** = $p<0.0001$, *** = $p<0.001$, ** = $p<0.01$, * = $p<0.05$, ns = $p>0.05$. Individual dots represent single flies, bars represent mean ± SEM.

Bibliography

1. Anafi, R. C., Kayser, M. S. & Raizen, D. M. Exploring phylogeny to find the function of sleep. *Nature Reviews Neuroscience* **20,** 109–116. ISSN: 14710048 (2019).
2. Lakhiani, R., Shanavas, S. & Melnattur, K. Comparative biology of sleep in diverse animals. *Journal of Experimental Biology* **226.** ISSN: 14779145 (July 2023).
3. Miyazaki, S., Liu, C. Y. & Hayashi, Y. Sleep in vertebrate and invertebrate animals, and insights into the function and evolution of sleep. *Neuroscience Research* **118,** 3–12. ISSN: 18728111 (May 2017).
4. Campbell, S. S. & Tobler, I. Animal sleep: a review of sleep duration across phylogeny. *Neuroscience and biobehavioral reviews* **8,** 269–300. ISSN: 0149-7634 (1984).
5. Adamantidis, A. R., Gutierrez Herrera, C. & Gent, T. C. *Oscillating circuitries in the sleeping brain* Dec. 2019.
6. Aserinsky, E. & Kleitman, N. Regularly occurring periods of eye motility, and concomitant phenomena, during sleep. *Science (New York, N.Y.)* **118,** 273–4. ISSN: 0036-8075 (Sept. 1953).
7. Dement, W. & Kleitman, N. Cyclic variations in EEG during sleep and their relation to eye movements, body motility, and dreaming. *Electroencephalography and clinical neurophysiology* **9,** 673–90. ISSN: 0013-4694 (Nov. 1957).
8. Nath, R. D. *et al.* The Jellyfish Cassiopea Exhibits a Sleep-like State. *Current Biology* **27,** 2984–2990. ISSN: 09609822 (Oct. 2017).
9. Kanaya, H. J. *et al.* A sleep-like state in Hydra unravels conserved sleep mechanisms during the evolutionary development of the central nervous system. *Science advances* **6,** eabb9415. ISSN: 23752548 (Oct. 2020).
10. Manaceine, D. M. Quelques observations experimentales sur l'influence de l'insomnie absolue. *Arch Ital. Biol.* **21,** 322–325 (1894).
11. Rechtschaffen, A., Gilliland, M. A., Bergmann, B. M. & Winter, J. B. Physiological correlates of prolonged sleep deprivation in rats. *Science* **221,** 182–184. ISSN: 00368075 (July 1983).
12. Tononi, G. & Cirelli, C. Sleep and synaptic homeostasis: A hypothesis. *Brain Research Bulletin* **62,** 143–150. ISSN: 03619230 (2003).

13. Tononi, G. & Cirelli, C. Sleep function and synaptic homeostasis. *Sleep Medicine Reviews* **10,** 49–62. ISSN: 10870792 (Feb. 2006).
14. Bushey, D., Tononi, G. & Cirelli, C. Sleep and Synaptic Homeostasis: Structural Evidence in Drosophila. *Science* **332,** 1576–1581. ISSN: 0036-8075 (June 2011).
15. Gilestro, G. F., Tononi, G. & Cirelli, C. Widespread Changes in Synaptic Markers as a Function of Sleep and Wakefulness in Drosophila. *Science* **324,** 109–112. ISSN: 0036-8075 (Apr. 2009).
16. Appelbaum, L. *et al.* Circadian and homeostatic regulation of structural synaptic plasticity in hypocretin neurons. *Neuron* **68,** 87–98. ISSN: 08966273 (Oct. 2010).
17. Suppermpool, A., Lyons, D. G., Broom, E. & Rihel, J. Sleep pressure modulates single-neuron synapse number in zebrafish. *Nature* **629,** 639–645. ISSN: 14764687 (May 2024).
18. Vyazovskiy, V. V., Cirelli, C., Pfister-Genskow, M., Faraguna, U. & Tononi, G. Molecular and electrophysiological evidence for net synaptic potentiation in wake and depression in sleep. *Nature Neuroscience* **11,** 200–208. ISSN: 10976256 (Feb. 2008).
19. Diering, G. H. *et al.* Homer1a drives homeostatic scaling-down of excitatory synapses during sleep. *Science* **355,** 511–515. ISSN: 0036-8075 (Feb. 2017).
20. Huber, R. *et al.* Human cortical excitability increases with time awake. *Cerebral Cortex* **23,** 332–338. ISSN: 10473211 (Feb. 2013).
21. Xie, L. *et al.* Sleep drives metabolite clearance from the adult brain. *Science* **342,** 373–377. ISSN: 10959203 (Oct. 2013).
22. Holth, J. K. *et al.* The sleep-wake cycle regulates brain interstitial fluid tau in mice and CSF tau in humans. *Science* **363,** 880–884. ISSN: 0036-8075 (Feb. 2019).
23. Eide, P. K., Vinje, V., Pripp, A. H., Mardal, K.-A. & Ringstad, G. Sleep deprivation impairs molecular clearance from the human brain. *Brain* **144,** 863–874. ISSN: 0006-8950 (Apr. 2021).
24. Ungurean, G. *et al.* Wide-spread brain activation and reduced CSF flow during avian REM sleep. *Nature Communications* **14.** ISSN: 20411723 (Dec. 2023).
25. Van Alphen, B., Semenza, E. R., Yap, M., van Swinderen, B. & Allada, R. A deep sleep stage in Drosophila with a functional role in waste clearance. *Science Advances* **7,** eabc2999. ISSN: 2375-2548 (Jan. 2021).

26. Hill, V. M. *et al.* A bidirectional relationship between sleep and oxidative stress in Drosophila. *PLoS Biology* **16,** e2005206. ISSN: 15457885 (July 2018).
27. Reimund, E. The free radical flux theory of sleep. *Medical Hypotheses* **43,** 231–233. ISSN: 03069877 (1994).
28. Borbély, A. A. A two process model of sleep regulation. *Human neurobiology* **1,** 195–204. ISSN: 0721-9075 (1982).
29. Borbély, A. A., Daan, S., Wirz-Justice, A. & Deboer, T. The two-process model of sleep regulation: A reappraisal. *Journal of Sleep Research* **25,** 131–143. ISSN: 13652869 (Apr. 2016).
30. Vyazovskiy, V. V. *et al.* Cortical firing and sleep homeostasis. *Neuron* **63,** 865–78. ISSN: 1097-4199 (Sept. 2009).
31. Allada, R. & Chung, B. Y. Circadian organization of behavior and physiology in Drosophila. *Annual Review of Physiology* **72,** 605–624. ISSN: 00664278 (Mar. 2009).
32. Dubowy, C. & Sehgal, A. Circadian rhythms and sleep in Drosophila melanogaster. *Genetics* **205,** 1373–1397. ISSN: 19432631 (Apr. 2017).
33. Takahashi, J. S. Transcriptional architecture of the mammalian circadian clock. *Nature Reviews Genetics* **18,** 164–179. ISSN: 14710064 (Mar. 2017).
34. Morgan, T. H. Sex Limited Inheritance in Drosophila. *Science* **32,** 120–122. ISSN: 0036-8075 (July 1910).
35. Konopka, R. J. & Benzer, S. Clock Mutants of Drosophila melanogaster. *Proceedings of the National Academy of Sciences* **68,** 2112–2116. ISSN: 0027-8424 (Sept. 1971).
36. Benzer, S. From the gene to behavior. *JAMA* **218,** 1015–22. ISSN: 0098-7484 (Nov. 1971).
37. Adams, M. D. *et al.* The Genome Sequence of Drosophila melanogaster. *Science* **287,** 2185–2195. ISSN: 0036-8075 (Mar. 2000).
38. Myers, E. W. *et al.* A Whole-Genome Assembly of Drosophila. *Science* **287,** 2196–2204. ISSN: 0036-8075 (Mar. 2000).
39. Goffeau, A. *et al.* Life with 6000 Genes. *Science* **274,** 546–567. ISSN: 0036-8075 (Oct. 1996).
40. Bargmann, C. I. Neurobiology of the Caenorhabditis elegans Genome. *Science* **282,** 2028–2033. ISSN: 0036-8075 (Dec. 1998).

41. The C. elegans sequencing consortium. Genome Sequence of the Nematode C. elegans: A Platform for Investigating Biology. *Science* **282,** 2012–2018. ISSN: 0036-8075 (Dec. 1998).
42. Zheng, Z. *et al.* A Complete Electron Microscopy Volume of the Brain of Adult Drosophila melanogaster. *Cell* **174,** 730–743. ISSN: 10974172 (2018).
43. Scheffer, L. K. *et al.* A connectome and analysis of the adult drosophila central brain. *eLife* **9,** 1–74. ISSN: 2050084X (Sept. 2020).
44. Hulse, B. K. *et al.* A connectome of the drosophila central complex reveals network motifs suitable for flexible navigation and context-dependent action selection. *eLife* **10.** ISSN: 2050084X (Oct. 2021).
45. Dorkenwald, S. *et al.* Neuronal wiring diagram of an adult brain. *Nature* **634,** 124–138. ISSN: 0028-0836 (Oct. 2024).
46. Takemura, S.-y. *et al.* A Connectome of the Male Drosophila Ventral Nerve Cord. *eLife* (May 2024).
47. Marin, E. C. *et al.* Systematic annotation of a complete adult male Drosophila nerve cord connectome reveals principles of functional organisation (July 2024).
48. Azevedo, A. *et al.* Connectomic reconstruction of a female Drosophila ventral nerve cord. *Nature* **631,** 360–368. ISSN: 0028-0836 (July 2024).
49. Stürner, T. *et al.* Comparative connectomics of Drosophila descending and ascending neurons. *Nature.* ISSN: 0028-0836 (Apr. 2025).
50. Fischer, J. A., Giniger, E., Maniatis, T. & Ptashne, M. GAL4 activates transcription in Drosophila. *Nature* **332,** 853–6. ISSN: 0028-0836 (Apr. 1988).
51. Brand, A. H. & Perrimon, N. Targeted gene expression as a means of altering cell fates and generating dominant phenotypes. *Development* **118,** 401–415. ISSN: 09501991 (1993).
52. Jenett, A. *et al.* A GAL4-Driver Line Resource for Drosophila Neurobiology. *Cell Reports* **2,** 991–1001. ISSN: 22111247 (Oct. 2012).
53. Luan, H., Peabody, N. C., Vinson, C. R. R. & White, B. H. Refined Spatial Manipulation of Neuronal Function by Combinatorial Restriction of Transgene Expression. *Neuron* **52,** 425–436. ISSN: 08966273 (Nov. 2006).
54. Pfeiffer, B. D. *et al.* Refinement of tools for targeted gene expression in Drosophila. *Genetics* **186,** 735–755. ISSN: 00166731 (Oct. 2010).

55. Wolff, T. *et al.* Cell type-specific driver lines targeting the Drosophila central complex and their use to investigate neuropeptide expression and sleep regulation. *eLife* **14.** ISSN: 2050-084X (Apr. 2025).
56. Meissner, G. W. *et al.* A split-GAL4 driver line resource for Drosophila neuron types. *eLife* **13.** ISSN: 2050-084X (Jan. 2025).
57. Perkins, L. A. *et al.* The transgenic RNAi project at Harvard medical school: Resources and validation. *Genetics* **201,** 843–852. ISSN: 19432631 (Nov. 2015).
58. Perrimon, N., Ni, J. Q. & Perkins, L. In vivo RNAi: today and tomorrow. *Cold Spring Harbor perspectives in biology* **2,** a003640. ISSN: 19430264 (Aug. 2010).
59. Ni, J.-Q. *et al.* A genome-scale shRNA resource for transgenic RNAi in Drosophila. *Nature Methods* **8,** 405–407. ISSN: 1548-7091 (May 2011).
60. Heigwer, F., Port, F. & Boutros, M. Rna interference (RNAi) screening in Drosophila. *Genetics* **208,** 853–874. ISSN: 19432631 (Mar. 2018).
61. Dietzl, G. *et al.* A genome-wide transgenic RNAi library for conditional gene inactivation in Drosophila. *Nature* **448,** 151–156. ISSN: 14764687 (2007).
62. Meltzer, H. *et al.* Tissue-specific (ts)CRISPR as an efficient strategy for in vivo screening in Drosophila. *Nature Communications* **10,** 1–9. ISSN: 20411723 (Dec. 2019).
63. Gratz, S. J. *et al.* Genome engineering of Drosophila with the CRISPR RNA-guided Cas9 nuclease. *Genetics* **194,** 1029–1035. ISSN: 00166731 (Aug. 2013).
64. Gratz, S. J., Rubinstein, C. D., Harrison, M. M., Wildonger, J. & O'Connor-Giles, K. M. CRISPR-Cas9 genome editing in Drosophila. *Current Protocols in Molecular Biology* **2015,** 1–31. ISSN: 19343647 (2015).
65. Port, F. *et al.* A large-scale resource for tissue-specific CRISPR mutagenesis in Drosophila. *eLife* **9,** 1–20. ISSN: 2050084X (2020).
66. Nässel, D. R., Pauls, D. & Huetteroth, W. *Neuropeptides in modulation of Drosophila behavior: how to get a grip on their pleiotropic actions* Dec. 2019.
67. Lacin, H. *et al.* Neurotransmitter identity is acquired in a lineage-restricted manner in the Drosophila CNS. *eLife* **8.** ISSN: 2050084X (Mar. 2019).
68. Collin, C. *et al.* Two types of muscarinic acetylcholine receptors in Drosophila and other arthropods. *Cellular and Molecular Life Sciences* **70,** 3231–3242. ISSN: 1420682X (Sept. 2013).

69. Lee, D. & O'Dowd, D. K. Fast Excitatory Synaptic Transmission Mediated by Nicotinic Acetylcholine Receptors in Drosophila Neurons. *The Journal of Neuroscience* **19,** 5311–5321. ISSN: 0270-6474 (July 1999).

70. Littleton, J. & Ganetzky, B. Ion Channels and Synaptic Organization. *Neuron* **26,** 35–43. ISSN: 08966273 (Apr. 2000).

71. Lee, D., Su, H. & O'Dowd, D. K. GABA Receptors Containing Rdl Subunits Mediate Fast Inhibitory Synaptic Transmission in Drosophila Neurons. *The Journal of Neuroscience* **23,** 4625–4634. ISSN: 0270-6474 (June 2003).

72. Rohrbough, J. & Broadie, K. Electrophysiological analysis of synaptic transmission in central neurons of Drosophila larvae. *Journal of neurophysiology* **88,** 847–60. ISSN: 0022-3077 (Aug. 2002).

73. Mezler, M., Müller, T. & Raming, K. Cloning and functional expression of GABAB receptors from Drosophila. *European Journal of Neuroscience* **13,** 477–486. ISSN: 0953816X (2001).

74. Jan, L. Y. & Jan, Y. N. L-glutamate as an excitatory transmitter at the Drosophila larval neuromuscular junction. *The Journal of Physiology* **262,** 215–236. ISSN: 0022-3751 (Oct. 1976).

75. Bogdanik, L. *et al.* The Drosophila metabotropic glutamate receptor DmGluRA regulates activity-dependent synaptic facilitation and fine synaptic morphology. *Journal of Neuroscience* **24,** 9105–9116. ISSN: 02706474 (2004).

76. Liu, W. W. & Wilson, R. I. Glutamate is an inhibitory neurotransmitter in the Drosophila olfactory system. *Proceedings of the National Academy of Sciences of the United States of America* **110,** 10294–10299. ISSN: 00278424 (2013).

77. Li, Y. *et al.* Novel Functional Properties of Drosophila CNS Glutamate Receptors. *Neuron* **92,** 1036–1048. ISSN: 10974199 (2016).

78. Cully, D. F., Paress, P. S., Liu, K. K., Schaeffer, J. M. & Arena, J. P. Identification of a Drosophila melanogaster Glutamate-gated Chloride Channel Sensitive to the Antiparasitic Agent Avermectin. *Journal of Biological Chemistry* **271,** 20187–20191. ISSN: 00219258 (Aug. 1996).

79. Hodgkin, A. L. & Huxley, A. F. A quantitative description of membrane current and its application to conduction and excitation in nerve. *The Journal of Physiology* **117,** 500–544. ISSN: 0022-3751 (Aug. 1952).

80. Neher, E., Sakmann, B. & Steinbach, J. H. The extracellular patch clamp: A method for resolving currents through individual open channels in biological membranes. *Pflügers Archiv European Journal of Physiology* **375,** 219–228. ISSN: 0031-6768 (July 1978).
81. Neher, E. & Sakmann, B. Single-channel currents recorded from membrane of denervated frog muscle fibres. *Nature* **260,** 799–802. ISSN: 0028-0836 (Apr. 1976).
82. Baines, R. A. & Bate, M. Electrophysiological development of central neurons in the Drosophila embryo. *The Journal of neuroscience : the official journal of the Society for Neuroscience* **18,** 4673–83. ISSN: 0270-6474 (June 1998).
83. Wilson, R. I., Turner, G. C. & Laurent, G. Transformation of Olfactory Representations in the Drosophila Antennal Lobe. *Science* **303,** 366–370. ISSN: 0036-8075 (Jan. 2004).
84. Feinberg, E. H. *et al.* GFP Reconstitution Across Synaptic Partners (GRASP) defines cell contacts and synapses in living nervous systems. *Neuron* **57,** 353–63. ISSN: 0896-6273 (Feb. 2008).
85. Ueno, T. *et al.* Identification of a dopamine pathway that regulates sleep and arousal in Drosophila. *Nature Neuroscience* **15,** 1516–1523. ISSN: 1097-6256 (Nov. 2012).
86. Singh, P. *et al.* Examining sleep modulation by Drosophila ellipsoid body neurons. *Eneuro* **10,** 0281–23. ISSN: 23732822 (2023).
87. Zhang, X. & Gaudry, Q. Examining monosynaptic connections in Drosophila using tetrodotoxin resistant sodium channels. *Journal of Visualized Experiments* **2018.** ISSN: 1940087X (Feb. 2018).
88. Sales, E. C., Heckman, E. L., Warren, T. L. & Doe, C. Q. Regulation of subcellular dendritic synapse specificity by axon guidance cues. *eLife* **8.** ISSN: 2050-084X (Apr. 2019).
89. Chen, D. *et al.* Genetic and neuronal mechanisms governing the sex-specific interaction between sleep and sexual behaviors in Drosophila. *Nature Communications* **8,** 1–14. ISSN: 20411723 (Dec. 2017).
90. Kato, Y. S., Tomita, J. & Kume, K. Interneurons of fan-shaped body promote arousal in Drosophila. *PLoS ONE* **17.** ISSN: 19326203 (Nov. 2022).
91. Raccuglia, D. *et al.* Coherent multi-level network oscillations create neural filters to favor quiescence over navigation in Drosophila. *bioRxiv* (Mar. 2022).

92. Fushiki, A. *et al.* A circuit mechanism for the propagation of waves of muscle contraction in Drosophila. *eLife* **5.** ISSN: 2050-084X (Feb. 2016).
93. Giachello, C. N. *et al.* Electrophysiological Validation of Monosynaptic Connectivity between Premotor Interneurons and the aCC Motoneuron in the Drosophila Larval CNS. *Journal of Neuroscience* **42,** 6724–6738. ISSN: 15292401 (2022).
94. Lu, J. *et al.* Transforming representations of movement from body- to world-centric space. *Nature* **601,** 98–104. ISSN: 14764687 (2022).
95. Berry, M. & Pentreath, V. Criteria for distinguishing between monosynaptic and polysynaptic transmission. *Brain Research* **105,** 1–20. ISSN: 00068993 (Mar. 1976).
96. Ho, M. C. *et al.* Sleep need-dependent changes in functional connectivity facilitate transmission of homeostatic sleep drive. *Current Biology* **32,** 4957–4966. ISSN: 18790445 (2022).
97. Suzuki, Y., Schenk, J. E., Tan, H. & Gaudry, Q. A Population of Interneurons Signals Changes in the Basal Concentration of Serotonin and Mediates Gain Control in the Drosophila Antennal Lobe. *Current Biology* **30,** 1110–1118. ISSN: 18790445 (Mar. 2020).
98. Li, Y. *et al.* Morphological Tracing and Functional Identification of Monosynaptic Connections in the Brain: A Comprehensive Guide. *Neuroscience Bulletin* **40,** 1364–1378. ISSN: 19958218 (Sept. 2024).
99. Shaw, P. J., Cirelli, C., Greenspan, R. J. & Tononi, G. Correlates of sleep and waking in Drosophila melanogaster. *Science* **287,** 1834–7. ISSN: 0036-8075 (Mar. 2000).
100. Hendricks, J. C. *et al.* Rest in Drosophila is a sleep-like state. *Neuron* **25,** 129–138. ISSN: 08966273 (2000).
101. Shaw, P. J., Tortoni, G., Greenspan, R. J. & Robinson, D. F. Stress response genes protect against lethal effects of sleep deprivation in Drosophila. *Nature* **417,** 287–291. ISSN: 00280836 (2002).
102. Helfrich-Förster, C. Differential Control of Morning and Evening Components in the Activity Rhythm of Drosophila melanogaster —Sex-Specific Differences Suggest a Different Quality of Activity. *Journal of Biological Rhythms* **15,** 135–154. ISSN: 0748-7304 (Apr. 2000).
103. Huber, R. *et al.* Sleep homeostasis in Drosophila melanogaster. *Sleep* **27,** 628–639. ISSN: 01618105 (June 2004).

104. Andretic, R. & Shaw, P. J. Essentials of sleep recordings in Drosophila: moving beyond sleep time. *Methods in enzymology* **393,** 759–72. ISSN: 1557-7988 (2005).

105. Beckwith, E. J. & French, A. S. Sleep in Drosophila and Its Context. *Frontiers in Physiology* **10.** ISSN: 1664042X (Sept. 2019).

106. Van Alphen, B., Yap, M. H., Kirszenblat, L., Kottler, B. & van Swinderen, B. A dynamic deep sleep stage in Drosophila. *Journal of Neuroscience* **33,** 6917–6937. ISSN: 02706474 (Apr. 2013).

107. Nitz, D. A., van Swinderen, B., Tononi, G. & Greenspan, R. J. Electrophysiological Correlates of Rest and Activity in Drosophila melanogaster. *Current Biology* **12,** 1934–1940. ISSN: 09609822 (Nov. 2002).

108. Stahl, B. A., Slocumb, M. E., Chaitin, H., DiAngelo, J. R. & Keene, A. C. Sleep-dependent modulation of metabolic rate in drosophila. *Sleep* **40.** ISSN: 15509109 (Aug. 2017).

109. Jagannathan, S. R., Jeans, T., Van De Poll, M. N. & van Swinderen, B. Multivariate classification of multichannel long-term electrophysiology data identifies different sleep stages in fruit flies. *Science Advances* **10,** 1–23. ISSN: 2375-2548 (Feb. 2024).

110. Wiggin, T. D. *et al.* Covert sleep-related biological processes are revealed by probabilistic analysis in Drosophila. *Proceedings of the National Academy of Sciences of the United States of America* **117,** 10024–10034. ISSN: 10916490 (2020).

111. Chowdhury, B., Abhilash, L., Ortega, A., Liu, S. & Shafer, O. Homeostatic control of deep sleep and molecular correlates of sleep pressure in Drosophila. *eLife* **12.** ISSN: 2050-084X (Oct. 2023).

112. Shafer, O. T. & Keene, A. C. The Regulation of Drosophila Sleep. *Current Biology* **31,** R38–R49. ISSN: 18790445 (2021).

113. Shafer, O. T. 25 years of Drosophila "Sleep genes". *Fly* **19.** ISSN: 19336942 (2025).

114. Tomita, J., Ban, G. & Kume, K. Genes and neural circuits for sleep of the fruit fly. *Neuroscience Research* **118,** 82–91. ISSN: 18728111 (2017).

115. Hanesch, U., Fischbach, K. .-. & Heisenberg, M. Neuronal architecture of the central complex in Drosophila melanogaster. *Cell and Tissue Research* **257,** 343–366. ISSN: 0302-766X (1989).

116. Young, J. & Armstrong, J. Structure of the adult central complex in Drosophila: Organization of distinct neuronal subsets. *Journal of Comparative Neurology* **518,** 1500–1524. ISSN: 0021-9967 (May 2010).

117. Pfeiffer, K. & Homberg, U. Organization and functional roles of the central complex in the insect brain. *Annual Review of Entomology* **59,** 165–184. ISSN: 00664170 (Jan. 2014).

118. Gillet, V., Kluge, J. & Patel, R. N. A historical perspective on the insect central complex: Anatomy, development, and function. *Molecular Psychology: Brain, Behavior, and Society* **2,** 19 (Aug. 2023).

119. Stone, T. *et al.* An Anatomically Constrained Model for Path Integration in the Bee Brain. *Current Biology* **27,** 3069–3085. ISSN: 09609822 (Oct. 2017).

120. Fisher, Y. E. Flexible navigational computations in the Drosophila central complex. *Current Opinion in Neurobiology* **73.** ISSN: 18736882 (Apr. 2022).

121. Lyu, C., Abbott, L. F. & Maimon, G. Building an allocentric travelling direction signal via vector computation. *Nature* **601,** 92–97. ISSN: 14764687 (2022).

122. Westeinde, E. A. *et al.* Transforming a head direction signal into a goal-oriented steering command. *Nature,* 2022.11.10.516039. ISSN: 0028-0836 (Feb. 2024).

123. Mussells Pires, P., Zhang, L., Parache, V., Abbott, L. F. & Maimon, G. Converting an allocentric goal into an egocentric steering signal. *Nature* **626,** 808–818. ISSN: 0028-0836 (Feb. 2024).

124. Matheson, A. M. *et al.* A neural circuit for wind-guided olfactory navigation. *Nature Communications* **13.** ISSN: 20411723 (2022).

125. Currier, T. A., Matheson, A. M. & Nagel, K. I. Encoding and control of orientation to airflow by a set of drosophila fan-shaped body neurons. *eLife* **9,** 1–29. ISSN: 2050084X (Dec. 2020).

126. Donlea, J. M., Thimgan, M. S., Suzuki, Y., Gottschalk, L. & Shaw, P. J. Inducing sleep by remote control facilitates memory consolidation in Drosophila. *Science* **332,** 1571–1576. ISSN: 00368075 (June 2011).

127. Donlea, J. M., Pimentel, D. & Miesenböck, G. Neuronal machinery of sleep homeostasis in Drosophila. *Neuron* **81,** 860–72. ISSN: 1097-4199 (Feb. 2014).

128. Pimentel, D. *et al.* Operation of a homeostatic sleep switch. *Nature* **536,** 333–337. ISSN: 0028-0836 (Aug. 2016).

129. Donlea, J. M. *et al.* Recurrent Circuitry for Balancing Sleep Need and Sleep. *Neuron* **97,** 378–389. ISSN: 10974199 (2018).

130. Liu, S., Liu, Q., Tabuchi, M. & Wu, M. N. Sleep drive is encoded by neural plastic changes in a dedicated circuit. *Cell* **165,** 1347–1360. ISSN: 10974172 (2016).

131. Kempf, A., Song, S. M., Talbot, C. B. & Miesenböck, G. A potassium channel β-subunit couples mitochondrial electron transport to sleep. *Nature* **568,** 230–234. ISSN: 0028-0836 (Apr. 2019).

132. Hasenhuetl, P. S., Sarnataro, R., Vrontou, E. & Rorsman, H. O. A half-centre oscillator encodes sleep pressure. *bioRxiv,* 1–43 (2024).

133. Sarnataro, R., Velasco, C. D. & Kempf, A. Mitochondrial origins of the pressure to sleep. *bioRxiv,* 1–46 (2024).

134. Dissel, S. *et al.* Sleep-promoting neurons remodel their response properties to calibrate sleep drive with environmental demands. *PLoS Biology* **20.** ISSN: 15457885 (Sept. 2022).

135. Qian, Y. *et al.* Sleep homeostasis regulated by 5HT2b receptor in a small subset of neurons in the dorsal fan-shaped body of drosophila. *eLife* **6,** 1–27. ISSN: 2050084X (2017).

136. Kayser, M. S., Yue, Z. & Sehgal, A. A Critical Period of Sleep for Development of Courtship Circuitry and Behavior in Drosophila (2014).

137. Troup, M. *et al.* Acute control of the sleep switch in drosophila reveals a role for gap junctions in regulating behavioral responsiveness. *eLife* **7,** 1–22. ISSN: 2050084X (2018).

138. Ammer, G., Vieira, R. M., Fendl, S. & Borst, A. Anatomical distribution and functional roles of electrical synapses in Drosophila. *Current Biology* **32,** 2022–2036. ISSN: 18790445 (May 2022).

139. Rorsman, H. O. *et al.* Sleep pressure accumulates in a voltage-gated lipid peroxidation memory. *Nature* **641,** 232–239. ISSN: 0028-0836 (May 2025).

140. De, J., Wu, M., Lambatan, V., Hua, Y. & Joiner, W. J. Re-examining the role of the dorsal fan-shaped body in promoting sleep in Drosophila. *Current biology* **33,** 3660–3668. ISSN: 1879-0445 (Sept. 2023).

141. Flores-Valle, A., Vishniakou, I. & Seelig, J. D. Dynamics of glia and neurons regulate homeostatic rest, sleep and feeding behavior in Drosophila. *Nature Neuroscience* **28,** 1226–1240. ISSN: 1097-6256 (June 2025).

142. Jones, J. D. *et al.* Regulation of sleep by cholinergic neurons located outside the central brain in Drosophila. *PLoS Biology* **21,** 1–29. ISSN: 15457885 (2023).

143. Tainton-Heap, L. A. *et al.* A Paradoxical Kind of Sleep in Drosophila melanogaster. *Current Biology* **31,** 578–590. ISSN: 09609822 (Feb. 2021).

144. Keleş, M. F. *et al.* FlyVISTA, an integrated machine learning platform for deep phenotyping of sleep in Drosophila. *Science Advances* **11.** ISSN: 2375-2548 (Mar. 2025).

145. Yap, M. H. *et al.* Oscillatory brain activity in spontaneous and induced sleep stages in flies. *Nature Communications* **8.** ISSN: 20411723 (2017).

146. Jones, J. D. *et al.* The dorsal fan-shaped body is a neurochemically heterogeneous sleep-regulating center in Drosophila. *PLOS Biology* **23** (ed Benton, R.) e3003014. ISSN: 1545-7885 (Mar. 2025).

147. Liu, Q., Liu, S., Kodama, L., Driscoll, M. R. & Wu, M. N. Two dopaminergic neurons signal to the dorsal fan-shaped body to promote wakefulness in Drosophila. *Current Biology* **22,** 2114–2123. ISSN: 09609822 (2012).

148. Li, W. *et al.* Chronic social isolation signals starvation and reduces sleep in Drosophila. *Nature* **597,** 239–244. ISSN: 0028-0836 (Sept. 2021).

149. Seelig, J. D. & Jayaraman, V. Feature detection and orientation tuning in the Drosophila central complex. *Nature* **503,** 262–266. ISSN: 00280836 (2013).

150. Neuser, K., Triphan, T., Mronz, M., Poeck, B. & Strauss, R. Analysis of a spatial orientation memory in Drosophila. *Nature* **453,** 1244–1247. ISSN: 14764687 (June 2008).

151. Ofstad, T. A., Zuker, C. S. & Reiser, M. B. Visual place learning in Drosophila melanogaster. *Nature* **474,** 204–209. ISSN: 00280836 (June 2011).

152. Seelig, J. D. & Jayaraman, V. Neural dynamics for landmark orientation and angular path integration. *Nature* **521,** 186–191. ISSN: 14764687 (May 2015).

153. Kim, S. S., Rouault, H., Druckmann, S. & Jayaraman, V. Ring attractor dynamics in the Drosophila central brain. *Science* **356,** 849–853. ISSN: 10959203 (May 2017).

154. Turner-Evans, D. *et al.* Angular velocity integration in a fly heading circuit. *eLife* **6.** ISSN: 2050-084X (May 2017).

155. Yan, W. *et al.* Subtype-Specific Roles of Ellipsoid Body Ring Neurons in Sleep Regulation in Drosophila. *Journal of Neuroscience* **43,** 764–786. ISSN: 15292401 (Feb. 2023).

156. Liu, C. *et al.* A Serotonin-Modulated Circuit Controls Sleep Architecture to Regulate Cognitive Function Independent of Total Sleep in Drosophila. *Current Biology* **29,** 3635–3646. ISSN: 09609822 (2019).

157. Raccuglia, D. *et al.* Network-Specific Synchronization of Electrical Slow-Wave Oscillations Regulates Sleep Drive in Drosophila. *Current Biology* **29,** 3611–3621. ISSN: 09609822 (2019).

158. Lamaze, A., Krätschmer, P., Chen, K. F., Lowe, S. & Jepson, J. E. A Wake-Promoting Circadian Output Circuit in Drosophila. *Current Biology* **28,** 3098–3105. ISSN: 09609822 (Oct. 2018).

159. Guo, F., Holla, M., Díaz, M. M. & Rosbash, M. A Circadian Output Circuit Controls Sleep-Wake Arousal in Drosophila. *Neuron* **100,** 624–635. ISSN: 10974199 (2018).

160. Dai, X., Le, J. Q., Ma, D. & Rosbash, M. Four SpsP neurons are an integrating sleep regulation hub in Drosophila. *Science Advances* **10.** ISSN: 2375-2548 (Nov. 2024).

161. Huang, S., Piao, C., Beuschel, C. B., Götz, T. & Sigrist, S. J. Presynaptic Active Zone Plasticity Encodes Sleep Need in Drosophila. *Current Biology* **30,** 1077–1091. ISSN: 18790445 (2020).

162. Huang, S., Piao, C., Beuschel, C. B., Zhao, Z. & Sigrist, S. J. A brain-wide form of presynaptic active zone plasticity orchestrates resilience to brain aging in Drosophila. *PLoS biology* **20** (ed Shaw, P. J.) e3001730 (Dec. 2022).

163. Andreani, T. *et al.* Circadian programming of the ellipsoid body sleep homeostat in Drosophila. *eLife* **11.** ISSN: 2050084X (June 2022).

164. French, A. S., Geissmann, Q., Beckwith, E. J. & Gilestro, G. F. Sensory processing during sleep in Drosophila melanogaster. *Nature* **20.** ISSN: 1476-4687 (2021).

165. Clements, J. *et al. neuPrint: Analysis Tools for EM Connectomics* Jan. 2020.

166. Buhmann, J. *et al.* Automatic detection of synaptic partners in a whole-brain Drosophila electron microscopy data set. *Nature Methods* **18,** 771–774. ISSN: 15487105 (July 2021).

167. Heinrich, L., Funke, J., Pape, C., Nunez-Iglesias, J. & Saalfeld, S. in *Medical Image Computing and Computer Assisted Intervention – MICCAI 2018. MICCAI 2018. Lecture Notes in Computer Science()* 317–325 (Springer Verlag, May 2018).

168. Vecsey, C. G., Koochagian, C., Porter, M. T., Roman, G. & Sitaraman, D. Analysis of Sleep and Circadian Rhythms from Drosophila Activity-Monitoring Data Using SCAMP. *Cold Spring Harbor Protocols* **2024,** pdb.prot108182. ISSN: 1940-3402 (Nov. 2024).

169. Donelson, N. C. *et al.* High-resolution positional tracking for long-term analysis of Drosophila sleep and locomotion using the "tracker" program. *PloS one* **7** (ed van Swinderen, B.) e37250. ISSN: 1932-6203 (May 2012).

170. White, J. G., Southgate, E., Thomson, J. N. & Brenner, S. The structure of the nervous system of the nematode Caenorhabditis elegans. *Philosophical transactions of the Royal Society of London. Series B, Biological sciences* **314,** 1–340. ISSN: 0962-8436 (Nov. 1986).

171. Cook, S. J. *et al.* Whole-animal connectomes of both Caenorhabditis elegans sexes. *Nature* **571,** 63–71. ISSN: 14764687 (July 2019).

172. Winding, M. *et al.* The connectome of an insect brain. *Science* **379.** ISSN: 10959203 (Mar. 2023).

173. Schlegel, P. *et al.* Whole-brain annotation and multi-connectome cell typing of Drosophila. *Nature* **634,** 139–152. ISSN: 0028-0836 (Oct. 2024).

174. Eckstein, N. *et al.* Neurotransmitter classification from electron microscopy images at synaptic sites in Drosophila melanogaster. *Cell* **187,** 2574–2594. ISSN: 10974172 (May 2024).

175. Auer, T. O. & Benton, R. Sexual circuitry in Drosophila. *Current Opinion in Neurobiology* **38,** 18–26. ISSN: 18736882 (June 2016).

176. Nojima, T. *et al.* A sex-specific switch between visual and olfactory inputs underlies adaptive sex differences in behavior. *Current Biology* **31,** 1175–1191. ISSN: 18790445 (Mar. 2021).

177. Ito, K. *et al.* A systematic nomenclature for the insect brain. *Neuron* **81,** 755–765. ISSN: 08966273 (Feb. 2014).

178. Talay, M. *et al.* Transsynaptic Mapping of Second-Order Taste Neurons in Flies by trans-Tango. *Neuron* **96,** 783–795. ISSN: 10974199 (2017).

179. Ni, J. D. *et al.* Differential regulation of the Drosophila sleep homeostat by circadian and arousal inputs. *eLife* **8.** ISSN: 2050-084X (Feb. 2019).

180. Reyes, M. *et al.* Octopamine regulates neural circuits in the mushroom body and central complex, influencing sleep and context-dependent arousal. *bioRxiv* (Mar. 2025).

181. Busch, S., Selcho, M., Ito, K. & Tanimoto, H. A map of octopaminergic neurons in the Drosophila brain. *Journal of Comparative Neurology* **513,** 643–667. ISSN: 10969861 (Apr. 2009).

182. Scaplen, K. M. *et al.* Transsynaptic mapping of drosophila mushroom body output neurons. *eLife* **10,** 1–29. ISSN: 2050084X (Feb. 2021).

183. Dolan, M.-J. *et al.* Neurogenetic dissection of the Drosophila lateral horn reveals major outputs, diverse behavioural functions, and interactions with the mushroom body. *eLife* **8.** ISSN: 2050-084X (May 2019).

184. Frechter, S. *et al.* Functional and anatomical specificity in a higher olfactory centre. *eLife* **8.** ISSN: 2050-084X (May 2019).

185. Landayan, D., Wang, B. P., Zhou, J. & Wolf, F. W. Thirst interneurons that promote water seeking and limit feeding behavior in Drosophila. *eLife* **10.** ISSN: 2050084X (May 2021).

186. Chen, H.-L., Motevalli, D., Stern, U. & Yang, C.-H. A functional division of Drosophila sweet taste neurons that is value-based and task-specific. *Proceedings of the National Academy of Sciences* **119.** ISSN: 0027-8424 (Jan. 2022).

187. Aso, Y. *et al.* The neuronal architecture of the mushroom body provides a logic for associative learning. *eLife* **3,** e04577. ISSN: 2050084X (2014).

188. Kim, H., Kirkhart, C. & Scott, K. Long-range projection neurons in the taste circuit of Drosophila. *eLife* **6.** ISSN: 2050-084X (Feb. 2017).

189. Li, F. *et al.* The connectome of the adult drosophila mushroom body provides insights into function. *eLife* **9,** 1–217. ISSN: 2050084X (Dec. 2020).

190. Matheson, A. M. M. *et al.* Addendum: A neural circuit for wind-guided olfactory navigation. *Nature Communications* **15,** 1903. ISSN: 2041-1723 (Mar. 2024).

191. Kathman, N. D., Lanz, A. J., Freed, J. D. & Nagel, K. I. Neural dynamics for working memory and evidence integration during olfactory navigation in Drosophila. *bioRxiv* (2024).

192. Hamada, F. N. *et al.* An internal thermal sensor controlling temperature preference in Drosophila. *Nature* **454,** 217–220. ISSN: 14764687 (July 2008).

193. Court, R. *et al.* Virtual Fly Brain—An interactive atlas of the Drosophila nervous system. *Frontiers in Physiology* **14.** ISSN: 1664042X (Jan. 2023).

194. Milyaev, N. *et al.* The virtual fly brain browser and query interface. *Bioinformatics* **28,** 411–415. ISSN: 13674803 (2012).

195. Clements, J. *et al.* NeuronBridge: an intuitive web application for neuronal morphology search across large data sets. *BMC Bioinformatics* **25.** ISSN: 14712105 (Dec. 2024).

196. Baines, R. A., Uhler, J. P., Thompson, A., Sweeney, S. T. & Bate, M. Altered Electrical Properties in Drosophila Neurons Developing without Synaptic Transmission (2001).

197. Johns, D. C., Marx, R., Mains, R. E., O'Rourke, B. & Marbán, E. Inducible Genetic Suppression of Neuronal Excitability. *The Journal of Neuroscience* **19,** 1691–1697. ISSN: 0270-6474 (Mar. 1999).

198. Lee, T. & Luo, L. Mosaic Analysis with a Repressible Cell Marker for Studies of Gene Function in Neuronal Morphogenesis. *Neuron* **22,** 451–461. ISSN: 08966273 (Mar. 1999).

199. McGuire, S. E., Le, P. T., Osborn, A. J., Matsumoto, K. & Davis, R. L. Spatiotemporal Rescue of Memory Dysfunction in Drosophila. *Science* **302,** 1765–1768. ISSN: 00368075 (Dec. 2003).

200. Gordon, M. D. & Scott, K. Motor Control in a Drosophila Taste Circuit. *Neuron* **61,** 373–384. ISSN: 08966273 (Feb. 2009).

201. Nicolaï, L. J. *et al.* Genetically encoded dendritic marker sheds light on neuronal connectivity in Drosophila. *Proceedings of the National Academy of Sciences of the United States of America* **107,** 20553–20558. ISSN: 10916490 (Nov. 2010).

202. Dana, H. *et al.* High-performance calcium sensors for imaging activity in neuronal populations and microcompartments. *Nature Methods* **16,** 649–657. ISSN: 15487105 (2019).

203. Klapoetke, N. C. *et al.* Independent optical excitation of distinct neural populations. *Nature Methods* **11,** 338–346. ISSN: 15487105 (2014).

204. Zemelman, B. V., Nesnas, N., Lee, G. A. & Miesenböck, G. Photochemical gating of heterologous ion channels: Remote control over genetically designated populations of neurons. *Proceedings of the National Academy of Sciences of the United States of America* **100,** 1352–1357. ISSN: 00278424 (2003).

205. Lima, S. Q. & Miesenböck, G. Remote control of behavior through genetically targeted photostimulation of neurons. *Cell* **121,** 141–152. ISSN: 00928674 (2005).

206. Barolo, S., Castro, B. & Posakony, J. W. New Drosophila transgenic reporters: Insulated P-element vectors expressing fast-maturing RFP. *BioTechniques* **36,** 436–442. ISSN: 07366205 (2004).

207. Robie, A. A. *et al.* Mapping the Neural Substrates of Behavior. *Cell* **170,** 393–406. ISSN: 10974172 (2017).

208. Aso, Y. *et al.* Neural circuit mechanisms for transforming learned olfactory valences into wind-oriented movement. *eLife* **12.** ISSN: 2050084X (Sept. 2023).

209. Parisky, K. M., Agosto Rivera, J. L., Donelson, N. C., Kotecha, S. & Griffith, L. C. Reorganization of Sleep by Temperature in Drosophila Requires Light, the Homeostat, and the Circadian Clock. *Current Biology* **26,** 882–892. ISSN: 09609822 (Apr. 2016).

210. Ishimoto, H., Lark, A. & Kitamoto, T. Factors that differentially affect daytime and nighttime sleep in Drosophila melanogaster. *Frontiers in Neurology* **FEB,** 1–5. ISSN: 16642295 (2012).

211. Cao, W. & Edery, I. A novel pathway for sensory-mediated arousal involves splicing of an intron in the period clock gene. *Sleep* **38,** 41–51. ISSN: 15509109 (Jan. 2015).

212. Chen, W.-F., Low, K. H., Lim, C. & Edery, I. Thermosensitive Splicing of a Clock Gene and Seasonal Adaptation. *Cold Spring Harbor Symposia on Quantitative Biology* **72,** 599–606. ISSN: 0091-7451 (Jan. 2007).

213. Pulver, S. R., Pashkovski, S. L., Hornstein, N. J., Garrity, P. A. & Griffith, L. C. Temporal dynamics of neuronal activation by channelrhodopsin-2 and TRPA1 determine behavioral output in Drosophila larvae. *Journal of Neurophysiology* **101,** 3075–3088. ISSN: 00223077 (June 2009).

214. Tomita, J., Ban, G., Kato, Y. S. & Kume, K. Protocerebral Bridge Neurons That Regulate Sleep in Drosophila melanogaster. *Frontiers in Neuroscience* **15.** ISSN: 1662453X (Oct. 2021).

215. Sarantopoulos, C., McCallum, J. B., Kwok, W. M. & Hogan, Q. β-escin diminishes voltage-gated calcium current rundown in perforated patch-clamp recordings from rat primary afferent neurons. *Journal of Neuroscience Methods* **139,** 61–68. ISSN: 01650270 (Oct. 2004).

216. Antic, S. D., Empson, R. M. & Knöpfel, T. Voltage imaging to understand connections and functions of neuronal circuits. *J Neurophysiol* **116,** 135–152 (2016).

217. Hao, Y. A. *et al.* A fast and responsive voltage indicator with enhanced sensitivity for unitary synaptic events. *Neuron* **112,** 3680–3696. ISSN: 08966273 (Nov. 2024).

218. Wolff, T. & Rubin, G. M. Neuroarchitecture of the Drosophila central complex: A catalog of nodulus and asymmetrical body neurons and a revision of the protocerebral bridge catalog. *Journal of Comparative Neurology* **526,** 2585–2611. ISSN: 10969861 (Nov. 2018).

219. Hensgen, R., England, L., Homberg, U. & Pfeiffer, K. Neuroarchitecture of the central complex in the brain of the honeybee: Neuronal cell types. *Journal of Comparative Neurology* **529,** 159–186. ISSN: 10969861 (Jan. 2021).

220. Heinze, S., Florman, J., Asokaraj, S., El Jundi, B. & Reppert, S. M. Anatomical basis of sun compass navigation II: the neuronal composition of the central complex of the monarch butterfly. *The Journal of comparative neurology* **521,** 267–98. ISSN: 1096-9861 (Feb. 2013).

221. Heinze, S. & Homberg, U. Neuroarchitecture of the central complex of the desert locust: Intrinsic and columnar neurons. *Journal of Comparative Neurology* **511,** 454–478. ISSN: 00219967 (Dec. 2008).

222. El Jundi, B., Warrant, E. J., Pfeiffer, K. & Dacke, M. Neuroarchitecture of the dung beetle central complex. *Journal of Comparative Neurology* **526,** 2612–2630. ISSN: 10969861 (Nov. 2018).

223. Jahn, S. *et al.* Neuroarchitecture of the central complex in the Madeira cockroach Rhyparobia maderae: Pontine and columnar neuronal cell types. *Journal of Comparative Neurology* **531,** 1689–1714. ISSN: 10969861 (Nov. 2023).

224. D'Atri, I. & DasGupta, S. *Neural Basis of Odometry in Drosophila* Mar. 2025.

225. Hamid, A. *et al.* The conserved RNA-binding protein Imp is required for the specification and function of olfactory navigation circuitry in Drosophila. *Current Biology* **34,** 473–488. ISSN: 18790445 (2024).

226. Chen, N. *et al.* Widespread posttranscriptional regulation of cotransmission. *Science Advances* **9.** ISSN: 23752548 (2023).

227. Croset, V., Treiber, C. D. & Waddell, S. Cellular diversity in the Drosophila midbrain revealed by single-cell transcriptomics. *eLife* **7.** ISSN: 2050084X (Apr. 2018).

228. Davie, K. *et al.* A Single-Cell Transcriptome Atlas of the Aging Drosophila Brain. *Cell* **174,** 982–998. ISSN: 10974172 (2018).

229. Nässel, D. R. Substrates for neuronal cotransmission with neuropeptides and small molecule neurotransmitters in drosophila. *Frontiers in Cellular Neuroscience* **12.** ISSN: 16625102 (Mar. 2018).

230. Bhatt, D. & Cooper, R. L. The pharmacological and physiological profile of glutamate receptors at the Drosophila larval neuromuscular junction. *Physiological Entomology* **30,** 205–210. ISSN: 03076962 (June 2005).

231. Hampel, S., Franconville, R., Simpson, J. H. & Seeds, A. M. A neural command circuit for grooming movement control. *eLife* **4.** ISSN: 2050-084X (Sept. 2015).

232. Elwyn Isaac, R., Li, C., Leedale, A. E. & Shirras, A. D. Drosophila male sex peptide inhibits siesta sleep and promotes locomotor activity in the post-mated female. *Proceedings of the Royal Society B: Biological Sciences* **277,** 65–70. ISSN: 14712970 (Jan. 2010).

233. Kitamoto, T. Conditional modification of behavior in Drosophila by targeted expression of a temperature-sensitive shibire allele in defined neurons. *Journal of Neurobiology* **47,** 81–92. ISSN: 0022-3034 (May 2001).

234. White, B. H. *et al.* Targeted attenuation of electrical activity in Drosophila using a genetically modified K(+) channel. *Neuron* **31,** 699–711. ISSN: 0896-6273 (Sept. 2001).

235. Markstein, M., Pitsouli, C., Villalta, C., Celniker, S. E. & Perrimon, N. Exploiting position effects and the gypsy retrovirus insulator to engineer precisely expressed transgenes. *Nature Genetics* **40,** 476–483. ISSN: 10614036 (Apr. 2008).

236. Tadres, D., Shiozaki, H. M., Tastekin, I., Stern, D. L. & Louis, M. An essential experimental control for functional connectivity mapping with optogenetics. *bioRxiv* (May 2022).

237. Sareen, P. F., McCurdy, L. Y. & Nitabach, M. N. A neuronal ensemble encoding adaptive choice during sensory conflict in Drosophila. *Nature Communications* **12.** ISSN: 20411723 (Dec. 2021).

238. Goldschmidt, D. *et al.* A neuronal substrate for translating nutrient state and resource density estimations into foraging decisions. *bioRxiv* (2023).

239. Kimura, K. I., Ote, M., Tazawa, T. & Yamamoto, D. Fruitless specifies sexually dimorphic neural circuitry in the Drosophila brain. *Nature* **438,** 229–233. ISSN: 14764687 (Nov. 2005).

240. Rideout, E. J., Dornan, A. J., Neville, M. C., Eadie, S. & Goodwin, S. F. Control of sexual differentiation and behavior by the doublesex gene in Drosophila melanogaster. *Nature Neuroscience* **13,** 458–466. ISSN: 10976256 (Apr. 2010).

241. Zhou, C., Pan, Y., Robinett, C. C., Meissner, G. W. & Baker, B. S. Central brain neurons expressing doublesex regulate female receptivity in Drosophila. *Neuron* **83,** 149–163. ISSN: 10974199 (July 2014).

242. Bormann, J., Hamill, O. P. & Sakmann, B. Mechanism of anion permeation through channels gated by glycine and gamma-aminobutyric acid in mouse cultured spinal neurones. *The Journal of Physiology* **385,** 243–286. ISSN: 0022-3751 (Apr. 1987).

243. Eick, A. K., Ogueta, M., Buhl, E., Hodge, J. J. & Stanewsky, R. The opposing chloride cotransporters KCC and NKCC control locomotor activity in constant light and during long days. *Current Biology* **32,** 1420–1428. ISSN: 18790445 (Mar. 2022).

244. Held, M. *et al.* Aminergic and peptidergic modulation of insulin-producing cells in Drosophila. *eLife* **13.** ISSN: 2050-084X (Mar. 2025).

245. Fenk, L. M. *et al.* Muscles that move the retina augment compound eye vision in Drosophila. *Nature* **612,** 116–122. ISSN: 14764687 (Dec. 2022).

246. Gouwens, N. W. & Wilson, R. I. Signal propagation in Drosophila central neurons. *Journal of Neuroscience* **29,** 6239–6249. ISSN: 02706474 (2009).

247. Ache, J. M., Namiki, S., Lee, A., Branson, K. & Card, G. M. State-dependent decoupling of sensory and motor circuits underlies behavioral flexibility in Drosophila. *Nature Neuroscience* **22,** 1132–1139. ISSN: 15461726 (July 2019).

248. Wilson, R. I. & Laurent, G. Role of GABAergic inhibition in shaping odor-evoked spatiotemporal patterns in the Drosophila antennal lobe. *Journal of Neuroscience* **25,** 9069–9079. ISSN: 02706474 (Oct. 2005).

249. Kondo, S. *et al.* Neurochemical Organization of the Drosophila Brain Visualized by Endogenously Tagged Neurotransmitter Receptors. *Cell Reports* **30,** 284–297. ISSN: 22111247 (Jan. 2020).

250. Omoto, J. J. *et al.* Neuronal constituents and putative interactions within the drosophila ellipsoid body neuropil. *Frontiers in Neural Circuits* **12,** 1–26. ISSN: 16625110 (2018).

251. Harris, R. M., Pfeiffer, B. D., Rubin, G. M. & Truman, J. W. Neuron hemilineages provide the functional ground plan for the Drosophila ventral nervous system. *eLife* **4.** ISSN: 2050-084X (July 2015).

252. Green, J., Vijayan, V., Mussells Pires, P., Adachi, A. & Maimon, G. A neural heading estimate is compared with an internal goal to guide oriented navigation. *Nature Neuroscience* **22,** 1460–1468. ISSN: 15461726 (Sept. 2019).

253. Shao, L. *et al.* Dissection of the Drosophila neuropeptide F circuit using a high-throughput two-choice assay. *Proceedings of the National Academy of Sciences of the United States of America* **114,** E8091–E8099. ISSN: 10916490 (2017).

254. Yuan, Q., Joiner, W. J. & Sehgal, A. A Sleep-Promoting Role for the Drosophila Serotonin Receptor 1A. *Current Biology* **16,** 1051–1062. ISSN: 09609822 (2006).

255. Knapp, E. M. *et al.* Mutation of the Drosophila melanogaster serotonin transporter dSERT impacts sleep, courtship, and feeding behaviors. *PLoS Genetics* **18.** ISSN: 15537404 (Nov. 2022).

256. Blenau, W., Stöppler, D., Balfanz, S., Thamm, M. & Baumann, A. Dm5-HT2B: Pharmacological characterization of the fifth serotonin receptor subtype of drosophila melanogaster. *Frontiers in Systems Neuroscience* **11,** 1–11. ISSN: 16625137 (2017).

257. Cao, H., Tang, J., Liu, Q., Huang, J. & Xu, R. Autism-like behaviors regulated by the serotonin receptor 5-HT2B in the dorsal fan-shaped body neurons of Drosophila melanogaster. *European Journal of Medical Research* **27,** 1–15. ISSN: 2047783X (2022).

258. Lau, C. K., Jelen, M. & Gordon, M. D. A closed-loop optogenetic screen for neurons controlling feeding in Drosophila. *G3: Genes, Genomes, Genetics* **11.** ISSN: 21601836 (May 2021).

259. Dionne, H., Hibbard, K. L., Cavallaro, A., Kao, J. C. & Rubin, G. M. Genetic reagents for making split-GAL4 lines in Drosophila. *Genetics* **209,** 31–35. ISSN: 19432631 (May 2018).

260. Blum, I. D. *et al.* Astroglial Calcium Signaling Encodes Sleep Need in Drosophila. *Current Biology* **31,** 150–162. ISSN: 18790445 (2021).

261. Flores-Valle, A., Gonçalves, P. J. & Seelig, J. D. Integration of sleep homeostasis and navigation in drosophila. *PLoS Computational Biology* **17.** ISSN: 15537358 (July 2021).

262. Green, J. *et al.* A neural circuit architecture for angular integration in Drosophila. *Nature* **546,** 101–106. ISSN: 14764687 (June 2017).

263. Beetz, M. J., Kraus, C. & el Jundi, B. Neural representation of goal direction in the monarch butterfly brain. *Nature Communications* **14.** ISSN: 20411723 (Dec. 2023).

264. Keene, A. C. *et al.* Clock and cycle limit starvation-induced sleep loss in drosophila. *Current Biology* **20,** 1209–1215. ISSN: 09609822 (2010).